INFORMATION TO USERS

This manuscript has been reproduced from the microfilm master. UMI films the text directly from the original or copy submitted. Thus, some thesis and dissertation copies are in typewriter face, while others may be from any type of computer printer.

The quality of this reproduction is dependent upon the quality of the copy submitted. Broken or indistinct print, colored or poor quality illustrations and photographs, print bleedthrough, substandard margins, and improper alignment can adversely affect reproduction.

In the unlikely event that the author did not send UMI a complete manuscript and there are missing pages, these will be noted. Also, if unauthorized copyright material had to be removed, a note will indicate the deletion.

Oversize materials (e.g., maps, drawings, charts) are reproduced by sectioning the original, beginning at the upper left-hand corner and continuing from left to right in equal sections with small overlaps. Each original is also photographed in one exposure and is included in reduced form at the back of the book.

Photographs included in the original manuscript have been reproduced xerographically in this copy. Higher quality 6" x 9" black and white photographic prints are available for any photographs or illustrations appearing in this copy for an additional charge. Contact UMI directly to order.

UMI

A Bell & Howell Information Company
300 North Zeeb Road, Ann Arbor MI 48106-1346 USA
313/761-4700 800/521-0600

ATTITUDE CONTROL OF SMALL SATELLITES USING FUZZY LOGIC

Bertrand Petermann

Department of Mechanical Engineering
McGill University, Montreal

A thesis submitted to the Faculty of Graduate Studies and Research
in partial fulfillment of the requirements of the degree of
Master of Engineering

ABSTRACT

Current interest in small satellites lies in the feasibility of achieving specific but limited objectives. By necessity, small spacecraft technology requires simple control schemes, where small attitude errors can be tolerated inside specified deadbands. The attitude control of a small satellite using fuzzy logic is examined in this thesis.

A realistic satellite is modelled as a central rigid body with a set of flexible appendages. The continuous flexible structures are discretized using the assumed modes method. Equations governing the attitude motion and the bending vibrations of the appendages are obtained from the Lagrangian formulation, while the orbital motion is assumed to be Keplerian.

The cases of thrusting and magneto-torquing are considered for the missions of three-axis and spin stabilization of the satellite, respectively. For each case, a set of control rules based on fuzzy logic is formulated to control the polarity and the switching time of the actuators. Control constraints are imposed on the actuators. Various simulations in the presence of environmental disturbances and uncontrolled vibrations of the appendages illustrate the effectiveness of the attitude fuzzy logic controllers.

RÉSUMÉ

L'intérêt actuel pour les mini-satellites repose sur la possibilité de réaliser des objectifs précis mais limités. Par nécessité, la technologie des mini-satellites requiert des stratégies simples de commande, où de petites erreurs sur l'orientation du satellite sont admises à l'intérieur de bandes de tolérance. Le contrôle d'attitude d'un mini-satellite par la logique floue est étudiée dans ce mémoire.

Un satellite est modélisé par un corps rigide central avec un ensemble de parties auxiliaires flexibles. Les structures flexibles continues sont discrétisées en utilisant la méthode des modes fictifs. Les équations régissant le mouvement d'attitude et les vibrations en flexion des parties auxiliaires sont obtenues à partir de la méthode Lagrangienne, tandis que le mouvement orbital est soumis aux lois de Kepler.

Les missions de stabilisation des trois axes de rotation et de stabilisation gyroscopique sont respectivement effectuées en utilisant des propulseurs et des bobines électro-magnétiques. Pour chaque cas, un ensemble de lois de contrôle basées sur la logique floue est énoncé pour commander la polarité et le temps de commutation des mécanismes créant le mouvement. Des contraintes de contrôle sont imposées sur ces mécanismes. Plusieurs simulations, en présence de perturbations environnementales et en présence de vibrations libres des parties flexibles, illustrent l'efficacité des contrôleurs d'attitude basés sur la logique floue.

ACKNOWLEDGMENTS

I would like to thank my research supervisor Professor A. K. Misra for his continuous guidance and support throughout the course of my work. His precise advise was highly appreciated.

I acknowledge the students with whom I share an office and computer facilities in the Department of Mechanical Engineering. I am especially grateful to Sun-Wook Kim and Christian Semler for their valuable advice. I also thank Barbara Whiston for her administrative expertise and kindness.

Finally, I would like to express my best regards to Isabelle Therrien, for her constant support and encouragement.

CONTENTS

NOMENCLATURE

General conventions

bold	bold variables represent a column vector or a matrix
non-bold	index or scalar
$\mathbf{a}^{\times}$	skew-symmetric cross-product matrix associated with vector **a**
$\mathbf{a}^{T}$	transpose of **a**
$\hat{\mathbf{a}}$	unit vector of **a**

Roman symbols

a	radial offset of the appendage from the satellite c. m.
A_c	coil cross sectional area
A_p	projected surface
b	geomagnetic field
$\mathbf{c}_p$	position vector of the centre of pressure of the surface
$\mathbf{c}_1$, $\mathbf{c}_2$	nondimensional vectors, Eq.(2.9)
$\mathbf{C}_3$, $\mathbf{C}_4$	nondimensional matrices, Eq.(2.9)
D	damping matrix
e	orbit eccentricity
E	modulus of elasticity of the beam material
EI_{in}	bending rigidity for in-plane displacements
EI_{out}	bending rigidity for out of plane displacements
f	vector of generalized forces
$\mathbf{f}_A$, $\mathbf{f}_D$, $\mathbf{f}_S$	vector of generalized forces corresponding to aerodynamics force, damping and solar pressure force, respectively

g_n^m, h_n^m	Gaussian coefficients
h	appendage offset along the axis of symmetry of the satellite
i	orbit inclination angle
i_c	coil current
I	total inertia matrix of the satellite about its centre of mass
I_{Tcb}	transverse moment of inertia of the central body about its c.m.
I_{Zcb}	moment of inertia of the central body about its axis of symmetry
K	stiffness matrix, Eq.(2.14)
L	length of the beam
m	magnetic dipole of the satellite
$\hat{\mathbf{m}}_e$	geomagnetic dipole unit vector
m_s	mass of the spacecraft
M	mass matrix, Eq.(2.8)
M_e	geomagnetic dipole strength
n	number of modes
$\hat{\mathbf{n}}_A$	inward normal to the surface
n_c	number of coil turns
$\hat{\mathbf{n}}_c$	unit vector normal to the coil area
N	number of appendages
p	semi-latus rectum
p_b	load distribution along the beam due to the solar radiation force
p_s	solar radiation pressure
P	kinematic transformation matrix
P_n^m	Legendre polynomials
q	vector of all generalized coordinates
$\mathbf{q}_i$	vector of generalized coordinates for the i^{th} elastic displacement
r_b	radius of the beam
$\mathbf{r}_G$	position vector of the satellite with respect to the Earth
R	universal gas constant

$\mathbf{R}$	rotational transformation matrix
R_e	radius of the Earth
$\hat{\mathbf{s}}$	incoming Sun unit vector
t	time
t_b	thickness of the beam
T	kinetic energy of the spacecraft
T_b	kinetic energy of one beam
$T_{b,e}$	elastic kinetic energy of one beam
$T_{b,r}$	rigid-body kinetic energy of one beam
T_e	kinetic energy of the flexible appendages
T_{orb}	orbital kinetic energy
$u(x,t)$	transverse displacement of a typical appendage
$\mathbf{v}$	absolute velocity of a point on an appendage
$\mathbf{v}_a$	velocity of the local atmosphere with respect the centre of mass of the satellite
v_b	speed of air related to the surface temperature
$\mathbf{v}_{orb}$	orbital velocity of the spacecraft
V	potential energy of the spacecraft
V_e	elastic potential energy of the flexible appendages
V_g	gravity-gradient potential energy
V_m	geomagnetic potential function
V_{orb}	gravitational orbital potential energy
w_b	width of the beam
X, Y, Z	body-fixed frame of reference
X_i, Y_i, Z_i	inertial geocentric frame
X_o, Y_o, Z_o	orbital frame

Greek symbols

α	angle of attack
$\boldsymbol{\alpha}$	vector of attitude Euler angles

α_S	right ascension of the Sun with respect to the vernal equinox
$\alpha_1, \alpha_2, \alpha_3$	attitude Euler angles
δ_S	declination angle of the Sun
ϕ_m	East longitude of the geomagnetic dipole
Φ	vectors of admissible function in nondimensional form
Γ	angular momentum vector due to deformations of the appendage
η	damping coefficient
μ	gravitational constant of Earth
θ	true anomaly
θ_{g0}	right ascension of the Greenwich meridian at some reference
θ_m	coelevation of the geomagnetic dipole
ρ	linear density of the uniform beam
ρ_a	density of the atmosphere
$\sigma_a, \sigma_{rd}, \sigma_{rs}$	radiation surface coefficients defined as absorption, diffused reflection and specular reflection coefficients respectively
σ_n, σ_t	surface accommodation coefficients for normal and tangential momentum exchange
τ	external nonconservative torque
τ_c, τ_d, τ_g	external torque corresponding to the control torque, the disturbance torque and the gravity-gradient torque, respectively
υ	argument of the perigee
ω	angular velocity of the spacecraft
ω_e	angular velocity of the Earth
ω_{in}^2	$EI_{in}/\rho L^4$
ω_m	right ascension of the geomagnetic dipole
ω_{out}^2	$EI_{out}/\rho L^4$
$\omega_x, \omega_y, \omega_z$	angular velocity components in the body-fixed frame
Ω	right ascension of the line of ascending node
ξ	nondimensional length variable

LIST OF FIGURES

LIST OF TABLES

Chapter 1

INTRODUCTION

1.1 Introductory Remarks

The last decade has seen the renaissance of interest in Low-Earth-Orbit small satellites. Their attraction lies in the feasibility of achieving specific but limited objectives with a relatively low-cost technology and a reduced research and development time-scale. For a focused mission, the tolerances are relaxed as much as possible: mechanisms are simplified, structural elements are limited to simple shapes, equipment redundancy is avoided. Also, small satellites can be released into orbit from small launch vehicles (e.g. Pegasus rocket) or as an auxiliary payload from big launchers (Delta rocket or Space Shuttle Get Away Special Canister). This reduces the cost of the overall mission and hence makes the use of small satellites all the more attractive. As a result, this low cost permits an access to the space era to commercial firms, research organizations and universities through scientific and testing experiments. For instance, the University of Surrey has met successful achievements through the UoSat satellite program in terms of cost-effective spacecraft technology and space education program [Hodgart et al.'87].

Small satellites are also considered for complex missions such as providing interactive data and mobile communications [Horais'91]. For such cases, a constellation of Low-Earth-Orbit small satellites can advantageously replace large and expensive geosynchronous satellites. Indeed, the reliability capability is distributed between a number of satellites and failure of one does not affect the total system operation.

The focus of this thesis is to examine novel attitude control schemes adapted to the small satellite requirements.

1.2 Attitude Dynamics of Flexible Spacecraft

Attitude dynamics of spacecraft, taking into account the effects of structural flexibility, has received increasing attention after the anomalous behavior of several early spacecraft. Pioneering contribution to this research area can be attributed to [Likins et al.'71], [Hughes'73], [Meirovitch et al.'66]. Since then, hundreds of papers have been written in this area. It is beyond the scope of this thesis to present an extensive literature review. Only some relevant papers are cited here. A more detailed review can be found in a volume edited by [Junkins'90].

Among the indispensable mathematical supports identified by [Modi'74] in a detailed literature review on satellites with flexible appendages, the concept of hybrid coordinates has provided a background for many researches. This method employs a combination of discrete and modal coordinates in the simulation of the motion of an assemblage of rigid bodies and flexible appendages: the attitude coordinates of the vehicle remain discrete while modes of linearly elastic appendages subject to small deformations are introduced. [Meirovitch'91] proposed a general method based on a modified Lagrangian approach to derive the equations of motion of translating and rotating flexible bodies. Another popular approach is to use Kane's method, which seems to have certain computational advantages [Huston'91].

The study of flexible bodies attached to a moving base has been pursued in connection with several disciplines such as helicopter dynamics, robotics, spacecraft dynamics. [Vigneron'71] used hybrid coordinates to study the attitude dynamics of a spinning spacecraft with four appendages in a crossed dipole configuration: the crucial effect of the geometric shortening of the beam was pointed out, as it leads to the correct theory in terms of centrifugal stiffening effect. [Kalaycioglu'87] analyzed the effect of the point of attachment of a rotating beam on the dynamics and stability of the system: offsets may have a destabilizing effect on the attitude motion while in some other cases increase the natural frequencies of the system. In a paper by [Kane et al.'87], a general comprehensive theory was derived for dealing with small vibrations of a general beam attached to a moving base. Although the paper made a significant advance, the authors' approach seemed to suffer from a confusion in using the deformed and undeformed

configuration coordinates. This drawback has been clearly pointed out by [Hanagud et al.'89], who presented the correct modelling.

Most of the work on the effect of the geometric stiffening on the dynamics of multibody flexible systems suffers from the drawback of being geometry-dependent, hence case-dependent. A general method has been proposed in [Banerjee et al.'90] for an arbitrary flexible body in large rotation and translation. The formulation is based on Kane's equations: firstly, generalized inertia forces are written using linearized modal coordinates; secondly, the linearization is compensated by means of a geometric stiffness matrix. This method is applied successfully to rotating beams and plates. [Sadigh et al.'93] compared three different methods of compensating for the missing terms in the equations of motion of a flexible structure: the method using nonlinear strain-displacement relations gave more precise results than those using the nonlinear strain energy or the pseudo-potential field.

Finally, a systematic procedure for obtaining the governing equations of a flexible multibody system is presented in [Huston et al.'95]: the dynamical stiffening effects are automatically incorporated into the analysis, which combines the finite element, finite segment, modal analysis methods.

1.3 Attitude Control of Flexible Spacecraft

The problem of control of flexible spacecraft has received a great deal of attention, especially for large flexible spacecraft. Numerous control schemes have been proposed, too many to be described here, but they all represent one form or another of modal control.

[Meirovitch et al.'77] proposed independent modal space control (IMSC), which involves a synthesizing control scheme for each mode separately after modal decoupling of the flexible spacecraft dynamical model. Both linear and nonlinear controllers can be applied advantageously using this approach. [Öz et al.'80] presented an optimization of the modal-space control of a flexible spacecraft by providing the spatial distribution of actuators and the optimal time control forces.

The modal reduction of a continuous flexible structure can induce control and observation spillover. [Balas'78] examined this phenomenon where the control effort affects and is affected by the uncontrolled modes. Spillover has to be reduced as it can lead to the instability of the system.

A comparison between coupled control and independent modal-space control for large flexible systems by [Meirovitch et al.'83] showed the superiority of independent modal-space control as it permits easier design and requires less computational effort. Also control spillover is circumvented in independent modal-space control, provided that the number of actuators equals the order of the discretized system.

In parallel to the increasing complexity of dynamical space system, challenging control schemes must be designed to achieve modal decoupling while actively eliminating the induced disturbances of the system. For instance, an orbiting platform supporting a multi-link flexible manipulator is considered in [Karray et al.'93], where the feedback linearization technique, used to separate the system dynamics into a set of decoupled equations, is combined to an active vibration suppression scheme using piezo-electric actuators.

1.4 Fuzzy Logic Control of Spacecraft Attitude

Spacecraft attitude control has been examined in the past using several approaches such as classical control theory or state-space techniques. In a detailed literature review, [Lee'90] reported a wide range of nonlinear systems controlled by fuzzy logic showing usually superior results over conventional control. Hence it is likely that this alternative control technique could also be applied to the attitude motion of a spacecraft.

[Berenji et al.'93] proposed a fuzzy control scheme for the attitude stabilization of the Space Shuttle. The control rules were designed to fire primary or vernier thrusters so that the attitude errors remain inside prescribed deadbands. [Chiang et al.'94] presented a fuzzy logic controller for Cassini spacecraft. The control rules were tuned to stabilize the satellite using bang-off-bang thrusters. The fuzzy controller was compared with the conventional bang-off-bang control scheme, showing better time response but larger thruster cycle. [Matsuzaki et al.'94] described the fuzzy logic control of the in-plane

pitching and the out of plane rolling motion of a tethered subsatellite during deployment, stationkeeping, and retrieval operations by changing the tether length rate. [Steyn'94] compared a rule-based fuzzy controller with an adaptive MIMO LQR controller for the Low-Earth-Orbit small satellite attitude control. The fuzzy logic controller achieved the best overall performance under various conditions while being less computationally demanding. Finally, [Satyadas et al.'95] proposed a Genetic Algorithm Optimized Fuzzy Control for the attitude control of the Space Station Freedom. The Genetic Algorithm is based on biological and mathematical concepts but, when applied to fuzzy logic control, allows a self-tuning of the control rules. The author concluded that this scheme has robustness and adaptation capability for the control of the steady-spin motion of the Space Station.

1.5 Objectives and Organization of the Thesis

In the few above-mentionned papers on attitude control using fuzzy logic, the dynamical models were fairly simplified: attitude equations were applied to rigid bodies while disturbances were taken into account in [Steyn'94] only, for a satellite spinning about the yaw-axis (i.e., axis along the nadir). This thesis considers attitude control using fuzzy logic in a more realistic situation: a satellite with a set of flexible appendages in a crossed-dipole configuration, spinning along the pitch axis (orbit normal) and subjected to environmental disturbances such as aerodynamic force, solar radiation pressure, and residual magnetic torque.

The control of the vibrations of the appendages is beyond the scope of this thesis. However, flexibility is taken into account as a perturbation on the attitude dynamics of the spacecraft.

Two kinds of attitude control will be presented with different actuators: three-axis stabilization using thrusters and spin-stabilization using magneto-torquing. For each case, a set of rules based on fuzzy logic is formulated. Simplicity, imposed by the design of a small satellite, requires actuators of constant magnitude, but constrains severely the control. The logic of the controller will be tuned to command the switching time of the actuators.

The lack of mathematical tools to establish the stability of the controlled system is a weakness of most fuzzy logic controllers. However, various simulations in the presence of environmental disturbances will be used to assess the effectiveness of the fuzzy logic attitude controller.

The thesis is organized as follows:

- Chapter 2 presents the equations governing the attitude motion of the spacecraft as well as the vibrational equations of the flexible appendages;
- Chapter 3 considers the environmental disturbances for a Low-Earth-Orbit satellite in terms of torques and generalized forces;
- Chapter 4 describes two fuzzy logic controllers for the attitude control of small spacecraft: three-axis stabilization using thrusters and spin-stabilization of the flexible spacecraft using fuzzy logic control with magneto-torquing;
- Chapter 5 provides numerical results and discussion;
- Chapter 6 presents the conclusions reached in the thesis and recommendations for future work.

Chapter 2

EQUATIONS OF MOTION

2.1 Introductory Remarks

Most modern satellites can be effectively modelled in one of the four ways:

(i) rigid body or assemblage of rigid bodies;

(ii) quasi-rigid bodies;

(iii) rigid body or assemblage of rigid bodies with flexible appendages;

(iv) elastic bodies.

The third type is chosen in this thesis since many small satellites fall in this category.

Current designs of spacecraft employ flexible appendages such as antennas, booms or solar arrays, for which the major deformation results due to bending. In this thesis, bending is modelled while torsion, shear and axial compression of the appendages are neglected.

The general motion of the system can be divided into three components:

(i) orbital dynamics: motion of the centre of mass around the Earth;

(ii) attitude dynamics: rotation of the satellite around its centre of mass;

(iii) structural dynamics: transverse vibrations of flexible appendages due to bending.

2.2 System Description

The configuration of the satellite considered in this thesis is shown in Figure 2.1: the satellite is modelled as a central rigid body linked to four identical flexible appendages in a deployed configuration.

Each appendage is assumed to be inextensible and of uniform cross section. The length of each appendage is L. The constant mass per unit length is ρ, and the modulus of elasticity is E. The offset of the base of each beam with respect to the centre of mass of the satellite is the same for all beams and is specified by the radial offset a, and the z-offset h.

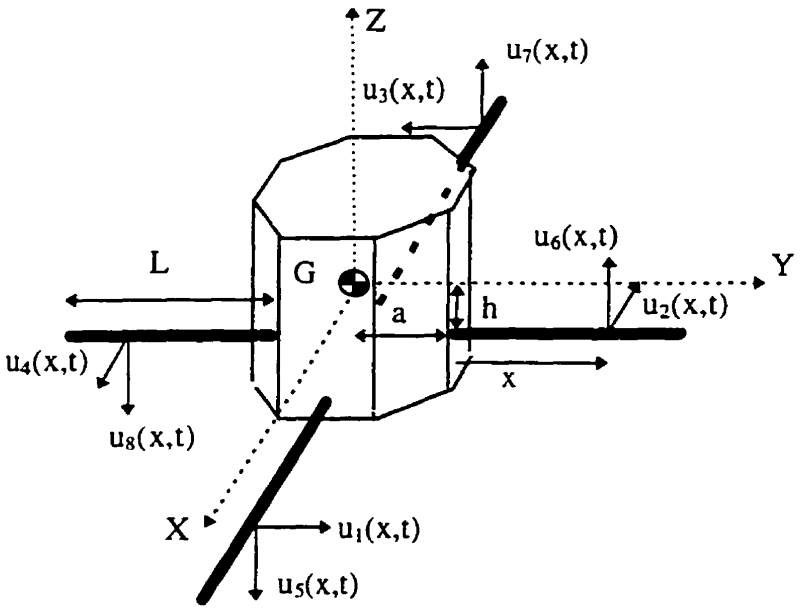

Figure 2.1 Satellite with Four Identical Flexible Appendages

In order to describe the dynamics, the definition of several coordinate frames is required.

The inertial frame X_i, Y_i, Z_i, is located at the centre of Earth and is defined as follows (Figure 2.2):

- X_i in the direction of the vernal equinox;
- Z_i along the spin axis of the Earth, i.e. towards the celestial north pole;
- Y_i completing the right-hand coordinate system.

The centre of mass of the satellite G is located with respect to the Earth centre by the radial vector $\mathbf{r}_G$. The position of the satellite in orbit is given by the true anomaly θ.

The orbital frame X_o, Y_o, Z_o has its origin at the centre of mass G and is oriented such that:

- X_o coincides with the local vertical, opposite to the nadir direction;
- Z_o is along the orbit normal;
- Y_o completes the triad.

These two frames are shown in Figure 2.2.

Finally, a body-fixed frame X, Y, Z is defined so that it coincides with the principal axes of the undeformed satellite. The attitude of the spacecraft with respect to the orbital frame is given by three right-hand positive rotations, conventional in spacecraft attitude dynamics, corresponding to the yaw angle α_1, the roll angle α_2 and the pitch angle α_3. The first rotation is yaw around the X_o-axis: the orbital frame is transformed into the intermediate set of axes X_1, Y_1, Z_1. The next rotation is roll around the Y_1-axis, which transforms the set of axes X_1, Y_1, Z_1 into the second intermediate frame X_2, Y_2, Z_2. Finally the body-fixed frame X, Y, Z is obtained by the pitch rotation of X_2, Y_2, Z_2 around the Z_2-axis. This set of rotations results in the 123 Euler transformation.

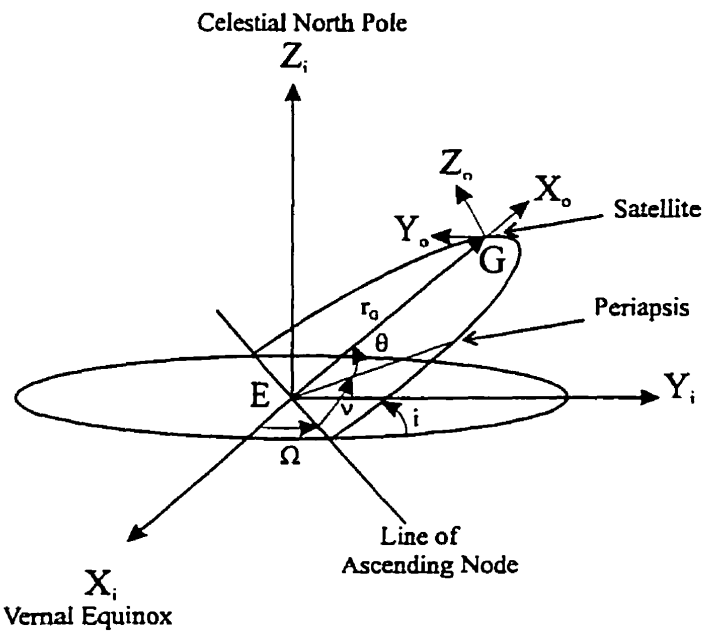

Figure 2.2 Definition of the Frames

2.3 Energy Expressions

2.3.1 Discretization

To derive the equations of motion, the kinetic energy and the potential energy of the satellite must be obtained first by considering separately the central body and the four identical appendages.

The appendages are modelled as Euler-Bernoulli beams, each undergoing bending vibrations in the two transverse directions denoted as in-plane and out of plane vibrations. Each displacement u_i, i= 1 to 8, is a function of both the distance from the base x and time t. For the modelled satellite, eight displacements are defined and are shown in Figure 2.1. Clearly, displacements u_1 to u_4 are in-plane, while displacements u_5 to u_8 are out of plane. These functions can be somewhat arbitrary: they can be polynomials, modes of uniform beams or those from a finite element analysis. However, in all cases they must satisfy at least the geometric boundary conditions.

The discretization of the flexible appendages is carried out using the well-known Ritz method. This method, based on the energy of the system, expresses the elastic displacements of a flexible structure as a sum of space-dependent functions multiplied by time-dependent generalized coordinates.

The discretization the displacements u_i, i=1 to 8 is given by:

$$u_i(x,t) = L\,\Phi^T(\xi)\,\mathbf{q}_i(t), \quad i = 1 \text{ to } 8, \text{ where } \xi = x/L,\ 0 \le \xi \le 1, \qquad (2.1)$$

and $\mathbf{q}_i$ is a vector of elastic generalized coordinates. The vector of admissible functions Φ must satisfy the geometric boundary conditions:

$$\Phi(0) = \Phi'(0) = \mathbf{0}. \qquad (2.2)$$

The length of the vector Φ represents the number of shape functions chosen in the discretization scheme. In this thesis, both polynomials and the eigenfunctions of a cantilever beam under flexion were considered as the admissible functions, but the latter involved less computational effort for the same accuracy. These and their properties are given in Appendix A.

The discretized expressions of the kinetic and potential energy can now be obtained.

2.3.2 Kinetic Energy

The kinetic energy of a beam is given by

$$T_b = \frac{1}{2}\int \mathbf{v}^T \mathbf{v}\, dm \tag{2.3}$$

where **v** represents the absolute velocity of a point on the beam, arising due to the orbital motion, rotational motion of the satellite and elastic oscillations of the beam. For the i^{th} beam, two transverse displacements are considered, namely $u_i(x,t)$ and $u_{i+N}(x,t)$, where N is the number of appendages. The kinetic energy of the beam can be split into two parts:

$$T_b = T_{b.r} + T_{b.e}(u_i, \dot{u}_i, u_{i+N}, \dot{u}_{i+N}) \tag{2.4}$$

where $T_{b.r}$ is the rigid-body kinetic energy of the beam and $T_{b.e}$ is the elastic kinetic energy of the beam. The axial shortening effect, also known as the geometric stiffening effect, is considered in the derivation of $T_{b.e}$.

Then substituing the discretization equation (2.1) into Eq.(2.4) and considering all beams, the kinetic energy of the satellite with four beams can be written in the form:

$$T = T_{orb} + T_e(\dot{\mathbf{q}}) + \frac{1}{2}\boldsymbol{\omega}^T \mathbf{I}(\mathbf{q})\boldsymbol{\omega} + \boldsymbol{\omega}^T \Gamma(\mathbf{q},\dot{\mathbf{q}}), \tag{2.5}$$

where **q** is the vector containing the elastic coordinates of all beams, **I(q)** is the inertia matrix of the satellite about its centre of gravity, $\boldsymbol{\omega}$ is the angular velocity of the spacecraft, and $\Gamma(\mathbf{q},\dot{\mathbf{q}})$ is the vector of angular momentum due to the vibrations of the beams. T_{orb} is the linear kinetic energy of the spacecraft due to the orbital motion:

$$T_{orb} = \frac{1}{2} m_S \dot{\mathbf{r}}_G{}^T \dot{\mathbf{r}}_G \tag{2.6}$$

where $\dot{\mathbf{r}}_G$ is the absolute velocity of the centre of mass of the satellite.

T_e is the kinetic energy associated with the elastic oscillations of the beam:

$$T_e(\dot{\mathbf{q}}) = \frac{\rho L^3}{2}\sum_{i=1}^{8} \dot{\mathbf{q}}_i^T \mathbf{M} \dot{\mathbf{q}}_i \tag{2.7}$$

where **M** is the nondimensional matrix given by:

$$\mathbf{M} = \int_0^1 \mathbf{\Phi}(\xi)\mathbf{\Phi}^T(\xi)d\xi \tag{2.8}$$

The following nondimensional vectors $\mathbf{c}_1$, $\mathbf{c}_2$ and the nondimensional matrices $\mathbf{C}_3$, $\mathbf{C}_4$ appear during the derivation of the kinetic energy in terms of discretized coordinates:

$$\begin{aligned} \mathbf{c}_1 &= \int_0^1 \xi\,\mathbf{\Phi}(\xi)d\xi & \mathbf{c}_2 &= \int_0^1 \mathbf{\Phi}(\xi)\,d\xi \\ \mathbf{C}_3 &= \int_0^1 \eta \int_0^\eta \frac{d\mathbf{\Phi}}{d\xi}\frac{d\mathbf{\Phi}^T}{d\xi}\,d\xi d\eta & \mathbf{C}_4 &= \int_0^1 \int_0^\eta \frac{d\mathbf{\Phi}}{d\xi}\frac{d\mathbf{\Phi}^T}{d\xi}\,d\xi d\eta \end{aligned} \tag{2.9}$$

The values of these integrals are given in Appendix A.

The inertia matrix $\mathbf{I}(\mathbf{q})$ is the sum of two matrices: a constant one corresponding to the satellite with undeformed appendages and an additional one involving the elastic generalized coordinates of the beams. The expressions for $\mathbf{I}(\mathbf{q})$, $\Gamma(\mathbf{q},\dot{\mathbf{q}})$ are given in Appendix B.

2.3.3 Potential Energy

The potential energy of the spacecraft can be written in the form:

$$V = V_{orb} + V_g(\mathbf{q},\alpha) + V_e(\mathbf{q}), \tag{2.10}$$

in which V_{orb} is the orbital potential energy given by:

$$V_{orb} = -m_s \frac{\mu}{r_G} \tag{2.11}$$

$V_g(\mathbf{q}, \alpha)$ is the gravity gradient potential energy of the spacecraft:

$$V_g(\mathbf{q},\alpha) = \frac{3\mu}{2r_G^3}\left[\mathbf{c}^T(\alpha)\mathbf{I}(\mathbf{q})\mathbf{c}(\alpha) - \frac{1}{3}\text{Trace}[\mathbf{I}(\mathbf{q})]\right] \tag{2.12}$$

where α is the vector of attitude angles and $\mathbf{c}$ is the unit vector in the direction of the Earth's radius, expressed in the body-fixed frame.

$V_e(\mathbf{q})$ is the strain energy of the beams involving two different flexural rigidities, denoted as in-plane and out of plane rigidities:

$$V_e(\mathbf{q}) = \frac{EI_{in}}{2L}\sum_{i=1}^{4}\mathbf{q}_i^T\mathbf{K}\mathbf{q}_i + \frac{EI_{out}}{2L}\sum_{i=5}^{8}\mathbf{q}_i^T\mathbf{K}\mathbf{q}_i \tag{2.13}$$

where $\mathbf{K}$ is the nondimensional matrix defined by:

$$\mathbf{K} = \int_0^1 \frac{d^2\Phi}{d\xi^2}\frac{d^2\Phi}{d\xi^2}^T d\xi \tag{2.14}$$

2.4 Orbital Dynamics

Although the kinetic energy T_{orb} and the potential energy V_{orb} associated with the orbital motion have no direct contributions to the attitude motion of the system, the orbital motion has an important effect on the attitude dynamics of the spacecraft through the orbital rate $\dot{\theta}$. The energy associated with the attitude motion is negligible compared to that involved in the orbital motion. As a result, the orbital motion can be calculated separately, and in this thesis will be assumed to be governed by Kepler's laws for a body in a spherical gravitational field.

2.5 Rotational Equations

The angular velocity components ω_x, ω_y, ω_z cannot be integrated to yield angular displacements, but can be regarded as quasi-coordinates. The kinematic relation between the angular velocity and the time derivatives of the attitude angles is given by:

$$\omega = \dot{\theta}\mathbf{R}(\alpha)\mathbf{Z}_o + \mathbf{P}(\alpha)\dot{\alpha} \tag{2.15}$$

where $\mathbf{R}(\alpha)$ is the transformation matrix between the orbital frame and the body-fixed frame, $\mathbf{Z}_o$ is the unit vector along the orbit normal expressed in the orbital frame, while $\mathbf{P}(\alpha)$ is a transformation matrix given in Eq.(2.16) for the 123 attitude angles sequence:

$$\mathbf{P}(\alpha)=\begin{bmatrix}\cos\alpha_3\cos\alpha_2 & \sin\alpha_3 & 0\\ -\sin\alpha_3\cos\alpha_2 & \cos\alpha_3 & 0\\ \sin\alpha_2 & 0 & 1\end{bmatrix} \tag{2.16}$$

The transformation matrix $\mathbf{P}(\alpha)$ for the rates of yaw, roll and pitch angles is singular at some configurations, as all trigonometric representations of the angular velocity are. However, the singularity $\alpha_2=\pm\frac{\pi}{2}$ is never encountered in the simulations in Chapter 5.

The equations of motion describing the attitude of the spacecraft can be derived using the angular-velocity components as quasi-coordinates [Meirovitch'91]:

$$\frac{d}{dt}\left(\frac{\partial T}{\partial \omega}\right)+\omega^{\times}\left(\frac{\partial T}{\partial \omega}\right)+\left(\mathbf{P}^{-1}\right)^{T}\left(\frac{\partial V}{\partial \alpha}\right)=\tau, \tag{2.17}$$

where τ is the external nonconservative torque vector, including the external disturbance torque τ_d and the control torque τ_c, while $\omega^{\times}$ is the cross-product matrix for ω. The third term on the left-hand side in Eq.(2.17) represents the negative of the gravity-gradient torque τ_g, as shown in Appendix C:

$$\tau_g=-\left(\mathbf{P}^{-1}\right)^{T}\left(\frac{\partial V}{\partial \alpha}\right)=-\left(\mathbf{P}^{-1}\right)^{T}\left(\frac{\partial V_g}{\partial \alpha}\right) \tag{2.18}$$

The three rotational equations can be written in the body-fixed frame in the form:

$$\mathbf{I}(\mathbf{q})\dot{\omega}+\dot{\mathbf{I}}(\mathbf{q},\dot{\mathbf{q}})\omega+\dot{\Gamma}(\mathbf{q},\dot{\mathbf{q}},\ddot{\mathbf{q}})+\omega^{\times}[\Gamma(\mathbf{q},\dot{\mathbf{q}})+\mathbf{I}(\mathbf{q})\omega]=\tau_c+\tau_g+\tau_d \tag{2.19}$$

2.6 Vibrational Equations

The equations governing the vibrations of the beams are obtained using Lagrange's equations:

$$\frac{d}{dt}\left(\frac{\partial T}{\partial \dot{\mathbf{q}}}\right)-\left(\frac{\partial T}{\partial \mathbf{q}}\right)+\left(\frac{\partial V}{\partial \mathbf{q}}\right)=\mathbf{f} \tag{2.20}$$

where $\mathbf{q}$ is a vector composed of sub-vectors $\mathbf{q}_i$, i=1 to 8 and hence $\mathbf{f}$ consists of eight sub-vectors. The generalized force $\mathbf{f}_i$, associated with the i^{th} elastic displacement, accounts for the environmental forces $\mathbf{f}_{e,i}$ and the structural damping force $\mathbf{f}_{d,i}$. A modal viscous model is assumed for the damping of each appendage:

$$\mathbf{f}_{d,i} = -2\eta_i \omega_i \mathbf{D}\dot{\mathbf{q}}_i \text{ , where i=1 to 8} \tag{2.21}$$

where η_i is the damping coefficient associated with the elastic coordinate vector $\mathbf{q}_i$, ω_i is a beam parameter (a scalar equal to ω_{in} for in-plane vibration or to ω_{out} for out of plane vibration), and $\mathbf{D}$ is the nondimensional damping matrix given in Appendix B.

The equation for the generalized coordinate vector $\mathbf{q}_1$ is given below as an example:

$$\begin{aligned}\mathbf{M}\ddot{\mathbf{q}}_1 + 2\eta_1\omega_{in}\mathbf{D}\dot{\mathbf{q}}_1 + [\omega_{in}^2\mathbf{K} - (\omega_x^2+\omega_z^2)\mathbf{M} + (\omega_y^2+\omega_z^2)(\frac{a}{L}\mathbf{C}_4 + \mathbf{C}_3) - \frac{h}{L}(\dot{\omega}_y + \omega_x\omega_z)\mathbf{C}_4]\mathbf{q}_1 + \\ 2\omega_x\mathbf{M}\dot{\mathbf{q}}_5 + (\dot{\omega}_x - \omega_y\omega_z)\mathbf{M}\mathbf{q}_5 = \frac{1}{\rho L^3}(\mathbf{f}_{e1} - \frac{\partial V_g}{\partial \mathbf{q}_1}) + \frac{h}{L}(\dot{\omega}_x - \omega_y\omega_z)\mathbf{c}_2 - (\dot{\omega}_z + \omega_x\omega_y)(\frac{a}{L}\mathbf{c}_2 + \mathbf{c}_1)\end{aligned} \tag{2.22}$$

Equations similar to Eq.(2.22) can be obtained for the other generalized coordinate vectors, which are presented in Appendix B.

Chapter 3

ENVIRONMENTAL DISTURBANCES

The effectiveness of the control laws developed in this thesis is tested in the presence of environmental disturbances. The models for the environmental forces are based on [Hughes'86]. The corresponding generalized forces are derived below.

3.1 Solar Pressure Disturbance

The momentum flux of photons emitted by the Sun and arrested by a material surface results in the radiation pressure. The assumptions about the Sun are as follows:

(i) the parallax of the Sun is negligible;

(ii) the reflected solar radiation of the Earth and its own emittance are ignored;

(iii) the solar radiation pressure is constant along the orbit.

In the Earth centered inertial frame, the unit vector pointing to the Sun is given by:

$$\hat{\mathbf{s}}_{\text{to Sun}} = \cos\delta_S \cos\alpha_S \mathbf{X}_i + \cos\delta_S \sin\alpha_S \mathbf{Y}_i + \sin\delta_S \mathbf{Z}_i \tag{3.1}$$

where α_S is the right ascension of the Sun with respect to the vernal equinox, δ_S is the declination of the Sun and $\mathbf{X}_i$, $\mathbf{Y}_i$, $\mathbf{Z}_i$ are the unit vectors for the inertial frame.

3.1.1 Solar Radiation Pressure Force and Torque

The radiation surface properties of the material are defined by three coefficients, which must add up to one if the surface is not transparent: the absorption coefficient σ_a, the diffused reflection coefficient σ_{rd}, and the specular reflection coefficient σ_{rs}.

The unit vector incoming to an element of surface with inward normal unit vector $\hat{\mathbf{n}}_A$ is defined as: $\hat{\mathbf{s}} = -\hat{\mathbf{s}}_{\text{to Sun}}$

Following the derivation in [Hughes'86], the solar radiation force is given by:

$$\mathbf{f} = p_S\left[2\sigma_{rs}\mathbf{a}_{pp} + \frac{2}{3}\sigma_{rd}\mathbf{a}_p + (\sigma_a + \sigma_{rd})A_p\hat{\mathbf{s}}\right] \tag{3.2}$$

where p_S is the solar radiation pressure and the geometrical integrals are given by:

$$\begin{aligned}\mathbf{a}_{pp} &= \oiint H(\cos\alpha)\cos^2\alpha d\mathbf{A}\\ \mathbf{a}_p &= \oiint H(\cos\alpha)\cos\alpha d\mathbf{A}\\ A_p &= \oiint H(\cos\alpha)\cos\alpha dA\end{aligned} \tag{3.3}$$

where the surface vector $d\mathbf{A}$ is defined by $dA\,\hat{\mathbf{n}}_A$; the angle of attack α is defined by: $\cos\alpha = \hat{\mathbf{s}}^T\hat{\mathbf{n}}_A$; the projected area is A_p; the Heaviside function H is defined as: $H(x) = 1$ if $x \geq 0$; $H(x) = 0$ otherwise.

Similarly, the torque expression about the centre of mass of the spacecraft is:

$$\tau = p_S\left[2\sigma_{rs}\mathbf{b}_{pp} + \frac{2}{3}\sigma_{rd}\mathbf{b}_p + (\sigma_a + \sigma_{rd})A_p\mathbf{c}_p^{\times}\hat{\mathbf{s}}\right] \tag{3.4}$$

where the new geometrical integrals are given by:

$$\begin{aligned}\mathbf{b}_{pp} &= \oiint H(\cos\alpha)\cos^2\alpha\,\mathbf{r}^{\times}d\mathbf{A}\\ \mathbf{b}_p &= \oiint H(\cos\alpha)\cos\alpha\,\mathbf{r}^{\times}d\mathbf{A}\\ A_p\mathbf{c}_p^{\times} &= \oiint H(\cos\alpha)\cos\alpha\,\mathbf{r}^{\times}dA\end{aligned} \tag{3.5}$$

where the position vector of the surface element dA with respect the centre of mass of the spacecraft is denoted by $\mathbf{r}$, and the position vector of the centre of pressure of the surface is defined by $\mathbf{c}_p$.

As a result of Eqs.(3.2) and (3.4), the solar pressure force and torque depend only on the shape of the surface. For some simple geometries, the surface integrals can be obtained analytically and are given in the following sections.

3.1.2 Flat Surface

Let G be the centre of mass of the spacecraft and C the geometrical centre of a flat surface of area A.

The total force is given by:

$$\mathbf{f} = p_S A \hat{\mathbf{s}}^T \hat{\mathbf{n}}_A \left[(\sigma_a + \sigma_{rd}) \hat{\mathbf{s}} + \left(\frac{2}{3} \sigma_{rd} + 2\sigma_{rs} \hat{\mathbf{s}}^T \hat{\mathbf{n}}_A \right) \hat{\mathbf{n}}_A \right] \tag{3.6}$$

It can be shown that the torque due to solar pressure is simply:

$$\tau = \mathbf{c}_p^{\times} \mathbf{f} \tag{3.7}$$

where $\mathbf{c}_p$ is the vector locating C with respect to G.

3.1.3 Right Circular Cylinder

Consider a right circular cylinder of length L and radius r along the unit vector $\hat{\mathbf{t}}$. The projected area is given by A_p=2rL. The axis of symmetry makes an angle β with the radiation direction. Let $\mathbf{r}_{cm}$ be the position vector of the centre of mass of the cylinder with respect to the centre of mass of the spacecraft. The end effects are not included in the following derivation. One then obtains:

$$\mathbf{f} = p_S A_p \left[(\sigma_a + \sigma_{rd}) \sin\beta \hat{\mathbf{s}} + \left(\frac{\pi}{6} \sigma_{rd} + \frac{4}{3} \sigma_{rs} \sin\beta \right) \hat{\mathbf{t}}^{\times} \hat{\mathbf{s}}^{\times} \hat{\mathbf{t}} \right] \tag{3.8}$$

The expression for the torque about the centre of mass is given by:

$$\tau = \mathbf{r}_{cm}^{\times} \mathbf{f} - p_S A_p r \frac{\pi}{4} (\sigma_a + \sigma_{rd}) \hat{\mathbf{s}}^T \hat{\mathbf{t}} \left(\hat{\mathbf{s}}^{\times} \hat{\mathbf{t}} \right) \tag{3.9}$$

3.1.4 Generalized Force for a Flexible Beam

The generalized force due to solar radiation pressure is derived in this section for two types of geometry of the beam. For a short beam modelling a small satellite appendage, the transverse motion is expected to be very small so that the change of the surface normal along the length can be ignored. Therefore, the formulations derived for basic rigid shapes in the previous paragraph can be used.

Rectangular cross section

The generalized force on each appendage due to solar radiation pressure is investigated now. An infinitesimal element of a rectangular cross-section beam in its undeformed position is shown in Figure 3.1. The undeformed axis of the beam is directed by the vector $\hat{\mathbf{t}}$.

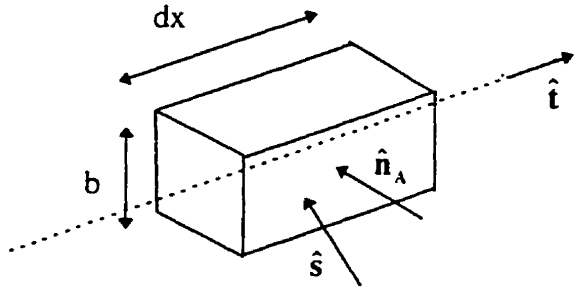

Figure 3.1 Rectangular Cross-section Beam

It is assumed that the two transverse bending directions of the beam correspond to the directions normal to the lateral surfaces. The generalized force corresponding to the generalized coordinate of positive displacement in the direction of $\hat{\mathbf{n}}_A$ is considered now. From Eq.(3.6), the force on the lateral surface of the element is given by:

$$df = p_S b dx \left\{ \left| \hat{\mathbf{s}}^T \hat{\mathbf{n}}_A \right| \left[(\sigma_a + \sigma_{rd}) \hat{\mathbf{s}} + 2\sigma_{rs} (\hat{\mathbf{s}}^T \hat{\mathbf{n}}_A) \hat{\mathbf{n}}_A \right] + \frac{2}{3} \sigma_{rd} (\hat{\mathbf{s}}^T \hat{\mathbf{n}}_A) \hat{\mathbf{n}}_A \right\} \quad (3.10)$$

The load per unit length due to the solar radiation pressure is then given by:

$$p_b(x,t) = \hat{\mathbf{n}}_A^T \frac{df}{dx} = p_S b \hat{\mathbf{s}}^T \hat{\mathbf{n}}_A \left[\left| \hat{\mathbf{s}}^T \hat{\mathbf{n}}_A \right| (\sigma_a + \sigma_{rd} + 2\sigma_{rs}) + \frac{2}{3} \sigma_{rd} \right] \quad (3.11)$$

Note that the above load distribution does not depend on the position along the beam.

The solar-pressure-induced generalized force for a rectangular cross-section beam is then:

$$\mathbf{Q}_S = \int_0^L L \Phi(x) p_b(x,t) dx = p_b L^2 \mathbf{c}_2 \quad (3.12)$$

where $\mathbf{c}_2$ is the nondimensional vector defined in Eq.(2.9).

Circular cross section

A small element of a circular cross-section beam is shown in Figure 3.2. The Sun unit vector makes an angle β with the undeformed axis directed by unit vector $\hat{\mathbf{t}}$.

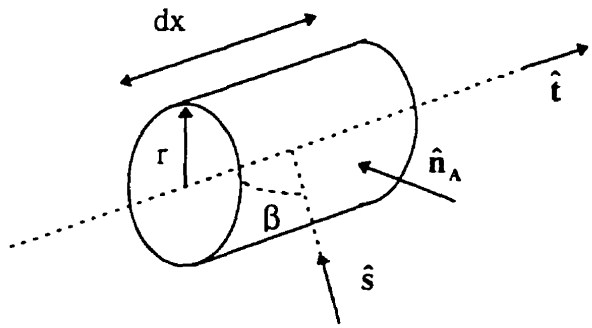

Figure 3.2 Circular Cross-section Beam

From Eq.(3.8), the solar pressure force on the infinitesimal cylinder is given by:

$$d\mathbf{f} = 2p_S r dx\left[(\sigma_a + \sigma_{rd})\sin\beta\hat{\mathbf{s}} + \left(\frac{\pi}{6}\sigma_{rd} + \frac{4}{3}\sigma_{rs}\sin\beta\right)\hat{\mathbf{t}}\times\hat{\mathbf{s}}\times\hat{\mathbf{t}}\right] \tag{3.13}$$

The load per unit length due to the solar radiation pressure is thus given by:

$$p_b(x,t) = \hat{\mathbf{n}}_A^T\frac{d\mathbf{f}}{dx} = 2p_S r\,\hat{\mathbf{s}}^T\hat{\mathbf{n}}_A\left[\sin\beta\left(\sigma_a + \sigma_{rd} + \frac{4}{3}\sigma_{rs}\right) + \frac{\pi}{6}\sigma_{rd}\right] \tag{3.14}$$

As in Eq.(3.11), the load distribution does not depend on the position along the beam. The solar-pressure-induced generalized force for a circular cross-section beam can then be obtained from Eq.(3.12) by substituting Eq.(3.14) for the transverse load.

3.2 Aerodynamic Disturbance

3.2.1 Aerodynamic Force and Torque

In this section, the aerodynamic forces on rigid surfaces are calculated, based on the derivations in [Hughes'86]. The assumptions about the aerodynamic model follow:

(i) the mean random speed of the atmosphere is much smaller than the speed of the spacecraft through the atmosphere (hyperthermal flow assumption);

(ii) the density of the atmosphere ρ_a is so low that molecules incoming to a surface and molecules outgoing from the surface can be dealt with separately (free-molecular flow assumption);

(iii) only the drag force expression is derived, with the aerodynamic drag coefficient equal to 2;

(iv) shielding effect due to the concavity of the surface is not taken into account.

Define $\mathbf{v}_a$ as the velocity of the local atmosphere relative to a surface element dA having an inward normal $\hat{\mathbf{n}}_A$. Denoting the accommodation coefficients for normal and tangential momentum exchange as σ_n and σ_t respectively, the force imparted to a surface element dA is given as [Hughes'86]:

$$\mathbf{df} = H(\cos\alpha)\rho_a v_a^2 \cos\alpha \left\{ \left[(2-\sigma_n-\sigma_t)\cos\alpha + \sigma_n \left(\frac{v_b}{v_a} \right) \right] \hat{\mathbf{n}}_A + \sigma_t \hat{\mathbf{v}}_a \right\} dA \qquad (3.15)$$

where the unit velocity vector is $\hat{\mathbf{v}}_a = \mathbf{v}_a / v_a$; the angle of attack α is defined by: $\cos\alpha = \hat{\mathbf{v}}_a^T \hat{\mathbf{n}}_A$; the speed v_b is related to the surface temperature T_S by: $v_b = \sqrt{\pi R T_S / 2m_g}$, where R is the universal gas constant (R=8313 J/(°K mol kg)) and m_g is the molecular weight of the gas.

The velocity of the local atmosphere with respect to a point on the spacecraft surface depends on the orbital velocity of the spacecraft $\mathbf{v}_{orb}$, the velocity of the atmosphere due its rotation about the axis of the Earth and the velocity of the point relative to the centre of mass of the spacecraft due to the attitude motion of the satellite. The last one is small compared to the other two so that it can be neglected in the formulation.

In the orbital frame, the angular velocity of the Earth is given by:

$$\boldsymbol{\omega}_e = \omega_e \left[\sin(\upsilon+\theta)\sin i \, \mathbf{X}_o + \cos(\upsilon+\theta)\sin i \, \mathbf{Y}_o + \cos i \, \mathbf{Z}_o \right] \qquad (3.16)$$

where υ is the argument of the perigee, θ is the true anomaly and i is the inclination of the orbit to the equatorial plane.

The velocity of the atmosphere with respect to the centre of mass of the satellite is given by:

$$\mathbf{v}_a = \boldsymbol{\omega}_e^{\times}\mathbf{r}_G - \mathbf{v}_{orb} = -\dot{r}_G\mathbf{X}_o + r_G\left(\omega_e \cos i - \dot{\theta}\right)\mathbf{Y}_o - r_G\omega_e \sin i \cos(\nu+\theta)\mathbf{Z}_o \qquad (3.17)$$

The aerodynamic torque about the centre of mass of the satellite arising due to the force imparted to dA is:

$$d\boldsymbol{\tau} = \mathbf{r}^{\times}d\mathbf{f} \qquad (3.18)$$

where $\mathbf{r}$ is the position vector of the surface element dA with respect the centre of mass of the spacecraft.

The force expression can be obtained by integrating Eq.(3.15) over the surface to yield:

$$\mathbf{f} = \rho_a v_a^2\left[\left(2-\sigma_n-\sigma_t\right)\mathbf{a}_{pp} + \sigma_n\frac{v_b}{v_a}\mathbf{a}_p + \sigma_t A_p\hat{\mathbf{v}}_a\right] \qquad (3.19)$$

where A_p, $\mathbf{a}_p$ and $\mathbf{a}_{pp}$ are integrals defined in Eq.(3.3). Mean values of the accommodation factors and of the surface temperature have been considered so that these quantities could be taken out of the integrals.

The torque expression can be obtained by integrating Eq.(3.18) over the surface :

$$\boldsymbol{\tau} = \rho_a v_a^2\left[\left(2-\sigma_n-\sigma_t\right)\mathbf{b}_{pp} + \sigma_n\frac{v_b}{v_a}\mathbf{b}_p + \sigma_t A_p\mathbf{c}_p^{\times}\hat{\mathbf{v}}_a\right] \qquad (3.20)$$

where $\mathbf{b}_p$, $\mathbf{b}_{pp}$, $\mathbf{c}_p^{\times}$ are integrals defined in Eq.(3.5).

3.2.2 Correspondence with Solar Radiation Pressure Expressions

It may be mentioned that the accommodation coefficients usually have average values in the range of $0.8<\sigma_n, \sigma_t<0.9$. The limiting cases, specular and diffuse reflections, are obtained by setting $\sigma_n=\sigma_t=0$ and $\sigma_n=\sigma_t=1$, respectively. Furthermore, the Earth gravity tends to keep the heaviest molecules close to the Earth, so that the composition of the atmosphere changes as a function of the altitude. From [Tribble'95], the main constituent of the neutral atmosphere, where LEO applications take place, are given in Table 3.1.

Altitude (km)	Dominant Constituent	Molecular Mass
0-175	Azote (N_2)	28
175-650	Atomic Oxygen (O)	16
650-1000	Helium (He)	2

Table 3.1 Dominant Air Constituents in Neutral Atmosphere

The expressions obtained for the aerodynamic force and the torque in Eqs.(3.19) and (3.20) have remarkably the same form as those found in Eqs.(3.2) and (3.4) for the force and torque, respectively, due to the solar radiation pressure. Hence it is really advantageous to use the correspondence of terms given in Table 3.2 to obtain the equivalent expressions developed in Section 3.1.

Solar pressure force	Aerodynamic force
$\hat{\mathbf{s}}$	$\hat{\mathbf{v}}_a$
p_S	$\rho_a v_a^2$
σ_{rs}	$\frac{1}{2}(2-\sigma_n-\sigma_t)$
σ_{rd}	$\frac{3}{2}\sigma_n\frac{v_b}{v_a}$
$\sigma_a+\sigma_{rd}$	σ_t

Table 3.2 Correspondence Between Solar Radiation Pressure and Aerodynamic Force Expressions

3.3 Geomagnetic Disturbance

3.3.1 Geomagnetic Field

The geomagnetic field can be represented as a tilted dipole. A detailed derivation of the dipole components is provided in Appendix D, while a summary is presented in this section.

In the inertial geocentric frame, the dipole vector is oriented by the following unit vector:

$$\hat{\mathbf{m}}_e = \left[\cos\omega_m \sin\theta_m \mathbf{X}_i + \sin\omega_m \sin\theta_m \mathbf{Y}_i + \cos\theta_m \mathbf{Z}_i\right] \tag{3.21}$$

where θ_m is the coelevation of the dipole, while ω_m is the right ascension of the dipole defined as:

$$\omega_m = \theta_{g0} + \omega_e t + \phi_m \tag{3.22}$$

where θ_{g0} is the right ascension of the Greenwich meridian at some reference, ω_e is the spin rate of the Earth, t is the time elapsed after the reference epoch, and ϕ_m is the East longitude of the dipole.

The right ascension of the Greenwich meridian can be obtained either from tables or from approximate equations based on the Julian Day, as found in [Kaplan'76] for instance.

The magnetic field at the satellite position due to the dipole is given by:

$$\mathbf{b} = \frac{M_e}{r_G^3}(3\hat{\mathbf{r}}^T\hat{\mathbf{r}} - \mathbf{I}_3)\hat{\mathbf{m}}_e \tag{3.23}$$

where $\hat{\mathbf{r}}$ is the radial unit vector, $\hat{\mathbf{m}}_e$ is the dipole unit vector, $\mathbf{I}_3$ is the identity matrix, r_G is the radial distance of the satellite centre of mass from the centre of the Earth, and M_e is the dipole strength.

Based on Eq.(3.23), the magnetic field vector can be expressed in any frame of interest by appropriate transformation of the Earth dipole vector given in Eq.(3.21) in the geocentric inertial frame.

The main properties of the geomagnetic field dipole appear clearly when the tilt angle of the dipole is neglected, i.e. the dipole axis coincides with the inertial $\mathbf{Z}_i$ axis. In this case, a simple expression for the Earth magnetic dipole can be obtained in the orbital frame:

$$\mathbf{b} = \frac{M_e}{r_G^3}\left[-2\sin i \sin(\theta + \nu)\mathbf{X}_o + \sin i \cos(\theta + \nu)\mathbf{Y}_o + \cos i \mathbf{Z}_o\right] \tag{3.24}$$

where i is the inclination of the orbit plane, ν is the argument of the perigee, and θ is the true anomaly of the spacecraft.

3.3.2 Magnetic Torque

The magnetic torque on a spacecraft results from the interaction of the dipole moment $\mathbf{m}$ of the spacecraft and the geomagnetic field:

$$\tau_{mag} = \mathbf{m}^{\times}\mathbf{b} \tag{3.25}$$

Magneto-torquing can be generated by an electromagnet fed by a controlled current, which is a well-known actuator for the attitude control of the spacecraft:

$$\mathbf{m} = n_c i_c A_c \hat{\mathbf{n}}_c \tag{3.26}$$

where n_c is the number of turns in the coil, i_c is the current in the coil, A_c is the coil cross sectional area, and $\hat{\mathbf{n}}_c$ is the unit vector normal to the coil area.

Even if an electromagnet is not used, a residual dipole moment always exists in the spacecraft due to the electronics on board, resulting in a disturbance torque.

Chapter 4

FUZZY LOGIC ATTITUDE CONTROL

4.1 Introduction to Fuzzy Logic Control

Fuzzy logic control is based on approximate reasoning, much closer to human thinking than traditional systems. Approximate reasoning is the process by which a possible imprecise conclusion can be deduced from a collection of imprecise premises. As a result, this modern control scheme shows a great flexibility for its design and can be implemented in different ways. A basic configuration of a fuzzy logic controller (FLC) is shown in Figure 4.1.

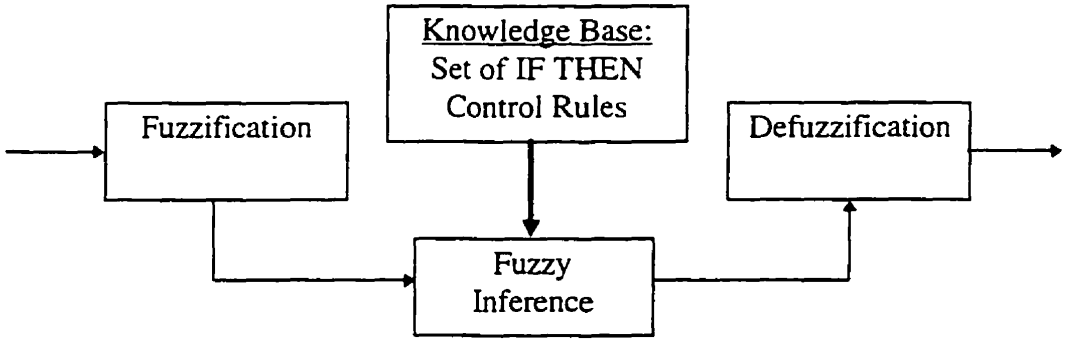

Figure 4.1 Basic Configuration of a Fuzzy Logic Controller

From Figure 4.1, the four components of a FLC can be identified as follows:

(i) Fuzzification interface: scale mapping of the input variables into associated linguistic values. An input variable can be associated with several fuzzy terms: typical variables for FLC are the state vector, the rate of the state vector and associated fuzzy terms describing these variables can be "Almost Zero", "Rather Big", for instance. The

membership function of each fuzzy term is used to grade the membership value of each variable between 0 and 1.

(ii) Knowledge base: set of implication rules characterizing the control goals. These control rules are given by an IF THEN relation formulated in vague terms.

(iii) Fuzzy inference: the control rules described in fuzzy terms are interpreted numerically following strict mathematical logic. Fuzzy output of each rule is then derived.

(iv) Defuzzification: scale mapping of the fuzzy output variables into an output variable by taking into account all rules.

As pointed out in [Ying et al.'90], a fuzzy logic controller results in a highly nonlinear control scheme, where nonlinearity appears in each of the four components described earlier.

In the following two sections, two attitude fuzzy logic controllers are derived for two different scenarios:

(i) three-axis stabilization using thrusters;

(ii) spin-stabilization using magneto-torquing.

For each case, actuators are active for a given duration. The controller has to evaluate the time and sign of the switch of each actuator. It is assumed that the measurements (or the estimations) of each attitude angle and each angular rate are available.

4.2 Fuzzy Logic Controller Using Thrusters

Six pairs of thrusters producing constant torques τ_X, τ_Y, τ_Z around the body-fixed axes X, Y, Z of the spacecraft are controlled by a Multi-Input and Single-Output (MISO) fuzzy logic. As a result of control with an actuator of constant magnitude, the response can only be obtained with a certain acceptable error around the desired setpoint.

As the fuzzy controller has the same structure for each rotation, the following analysis is given in term of e, which holds for any of the three errors in the attitude angles

of the spacecraft. The inputs of the Fuzzy Logic Controller associated with the error angle to be controlled by the torque components τ_X, τ_Y, τ_Z are given in Eq.(4.1):

$$x_1 = e \quad x_2 = \dot{e} \quad x_3 = e + k\dot{e} \,, \tag{4.1}$$

where x_1 is the angle error, x_2 the rate of the angle error and x_3 is defined as the linear switching function. In Eq.(4.1), k is a constant and has the dimension of time.

The control scheme for the attitude stabilization is represented in Figure 4.2.

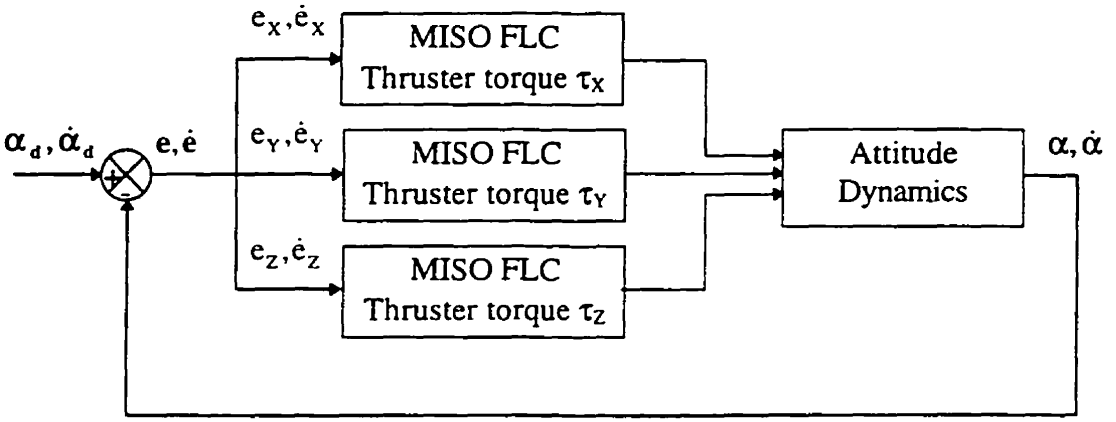

Figure 4.2 Block Diagram for the Three-Axis Stabilization Fuzzy Control

Three fuzzy sets, *Zero Positive* (ZP), *Zero Negative* (ZN) and *Non-Zero* (NZ) describe the inputs x_1 and x_2, while two fuzzy sets, *Positive* (P) and *Negative* (N) describe the variable x_3. The membership functions are represented in Figure 4.3.

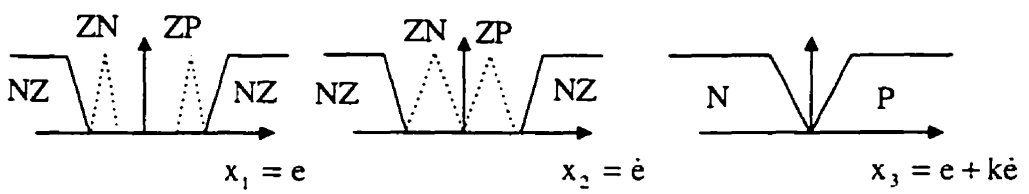

Figure 4.3 Membership Functions of the Input Variables of the FLC with Thrusters

In Figure 4.3, the scaling of the *Non-Zero* membership functions associated with x_1 and x_2 appears as a deadband for x_1 and x_2. The objectives of the controller are defined in the following two statements:

(i) reduce the error and the rate of the error inside prescribed deadbands where no control is applied;

(ii) maintain the error inside the deadband by periodic control.

Accordingly, a set of four rules is constructed. The output of each rule is only the sign of the torque. The rules are presented in Table 4.1: the fuzzy sets written in italics are linked by the conjunction OR.

Rules	x_1	x_2	x_3	**Output u**
R_1	*NZ*	*NZ*	P	-1
R_2	*NZ*	*NZ*	N	+1
R_3	ZN	ZN		+1
R_4	ZP	ZP		-1

Table 4.1 Control Rules for One Rotation

The first two rules govern the switching of the thruster when the angular error or its rate is not within certain range (i.e. deadbands on x_1 and x_2). As mentioned in [Bryson'94], the control can be implemented effectively by applying a torque of opposite sign to the linear switching function.

The last two rules are utilized to maintain the angle inside the deadband by one firing only.

The rule R_1 is interpreted as follows:

IF (x_1 is Non-Zero **OR** x_2 is Non-Zero) **AND** (x_3 is Positive) **THEN** u is Negative.

The algebraic sum is used for the conjunction **OR**, while the algebraic product is used for operation **AND**.

The condition of the first rule is then:

$$\mu_1 = (m_{NZ}(x_1) + m_{NZ}(x_2)) * m_P(x_3), \tag{4.2}$$

where m_{NZ} and m_P represent the membership functions defined in Figure 4.3.

The product operation rule of fuzzy implication is used to get the fuzzy output of each rule:

$$y_1 = \mu_1 * u \ . \tag{4.3}$$

All the rules are inferred in the same manner. Then, the defuzzication gives the output of the controller as:

$$\tau = \mathrm{sgn}(\sum_{i=1}^{4} y_i)|\tau|, \quad \text{where} \begin{cases} \mathrm{sgn}(x) = +1, & \text{if } x > 0, \\ \mathrm{sgn}(x) = -1, & \text{if } x < 0, \\ \mathrm{sgn}(x) = 0, & \text{if } x = 0. \end{cases} \tag{4.4}$$

and $|\tau|$ is the magnitude of the constant thrust produced by the thrusters.

At each instant, the rules of each MISO controller are evaluated, which gives the torque to be applied, if needed. Because of the weak coupling of the equations, when all angles defining the attitude are small, the thrusters are fired at the same time.

The concept of the simple MISO control scheme derived in this section will be partly used for the more complicated problem of spin-axis stabilization using magneto-torquing, as described now.

4.3 Fuzzy Logic Controller Using Magneto-Torquers

4.3.1 Introduction

The spin stabilization of a small satellite can be achieved by using magneto-torquing. Three coils around the body-fixed axes (X, Y, Z) of the spacecraft are fed by a constant current to produce a dipole **m**, which interacts with the geomagnetic field **b** to generate a torque $\boldsymbol{\tau}_{\mathbf{mag}}$ given by Eq.(3.25).

As described in Chapter 2, the attitude of the spacecraft is described by a set of rotations from the orbital frame defining the yaw angle α_1, roll angle α_2 and the

pitch angle α_3 in the 123 Euler transformation. In this section, advantage is taken of the satellite configuration and of the choice of the Euler sequence. Indeed, the spacecraft is spinning about the Z-axis, its axis of symmetry in the undeformed position. For such a case, it is convenient to use the second frame (i.e. after the first two rotations) as the nonspinning reference frame denoted by the set of axes X_{ref}, Y_{ref}, Z_{ref}. This convenience appears clearly through linearized torque-free attitude equations of an axisymmetric rigid spacecraft in an elliptic orbit of orbital rate $\dot{\theta}$, spinning about its axis of symmetry at the constant spinning rate ω_s with respect to the orbital frame:

$$\begin{cases} I_T\ddot{\alpha}_1 + \left[I_Z(\dot{\theta}+\omega_S) - 2I_T\dot{\theta}\right]\dot{\alpha}_2 + \left[I_Z\dot{\theta}(\dot{\theta}+\omega_S) - I_T\dot{\theta}^2\right]\alpha_1 - I_T\ddot{\theta}\alpha_2 = \tau_{Xref}, \\ I_T\ddot{\alpha}_2 - \left[I_Z(\dot{\theta}+\omega_S) - 2I_T\dot{\theta}\right]\dot{\alpha}_1 + \left[I_Z\dot{\theta}(\dot{\theta}+\omega_S) - I_T\dot{\theta}^2\right]\alpha_2 + I_T\ddot{\theta}\alpha_1 = \tau_{Yref}, \\ I_z\left(\ddot{\alpha}_3 + \ddot{\theta}\right) = \tau_{Zref}. \end{cases} \quad (4.5)$$

The magnetic torques τ_{Xref}., τ_{Yref} and τ_{Zref} appear as the yaw, roll and pitch torques respectively and are given in this reference frame by:

$$\begin{cases} \tau_{Xref} = m_{Yref}\, b_{Zref} - m_{Zref}\, b_{Yref}, \\ \tau_{Yref} = m_{Zref}\, b_{Xref} - m_{Xref}\, b_{Zref}, \\ \tau_{Zref} = m_{Xref}\, b_{Yref} - m_{Yref}\, b_{Xref}, \end{cases} \quad (4.6)$$

where m_{Xref}, m_{Yref}, m_{Zref} are the components of the magneto-torquer dipole moment along the reference axes and are given by:

$$\begin{cases} m_{Xref} = \cos\alpha_3\, m_X - \sin\alpha_3\, m_Y, \\ m_{Yref} = \sin\alpha_3\, m_X + \cos\alpha_3\, m_Y, \\ m_{Zref} = m_Z \end{cases} \quad (4.7)$$

The variables b_{Xref}, b_{Yref} and b_{Zref} are calculated similarly from the components of the magnetic field in the body-fixed frame, which can be obtained by an onboard magnetometer. From Eq.(4.6), the torque components provided by each coil can be obtained and are presented in Table 4.2.

	Coil m_X	Coil m_Y	Coil m_Z
τ_{Xref}	$m_X b_{Zref} \sin\alpha_3$	$m_Y b_{Zref} \cos\alpha_3$	$-m_Z b_{Yref}$
τ_{Yref}	$-m_X b_{Zref} \cos\alpha_3$	$m_Y b_{Zref} \sin\alpha_3$	$m_Z b_{Xref}$
τ_{Zref}	$m_X(b_{Yref} \cos\alpha_3 - b_{Xref} \sin\alpha_3)$	$-m_Y(b_{Yref} \sin\alpha_3 + b_{Xref} \cos\alpha_3)$	0

Table 4.2 Magnetic Torque Components for Each Coil

The magnetic field vector **b** is space-dependent. The untilted model described in Eq.(3.24) shows its dependence on the orbital position and orbit inclination. As pointed out in [Cvetkovic et al.'93], most LEO small satellites will be injected into Sun-synchronous orbits, as it guarantees an invariant illumination along the year and a simpler design of the solar arrays orientation. For such satellites, the inclination of the orbital plane is typically between 96 and 100 degrees for altitudes between 300 km and 1200 km, which makes the component of the geomagnetic field along the orbit normal small compared to the other two.

4.3.2 Control Limitations for a Polar LEO

Over the equatorial region, the b_{Yorb} component and thus the b_{Yref} are dominant. The X/Y magneto-torquers can be used to control the rate of pitch, while the Z magneto-torquer can be switched to control the yaw angle. Similarly over the polar region, the b_{Xorb} component is dominant. Then the magneto-torquers X/Y can control the pitch while the Z magneto-torquer can control the roll angle.

For a polar orbit, the b_{Zorb} component is always small. If m_X and m_Y are coils of large magnitude, they can be used to control yaw and roll. However, when switching those two coils, the resulting torque about the pitch axis is important and may disturb the spin motion.

As a result, the utilization of the geomagnetic field imposes two control limitations, namely: the availability of the magnetic torque along the orbit and the cross-coupling between the torques about the various rotation axes.

4.3.3 Fuzzy Logic Controller with Magneto-Torquers

The controller consists of three MISO fuzzy controllers, each associated with a coil. At each sampling time, each MISO controller analyses the torques produced by the switching of the coil and returns a weighted value of the control. Then the coil to be switched during the next interval will be the one with the output having the largest weight, while the other two are turned off.

The objectives of the controller are defined in the two following statements:

(i) reduce the roll and yaw errors into prescribed deadbands; i.e. reorient the spin-axis close to its nominal position along the orbit normal;

(ii) maintain the spin rate about the pitch axis within a band of tolerance.

The control scheme for the spin-stabilization is shown in Figure 4.4.

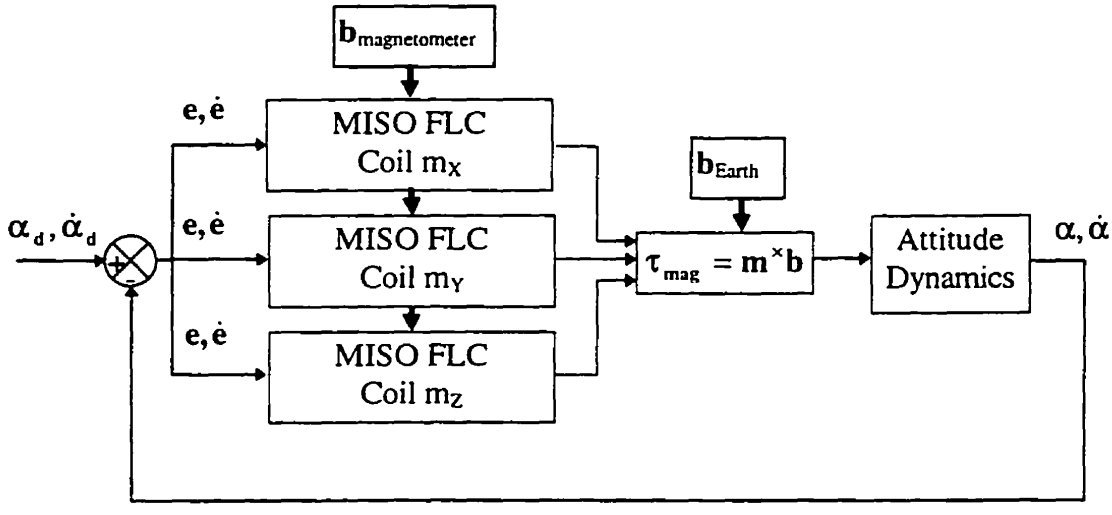

Figure 4.4 Block Diagram for Spin Stabilization Fuzzy Control

The first objective is similar to the thruster case of Section 4.1. Hence, the same approach is used, except that the torque to control the rotation is no longer constant and induces disturbances on the other rotations.

The following inputs to the control logic are defined:

$$x_1 = e_X \quad x_2 = \dot{e}_X \quad x_3 = e_X + k_X \dot{e}_X \quad x_4 = \tau_{Xref}$$
$$x_5 = e_Y \quad x_6 = \dot{e}_Y \quad x_7 = e_Y + k_Y \dot{e}_Y \quad x_8 = \tau_{Yref} \tag{4.8}$$

where x_1 is the error in yaw angle, x_2 is the error in the rate of yaw, x_3 is the linear switch function for yaw error, while x_4 is the torque to control the yaw motion. Similar definitions apply for the inputs related to the roll motion in Eq.(4.8).

For the control of the spin rate, the following inputs are needed:

$$x_9 = \dot{e}_Z \quad x_{10} = \tau_{Zref} \tag{4.9}$$

where x_9 is the error in the spin rate and x_{10} is the torque available along the Z-axis.

The input variables are mapped into fuzzy sets. Two fuzzy sets *Positive* and *Negative* are defined to control the attitude, while two other fuzzy sets are defined to limit the control action: a special fuzzy set *Zero* is associated with the torque τ_{Zref} to limit the effect on the pitch angle when the magneto-torquers m_X or m_Y are active while the fuzzy set *Non-Zero* is used to define the deadband on the errors and the rates of the errors in yaw and roll angles. The membership functions for the input variables associated with yaw and pitch are given in Figure 4.5. Those for the control of roll are the same as for the control of yaw and are not shown.

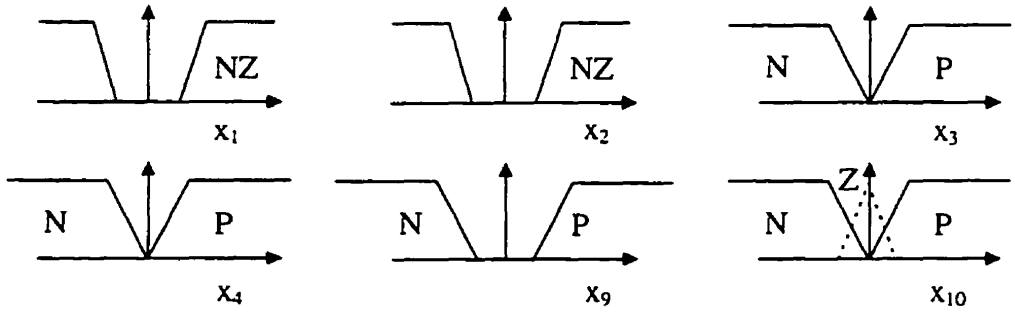

Figure 4.5 Membership Functions for the FLC with Magneto-torquers

The same set of twelve rules is used to decide on the switching of the coils m_X as well as m_Y and is presented in Table 4.3. The output of each rule represents the polarity of

the coil. According to Table 4.3, the rules R_1 to R_4, R_5 to R_8, R_9 to R_{12} are used to control the yaw angle, roll angle and the pitch rate, respectively. The rules are used as long as the requirements on the yaw and roll angles and their rates are not fulfilled.

For the control of the yaw and roll motions, the variable x_{10} associated with the membership function *Zero* is used to prevent the use of the coil m_X or m_Y, when the disturbance on the pitch axis is large.

In rules R_1 to R_8, the torque is computed with the positive polarity of the coil. Then the sign of the coil is chosen such that the resulting torque about the rotation axis is of opposite sign to the switching function associated with the corresponding angle, as was done for the thruster case.

The rules R_9 to R_{12} are designed such that the regulating torque about the pitch axis is of the opposite sign to the error in the spin rate.

Rules	x_1	x_2	x_3	x_4	x_5	x_6	x_7	x_8	x_9	x_{10}	**Output u**
R_1	*NZ*	*NZ*	P	P	*NZ*	*NZ*				Z	-1
R_2	*NZ*	*NZ*	P	N	*NZ*	*NZ*				Z	+1
R_3	*NZ*	*NZ*	N	P	*NZ*	*NZ*				Z	+1
R_4	*NZ*	*NZ*	N	N	*NZ*	*NZ*				Z	-1
R_5	*NZ*	*NZ*			*NZ*	*NZ*	P	P		Z	-1
R_6	*NZ*	*NZ*			*NZ*	*NZ*	P	N		Z	+1
R_7	*NZ*	*NZ*			*NZ*	*NZ*	N	P		Z	+1
R_8	*NZ*	*NZ*			*NZ*	*NZ*	N	N		Z	-1
R_9	*NZ*	*NZ*			*NZ*	*NZ*			P	P	-1
R_{10}	*NZ*	*NZ*			*NZ*	*NZ*			P	N	+1
R_{11}	*NZ*	*NZ*			*NZ*	*NZ*			N	P	+1
R_{12}	*NZ*	*NZ*			*NZ*	*NZ*			N	N	-1

Table 4.3 Control Rules for m_X and m_Y

Eight rules control the switching of the magneto-torquer m_Z, which can provide an effective control of the yaw and roll angles without disturbing the spin motion. These rules are presented in Table 4.4. As can be seen in Table 4.2, the switching of the coil m_Z has no influence on the spin rate. The rules are designed in a similar manner as in Table 4.3.

Rules	x_1	x_2	x_3	x_4	x_5	x_6	x_7	x_8	Output u
R_1	*NZ*	*NZ*	P	P	*NZ*	*NZ*			-1
R_2	*NZ*	*NZ*	P	N	*NZ*	*NZ*			+1
R_3	*NZ*	*NZ*	N	P	*NZ*	*NZ*			+1
R_4	*NZ*	*NZ*	N	N	*NZ*	*NZ*			-1
R_5	*NZ*	*NZ*			*NZ*	*NZ*	P	P	-1
R_6	*NZ*	*NZ*			*NZ*	*NZ*	P	N	+1
R_7	*NZ*	*NZ*			*NZ*	*NZ*	N	P	+1
R_8	*NZ*	*NZ*			*NZ*	*NZ*	N	N	-1

Table 4.4 Control Rules for m_Z

The fuzzy inference of the rules is the same as for thrusters except for the defuzzification where the output of each FLC is given as:

$$y_{coil} = \sum_{i=1}^{\text{Number of Rules}} y_i = \text{sgn}\left(\sum_{i=1}^{\text{Number of Rules}} y_i\right) \left| \sum_{i=1}^{\text{Number of Rules}} y_i \right| \tag{4.10}$$

As the control rules and membership functions have been designed, the output of all control rules cannot be valid simultaneously, since a non-zero variable cannot have a positive and negative membership value at the same time. Therefore, from Table 4.3, a maximum of three rules will be non-zero and from Table 4.4, a maximum of two rules will be non-zero.

The best case of coil utilization corresponds to the situation when the non-zero rules return the same sign, which means that switching the coil with this sign will satisfy all control requirements. Also, when the outputs of a controller from the rules are of opposite signs, this means that the switching of the coil will control one or two rotations but perturb the others. The summing of all rules in Eq.(4.10) cancels then the cross-disturbance, i.e. rule-based outputs of opposite signs are added up to a small value. On the other hand, if the outputs of the rules have the same sign for a coil, that coil is preferred. This defuzzification process returns then a weighted value of the control of each MISO controller at each sampling time.

The output of each fuzzy control from Eq.(4.10) is analyzed through its sign and absolute value. The resulting output then gives a weight of the controller if the coil were switched. As the effect of each coil is examined separately, only one coil among the three will be switched on at each sampling period with the sign of the output of the corresponding FLC.

Chapter 5

SIMULATIONS AND RESULTS

5.1 Introduction

5.1.1 Numerical Investigation

The interaction between structural and attitude dynamics appears clearly through the coupling of Eqs.(2.19) and (2.22). The equations governing the dynamics of the coupled system are then defined by the three attitude equations and the eight vibrational equations discretized with the same number of admissible functions. Also, the kinematic relation in Eq.(2.15) must be used to determine the physical attitude variables.

Since there is a large difference in the magnitudes of the frequencies associated with the attitude and flexible dynamics of a typical small spacecraft with short and stiff appendages, the equations of motion form a stiff system (in the sense of numerical analysis), which is solved numerically in this thesis using the well-known Gear's method.

Several simulations have been carried out using two admissible functions (modes) in the discretization of the flexible appendages and compared to the results obtained with one mode. In all cases, the contribution of the second mode is so weak that it can be neglected. Therefore the results in the following sections are given for one mode per appendage, which is also less computationally demanding.

5.1.2 Satellite Data

In this chapter, results of simulation of attitude control of a small satellite are presented using the spacecraft data specified in Table 5.1. Both cases of rigid and flexible appendages are considered.

The appendages are identical and may have either a rectangular cross-section to model solar arrays or a circular cross-section to model antennas. When taken as flexible solar arrays, the appendages have higher structural rigidity for the in-plane vibrations than for the out of plane vibrations. When taken as flexible antennas, the appendages have the same structural rigidity in the two transverse directions. Two different values for each structural rigidity are used in the simulations to study the effect of flexibility. Also, the effect of structural damping is investigated through two values of damping coefficient for the beam material.

mass of the spacecraft	m_S	201.92 kg
transverse mass moment of inertia of the central body about c.m.	I_{Tcb}	39.97 kg m^2
moment of inertia of the central body about its axis of symmetry	I_{Zcb}	32.28 kg m^2
linear mass density of the uniform beam	ρ	1.63 kg/m
radial offset of the appendage from the satellite c. m.	a	0.55 m
appendage offset along the axis of symmetry of the satellite	h	-0.585 m
length of the beam	L	2.30 m
width of the beam (rectangular cross-section beam)	w_b	0.455 m
thickness of the beam (rectangular cross-section beam)	t_b	0.02 m
radius of the beam (circular cross-section beam)	r_b	0.04 m
damping coefficient	η	0.005 or 0
bending rigidity for in-plane displacements	EI_{in}	10^5 Nm^2 or 10^3 Nm^2
bending rigidity for out of plane displacements	EI_{out}	10^3 Nm^2 or 10^2 Nm^2

Table 5.1 Spacecraft Data

5.1.3 Orbital Data

The five parameters defining the Keplerian orbit of the satellite are given in Table 5.2. The orbital parameters are chosen to meet the requirements of a Sun-synchronous orbit.

eccentricity	e	0.01
semi-latus rectum	p	7148 km
right ascension of the ascending node	Ω	90 deg
argument of the periapsis	υ	0 deg
inclination of the orbital plane	i	98.15 deg

Table 5.2 Orbital Data

The right ascension angle is chosen so as to guarantee exposure of the solar arrays to the Sun at all time.

5.1.4 Disturbance Data

Environmental disturbances are considered in most simulations in this thesis and include the effects of the aerodynamic drag, the solar radiation pressure and the magnetic torque due to a residual magnetic dipole in the spacecraft. Data specifying the properties of all surfaces of the satellite are presented in Table 5.3. The components of the residual dipole are the same along each body-fixed axis.

aerodynamical accommodation coefficients	σ_n, σ_t	0.85
radiative absorption coefficient	σ_a	0.8
radiative reflection coefficients	σ_{rs}, σ_{rd}	0.1
residual magnetic dipole component	m_{res}	1 Am^2

Table 5.3 Environmental Disturbance Data

In all simulations, the Earth is assumed to be at the summer solstice. This is the worst-case scenario, when the angle between the Sun direction and the pitch axis is maximum: the solar radiation pressure torque is then the maximum.

5.2 Three-Axis Stabilization

The angles of yaw, roll and pitch are initialized at 1, -1 and 1 degree, respectively. The objective is to drive these angles to values smaller than 0.1 degree. The thrusters can generate a torque of 0.2 Nm and are applied for a minimum duration of 0.5 seconds.

The effect of environmental disturbances, flexibility and damping are examined for various conditions which are summarized in Table 5.4. For each simulation, the time histories of the attitude angles and control torques are presented. When appendage flexibility is taken into account, the tip displacement of the beam along the X-axis is shown for the in-plane and out of plane vibrations.

Figure	Simulation Duration (sec)	Rigid/ Flexible	Environmental Disturbances	Cross-section	η	EI_{in} (Nm^2)	EI_{out} (Nm^2)
5.1 a&b	200	Rigid	No	N/A	N/A	N/A	N/A
5.2 a&b	200	Rigid	Yes	Rect.	N/A	N/A	N/A
5.3 a&b	200	Flexible	Yes	Rect.	0.005	100000	1000
5.4 a&b	20	Flexible	Yes	Rect.	0.005	100000	1000
5.5 a&b	20	Flexible	Yes	Rect.	0.005	100000	100
5.6 a&b	20	Flexible	Yes	Rect.	0.0	100000	100
5.7 a&b	20	Flexible	Yes	Circ.	0.0	1000	1000

Table 5.4 Simulation Conditions for Three-Axis Stabilization using Thrusters

In Figure 5.1, a long simulation duration is chosen to show the two steps involved in the control strategy developed in Chapter 4. Without environmental disturbances, the control is carried out efficiently, firstly by driving the attitude errors into the prescribed deadbands, and secondly by maintaining the errors inside the deadband by periodic switching. The need for maintenance occurs almost every minute, which can be explained by the small value chosen for the deadband (0.1 degree).

In Figure 5.2, disturbances are considered. The time history of the control changes slightly, and attitude is barely perturbed.

In Figures 5.3 to 5.7 for the flexible case, the control is carried out in a very similar manner as for the rigid case. However, the thruster firing is more frequent. In Figure 5.3, the damped response of the vibrations of the beams can be noticed especially in the out of plane direction.

In order to observe the high frequencies of the vibrations of the appendages, simulations are now shown for the first 20 seconds. Figure 5.4 represents an expansion of Figure 5.3 so as to make the comparison with the following cases convenient. Small residual oscillations appear in the time histories of angles of roll and yaw in Figure 5.5 and 5.6, although the tip displacements of the rectangular cross-section beams remain very small, especially in the in-plane direction. The case of flexible circular antennas is considered in Figure 5.7: the flexibility perturbs then the motion about pitch and frequent firing is then required.

5.3 Spin Stabilization

Control of a slowly spinning spacecraft using magneto-torquing is simulated in this section. The strength of the coils m_X, m_Y and m_Z are chosen as 100, 100 and 30 Am^2, respectively.

The errors on the roll and yaw angles are initialized at 2 degrees and the spin velocity is set to 0.6 deg/sec. The objective of the controller is to reduce the librations to 0.5 degrees while allowing an error in the spin velocity of 0.12 deg/sec. This tolerance is large, so that the use of the coils m_X and m_Y is made possible.

The tilted model of the geomagnetic field developed in Chapter 3 is used in all simulations.

The various conditions considered are presented in Table 5.5. For the rigid case, the effect of environmental disturbances and the dependence on the position around the Earth are investigated. For the flexible case, the effect of damping and bending rigidity is examined.

Figure	Simulation Duration (sec)	Rigid/ Flexible	Environmental Disturbance	Start	Cross section	η	EI_{in} (Nm^2)	EI_{out} (Nm^2)
5.8 a&b	1000	Rigid	No	perigee	N/A	N/A	N/A	N/A
5.9 a&b	1000	Rigid	Yes	perigee	rect.	N/A	N/A	N/A
5.10 a&b	1000	Rigid	Yes	North P.	rect.	N/A	N/A	N/A
5.11 a&b	1000	Rigid	Yes	apogee	rect.	N/A	N/A	N/A
5.12 a&b	1000	Rigid	Yes	South P.	rect.	N/A	N/A	N/A
5.13 a&b	400	Rigid	Yes	perigee	rect.	N/A	N/A	N/A
5.14 a&b	400	Flexible	Yes	perigee	rect.	0.005	100000	1000
5.15 a&b	400	Flexible	Yes	perigee	rect.	0.005	100000	100
5.16 a&b	400	Flexible	Yes	perigee	rect.	0	100000	100
5.17 a&b	400	Flexible	Yes	perigee	circ.	0	1000	1000

Table 5.5 Simulation Conditions for Spin Stabilization using Magneto-torquing

In Figures 5.8 to 5.12, a long simulation duration is chosen so as to observe the tendency of the time histories. In all cases, the control objectives are fulfilled, but in different manner. Without environmental disturbances, the responses appear to be smooth, especially inside the deadbands, as shown in Figure 5.8. However, when disturbances are taken into account in the attitude dynamics of the satellite, the control switchings are more frequent. Environmental disturbances are considered for all the remaining simulations.

As mentioned in Chapter 4, the geomagnetic field, and hence the magnetic torque, depends on the position around the Earth. Figures 5.9 to 5.12 represent simulations starting respectively at perigee, above the North Pole, at apogee and above the South Pole. The time history of the switching of the coils varies significantly from one case to the other. The most difficult case is shown in Figure 5.12, where chattering of coil m_z is observed for the first third of the simulation.

Figure 5.13 represents the first 400 seconds of the simulation presented in Figure 5.9, for a rigid spacecraft. This facilitates the comparison with the following results obtained for a spacecraft with flexible appendages.

The results shown in Figure 5.14 correspond to rather stiff rectangular cross-section appendages. Transverse displacements of the beams are very small and do not perturb the attitude motion in any perceptible manner. Even when the out of plane structural rigidity is reduced, minor changes appear in the time histories as shown in Figure 5.15, and control can still be carried out efficiently. Finally, when structural damping in the beams is ignored for rectangular and circular cross-section appendages in Figures 5.16 and 5.17 respectively, the attitude motion is slightly modified, especially when the attitude angles are inside their deadbands.

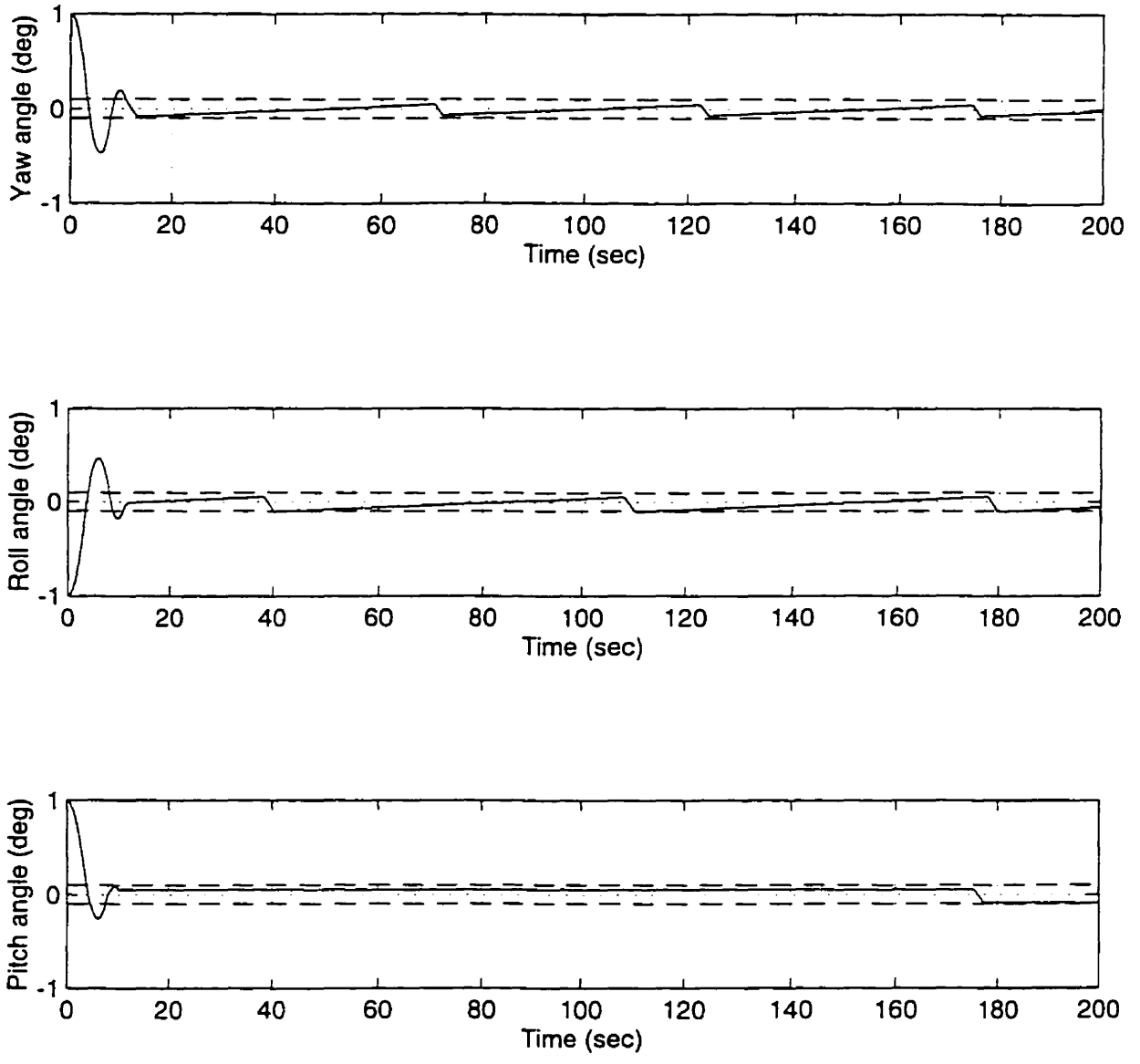

Figure 5.1a Three-Axis Stabilization: Attitude Angles

(Rigid Case, No Disturbances)

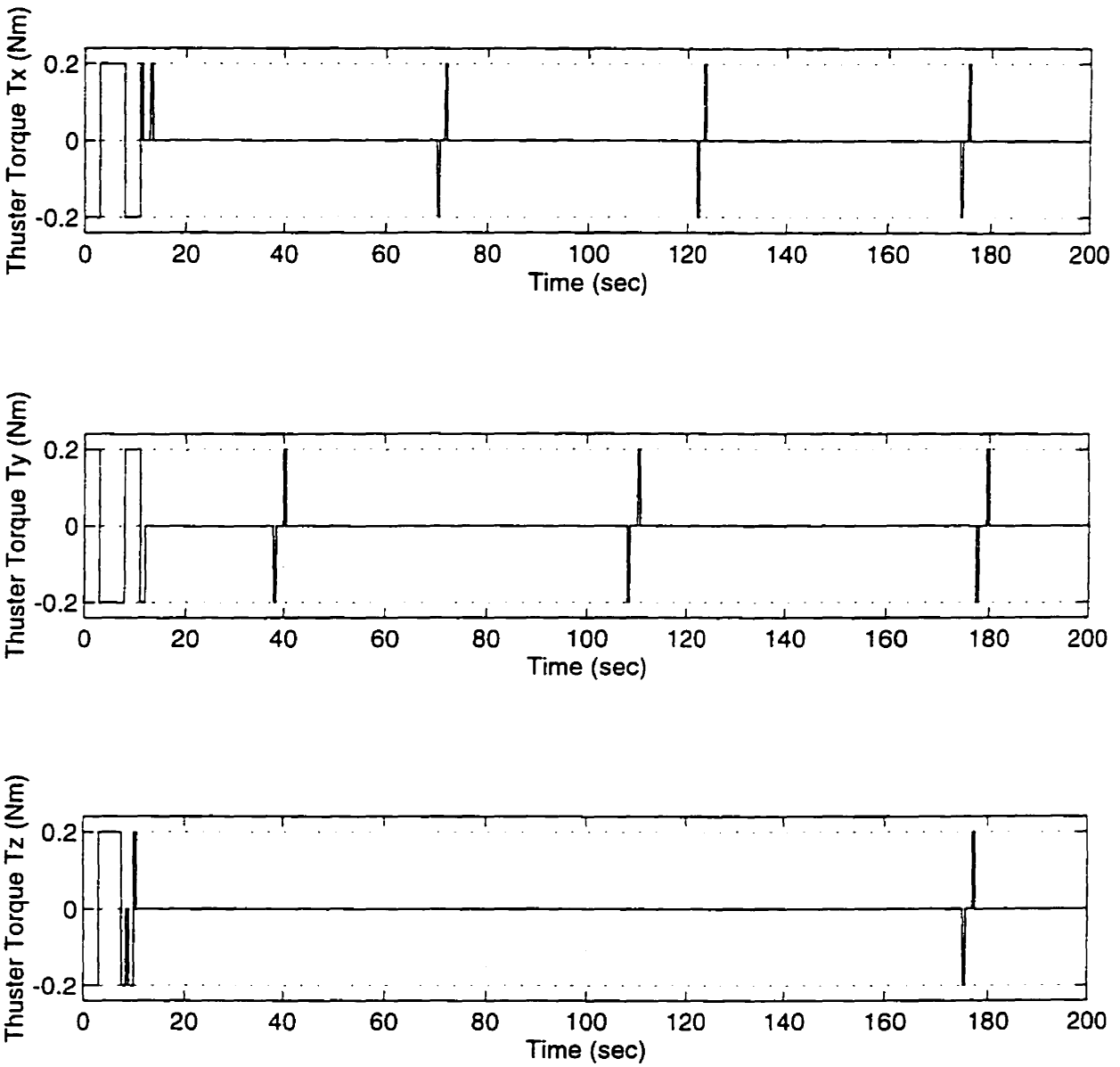

Figure 5.1b Three-Axis Stabilization: Thruster Torques

(Rigid Case, No Disturbances)

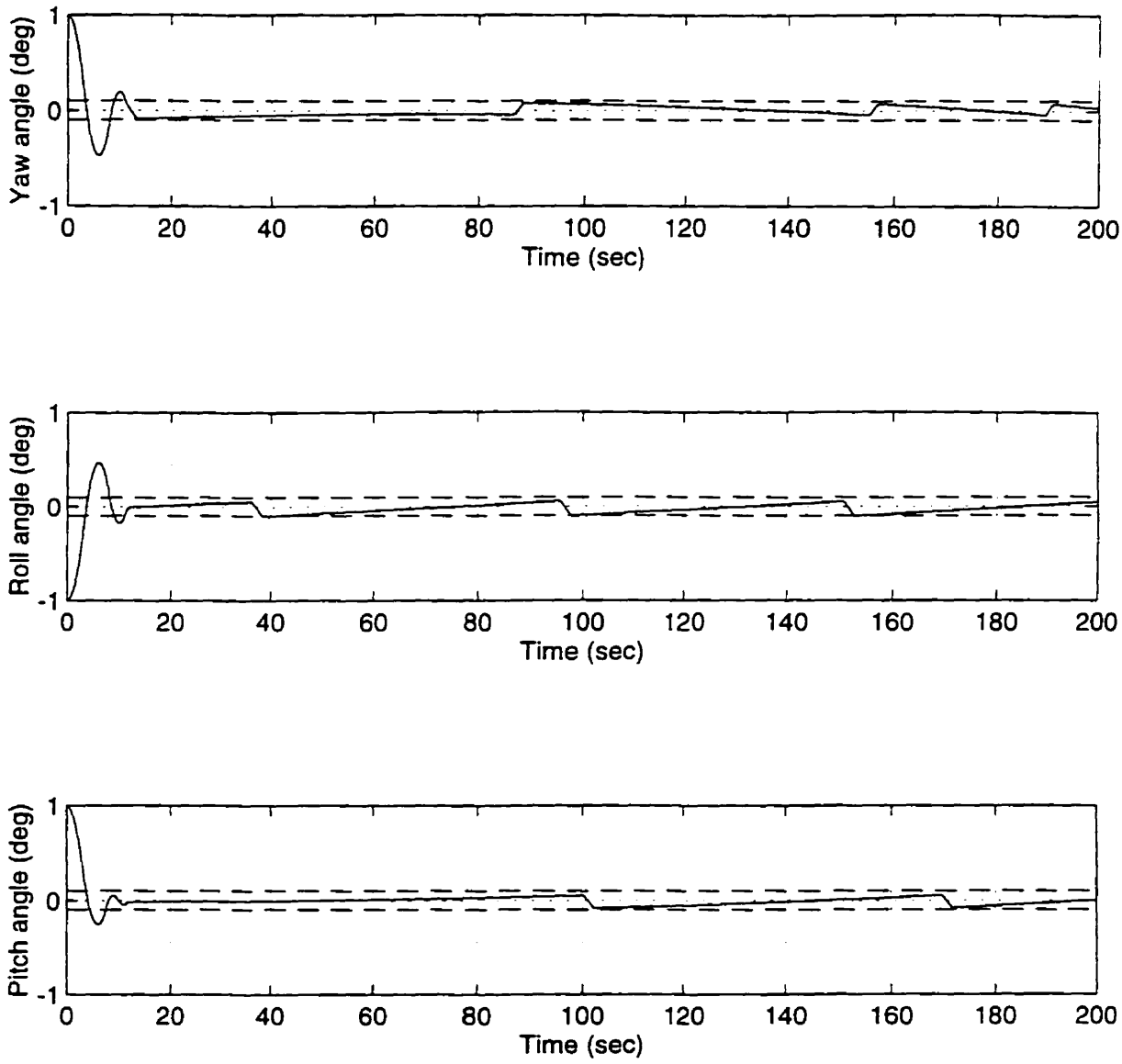

Figure 5.2a Three-Axis Stabilization: Attitude Angles
(Rigid Case, With Disturbances)

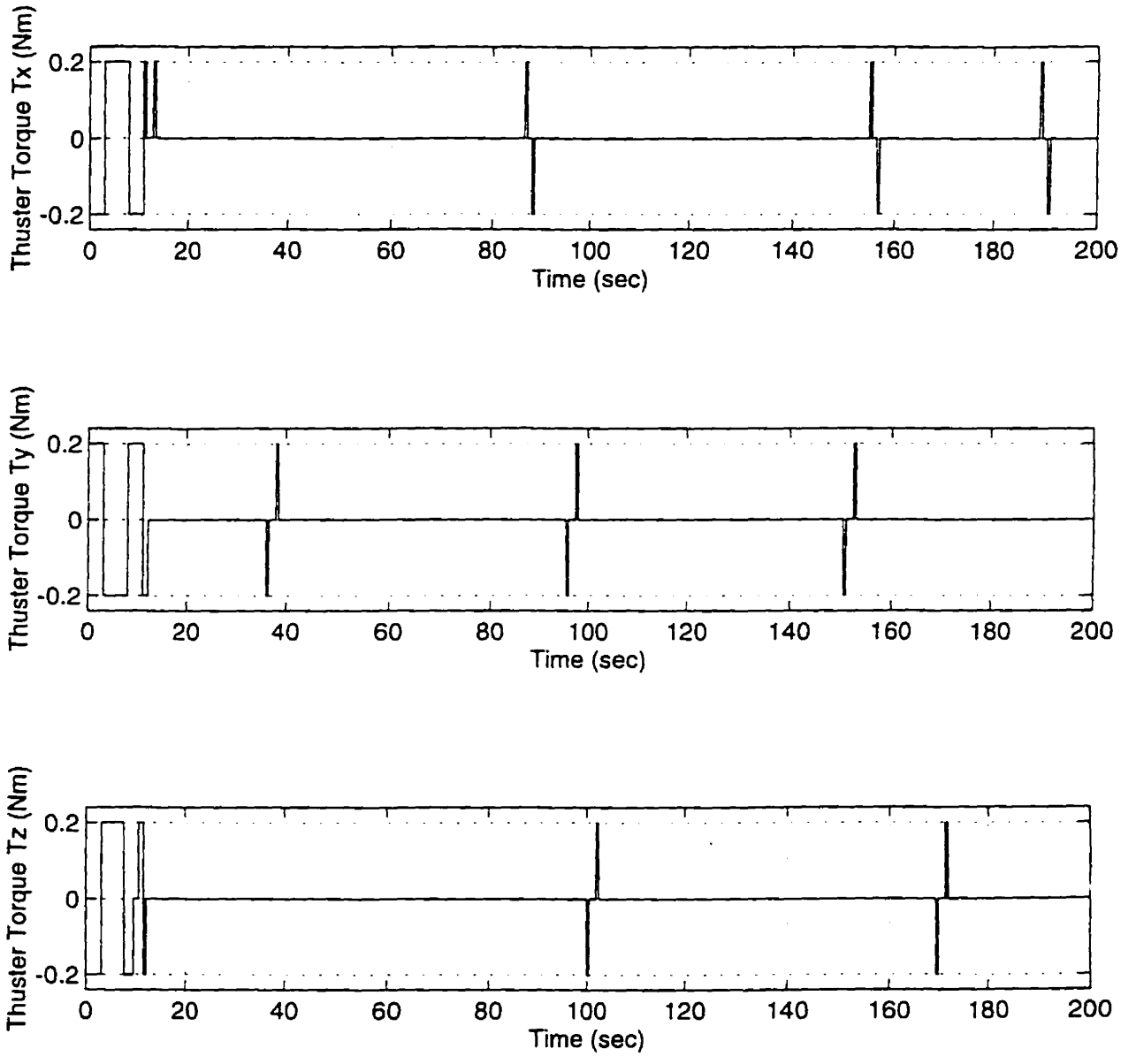

Figure 5.2b Three-Axis Stabilization: Thruster Torques

(Rigid Case, With Disturbances)

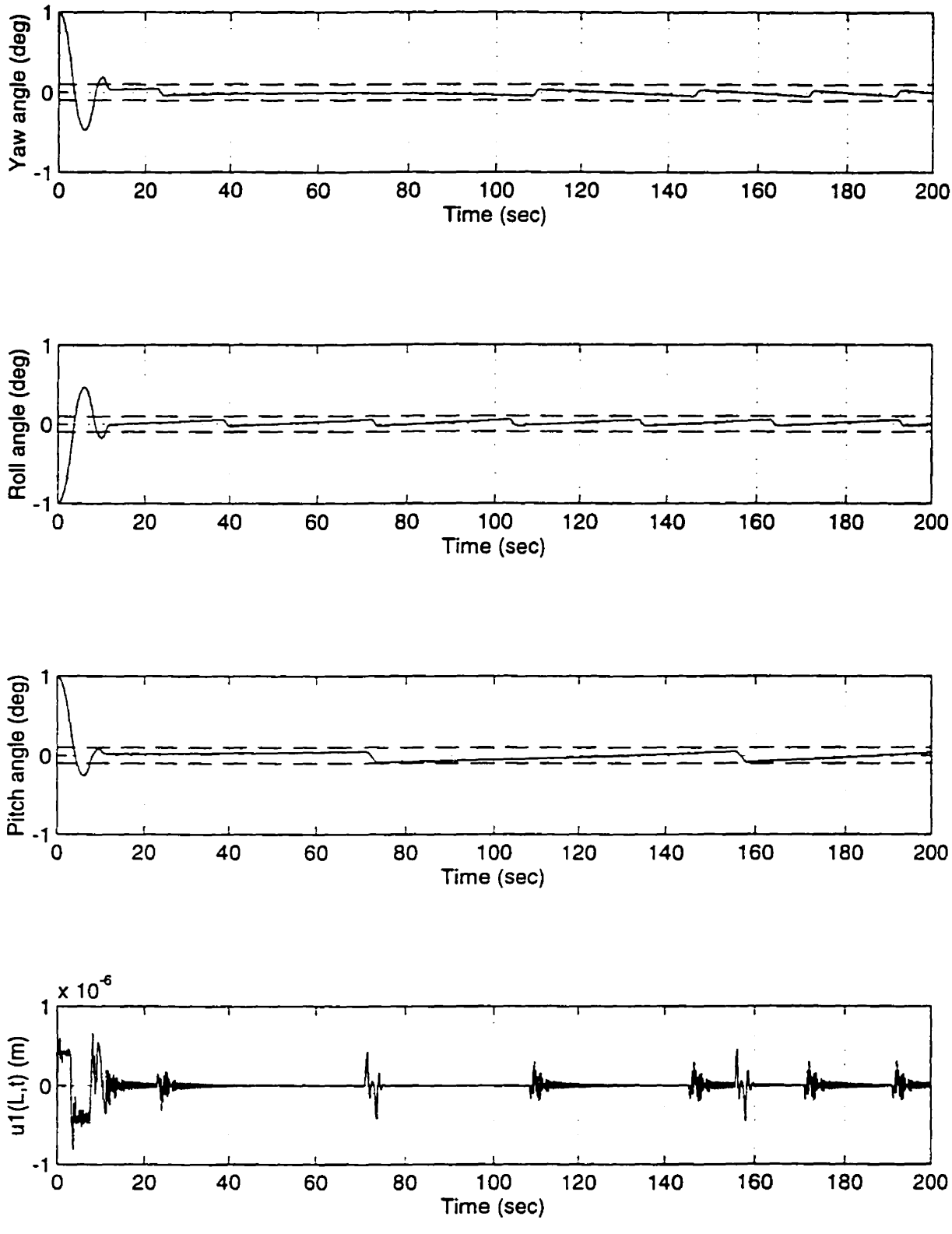

Figure 5.3a Three-Axis Stabilization: Attitude Angles, In-Plane Tip Vibration (Flexible Case, Rectangular cross-section, η=0.005, $EI_{in}=10^5$ Nm^2, $EI_{out}=10^3$ Nm^2)

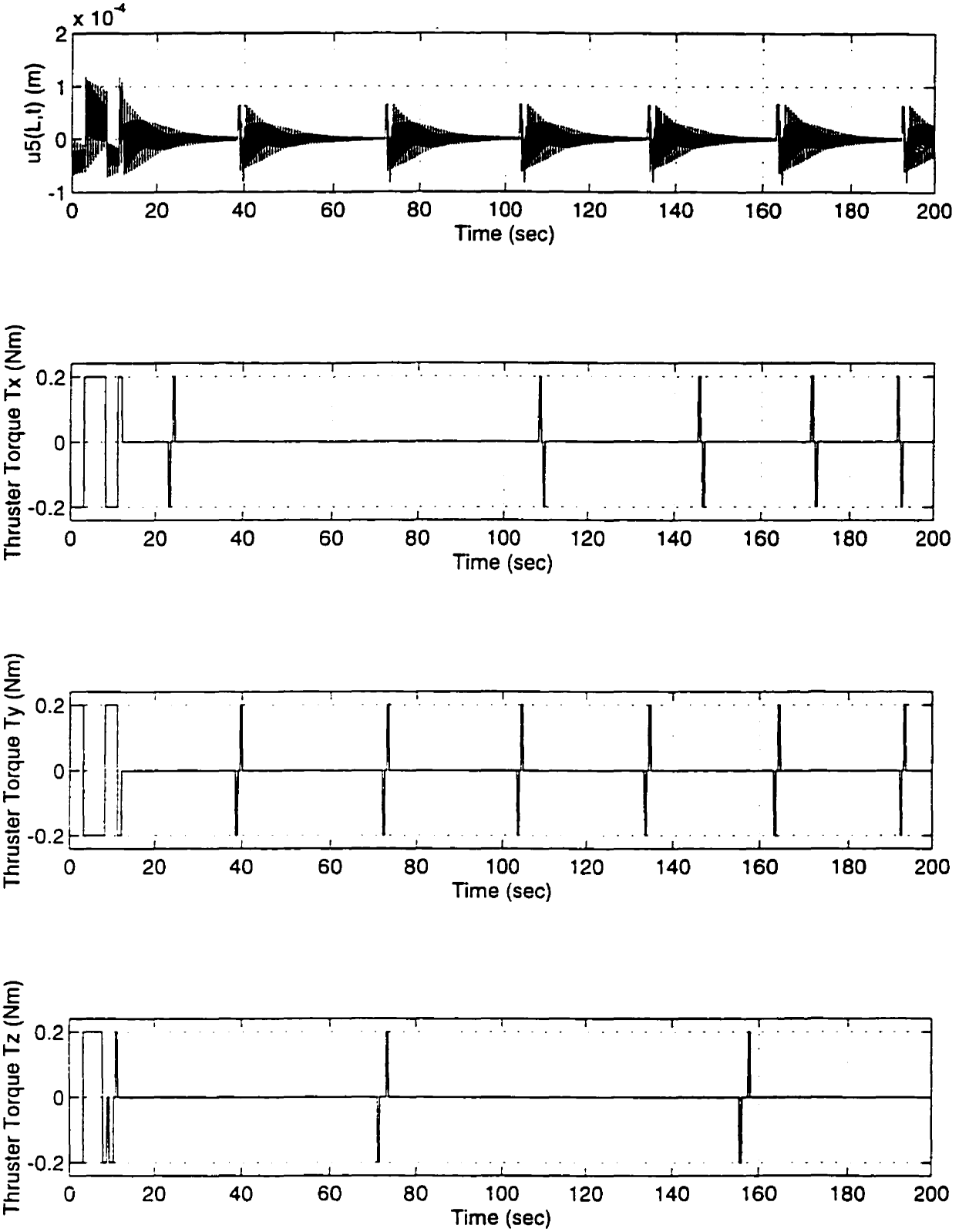

Figure 5.3b Three-Axis Stabilization: Out of plane Tip Vibration, Thruster Torques (Flexible Case, Rectangular cross-section, η=0.005, $EI_{in}=10^5$ Nm^2, $EI_{out}=10^3$ Nm^2)

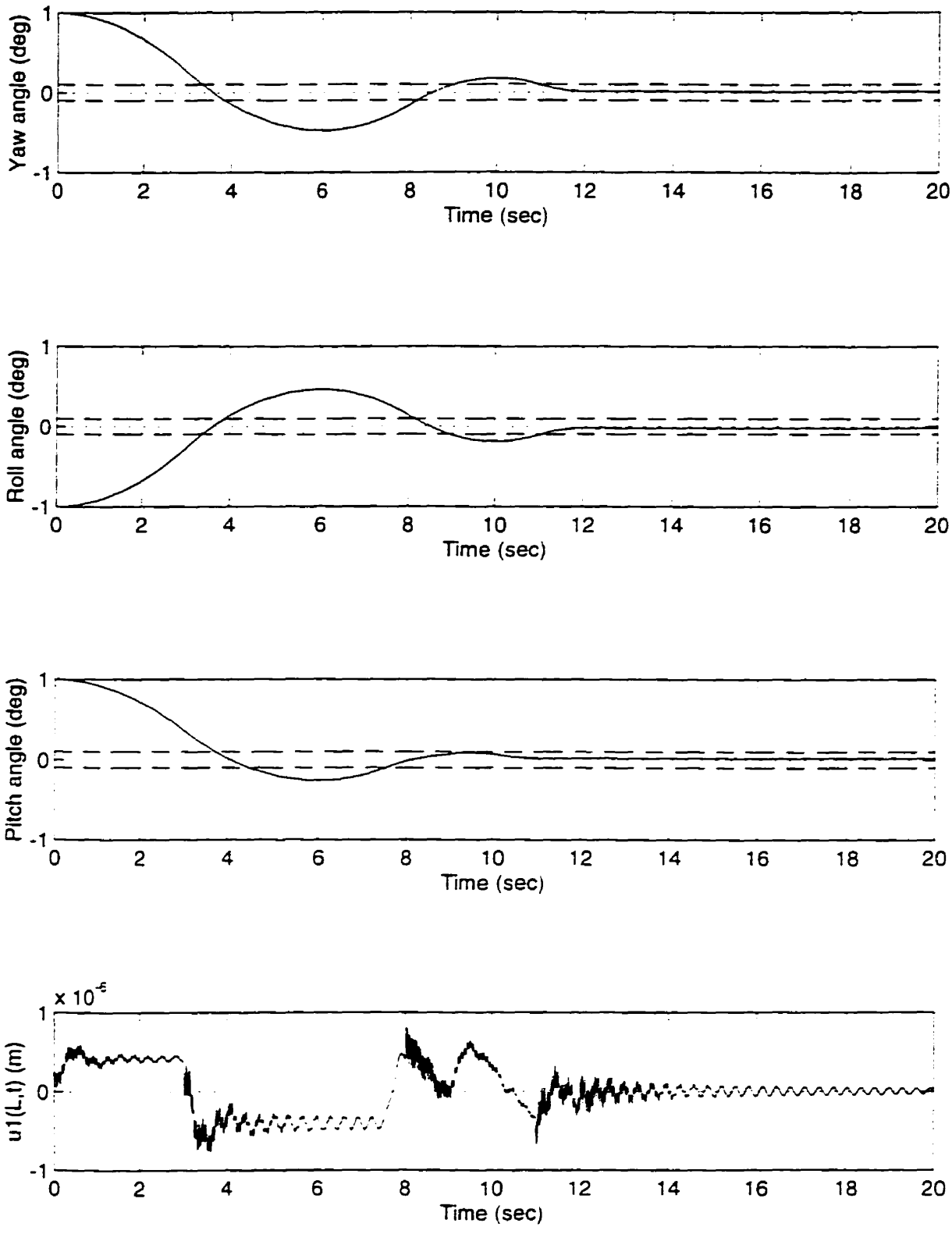

Figure 5.4a Three-Axis Stabilization: Attitude Angles. In-Plane Tip Vibration (Expansion of Figure 5.3a)

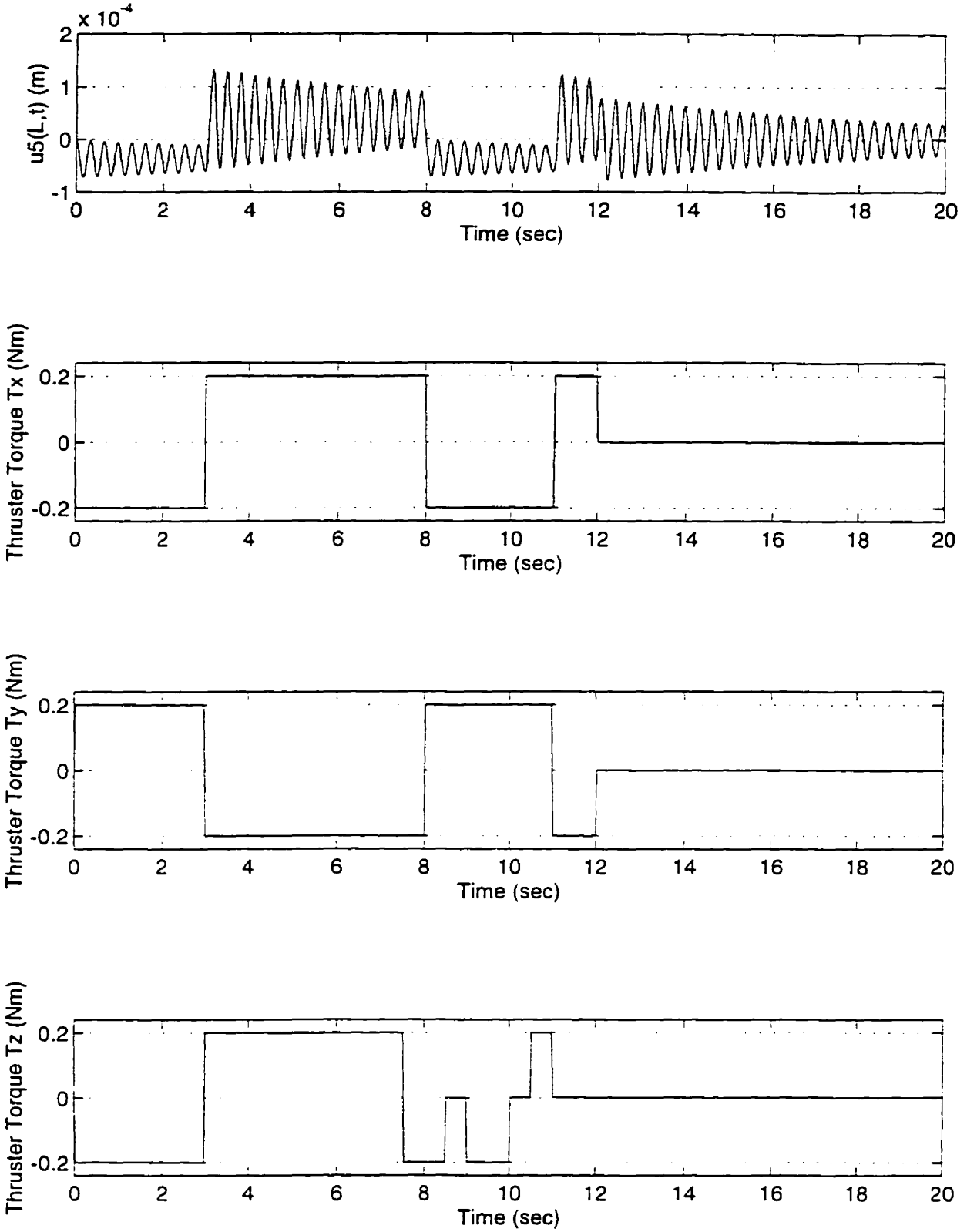

Figure 5.4b Three-Axis Stabilization: Out of plane Tip Vibration, Thruster Torques (Expansion of Figure 5.3b)

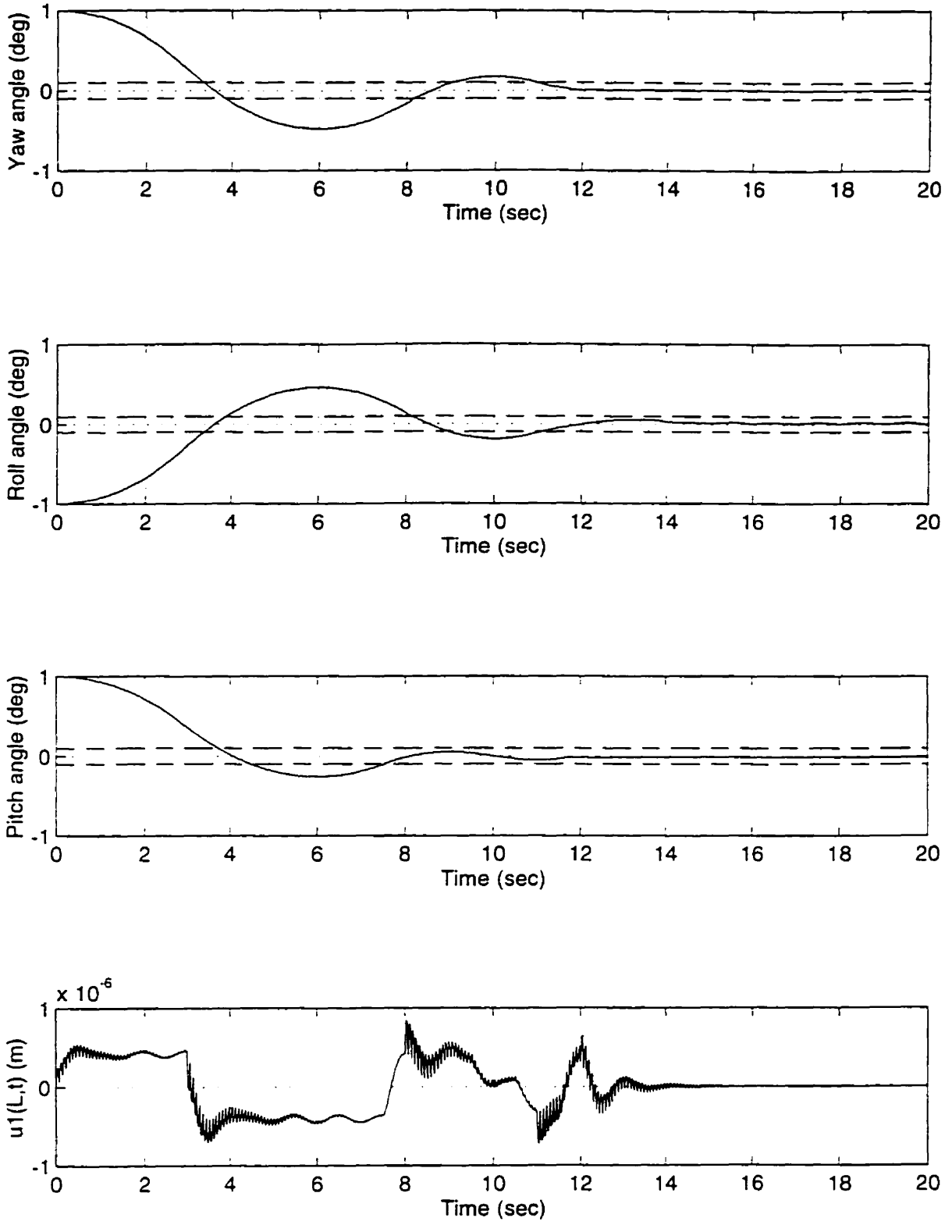

Figure 5.5a Three-Axis Stabilization: Attitude Angles, In-Plane Tip Vibration (Flexible Case, Rectangular cross-section, η=0.005, $EI_{in}=10^5$ Nm^2, $EI_{out}=10^2$ Nm^2)

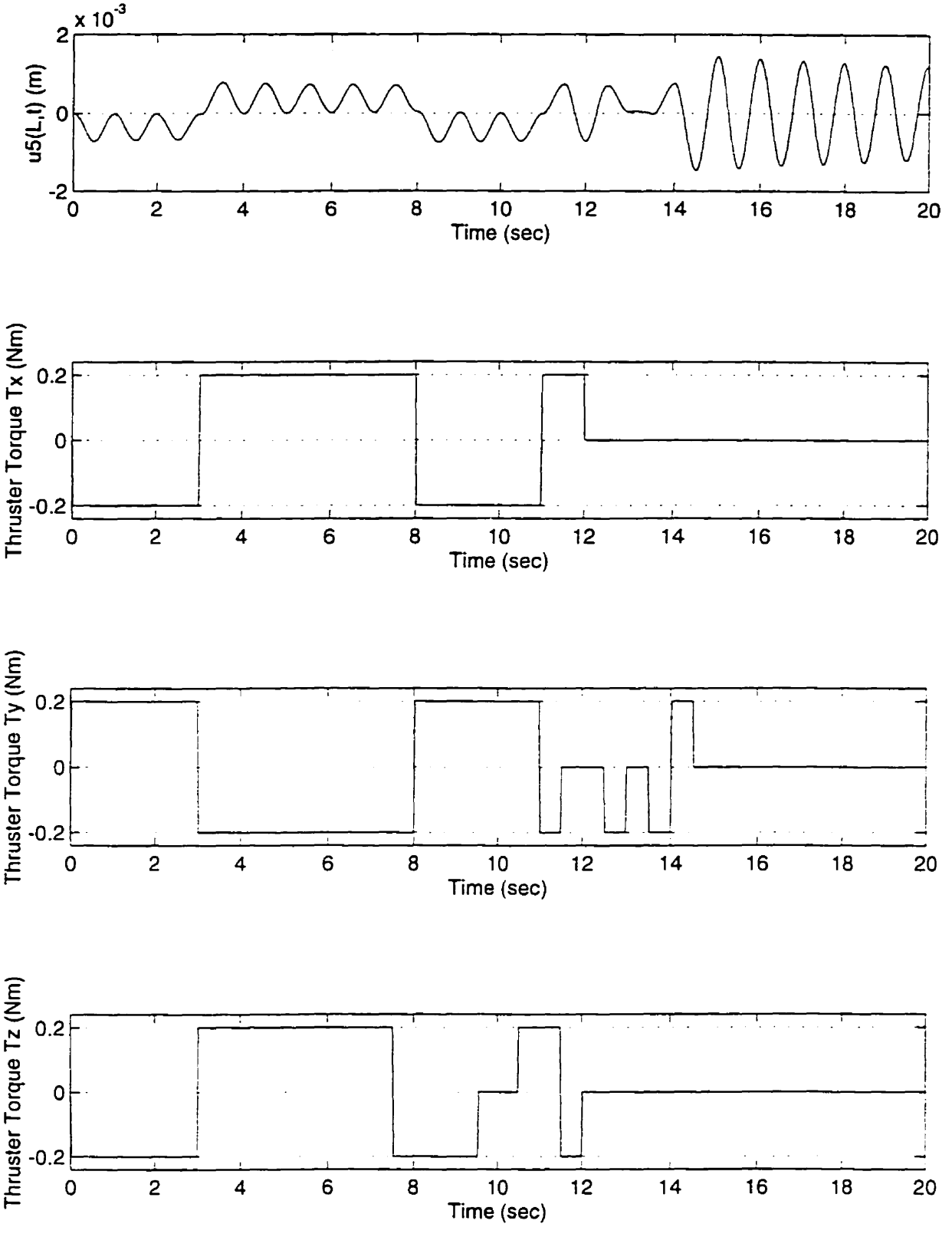

Figure 5.5b Three-Axis Stabilization: Out of plane Tip Vibration, Thruster Torques (Flexible Case, Rectangular cross-section, η=0.005, $EI_{in}=10^5$ Nm^2, $EI_{out}=10^2$ Nm^2)

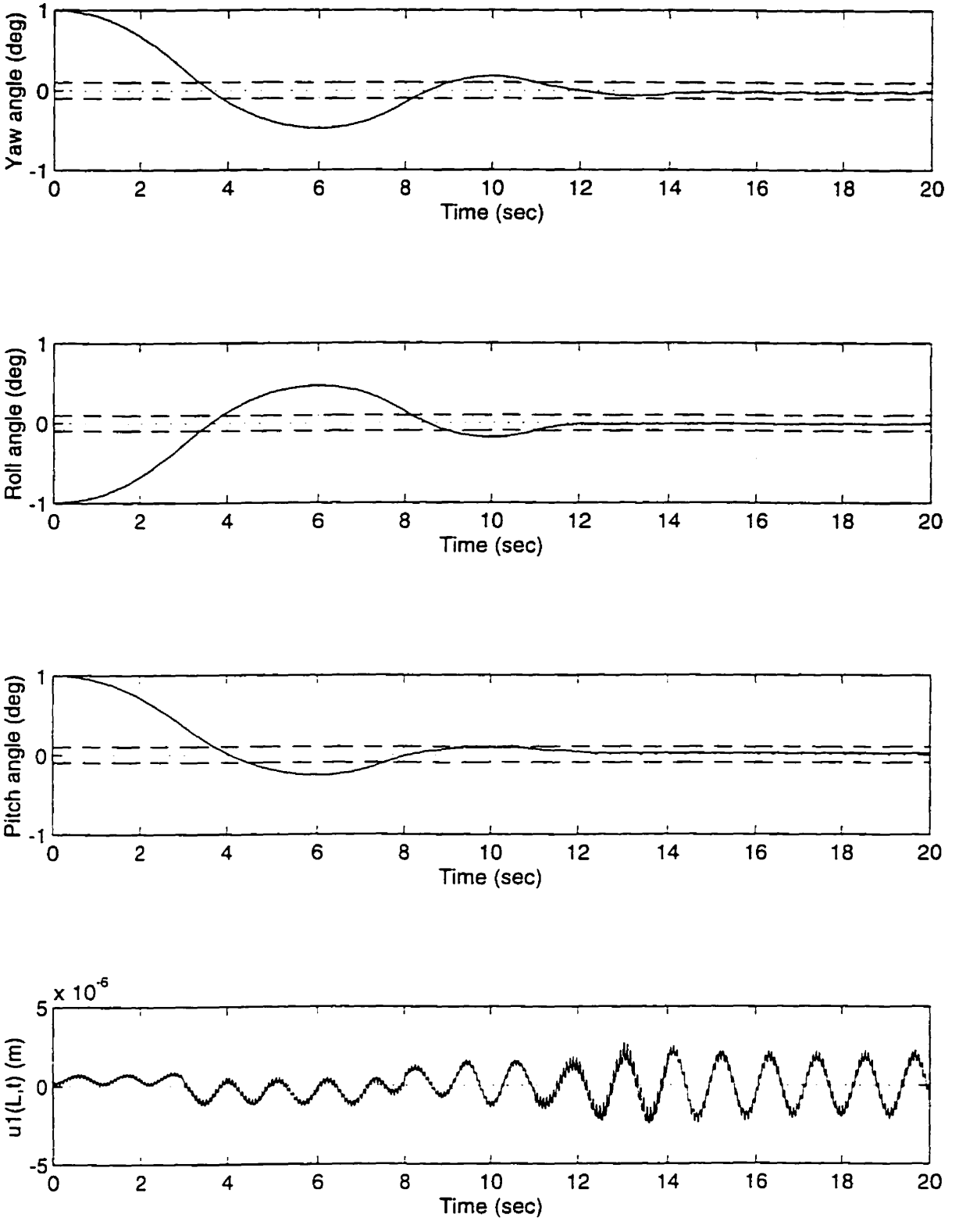

Figure 5.6a Three-Axis Stabilization: Attitude Angles, In-Plane Tip Vibration (Flexible Case, Rectangular cross-section, η=0.0, $EI_{in}=10^5$ Nm^2, $EI_{out}=10^2$ Nm^2)

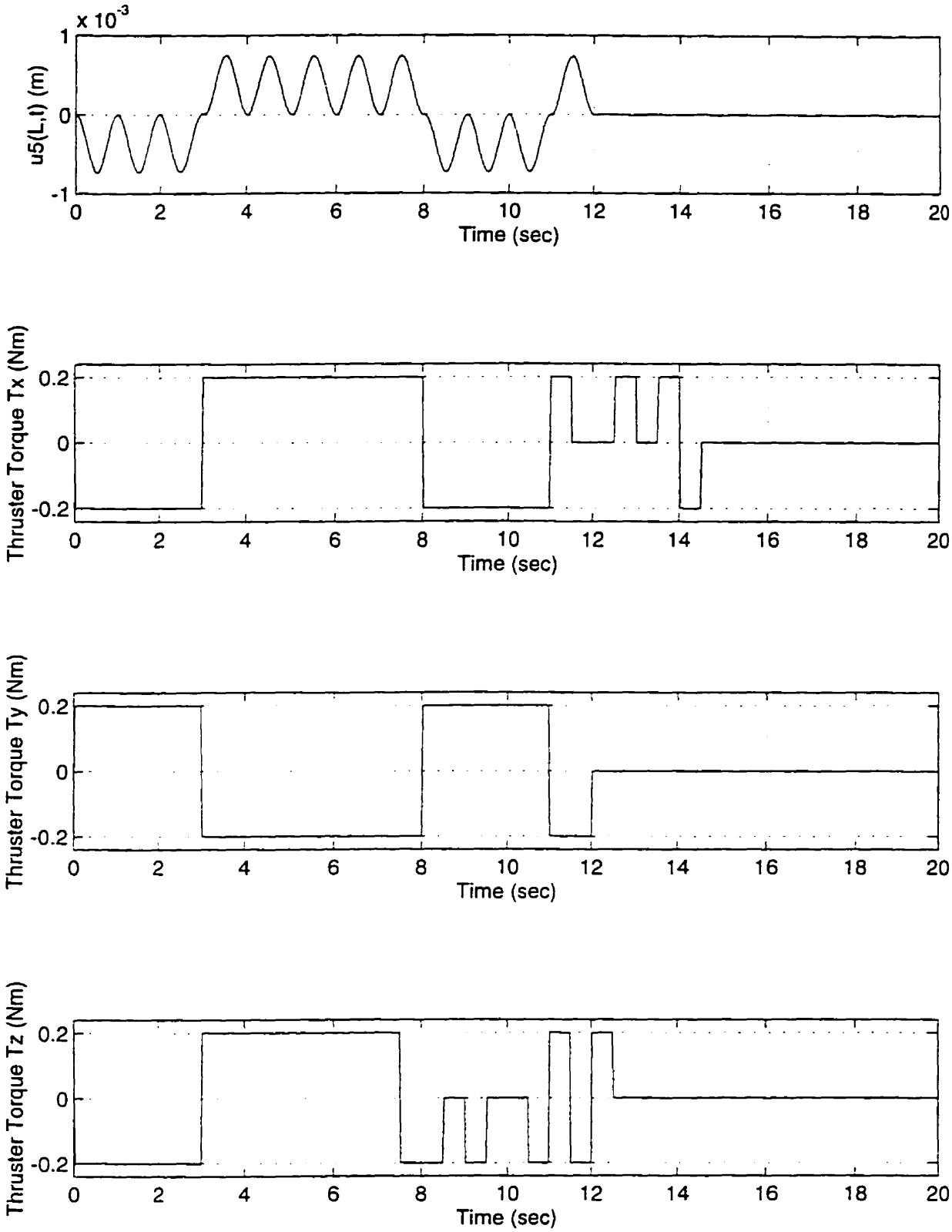

Figure 5.6b Three-Axis Stabilization: Out of plane Tip Vibration, Thruster Torques (Flexible Case, Rectangular cross-section, η=0.0, $EI_{in}=10^5$ Nm^2, $EI_{out}=10^2$ Nm^2)

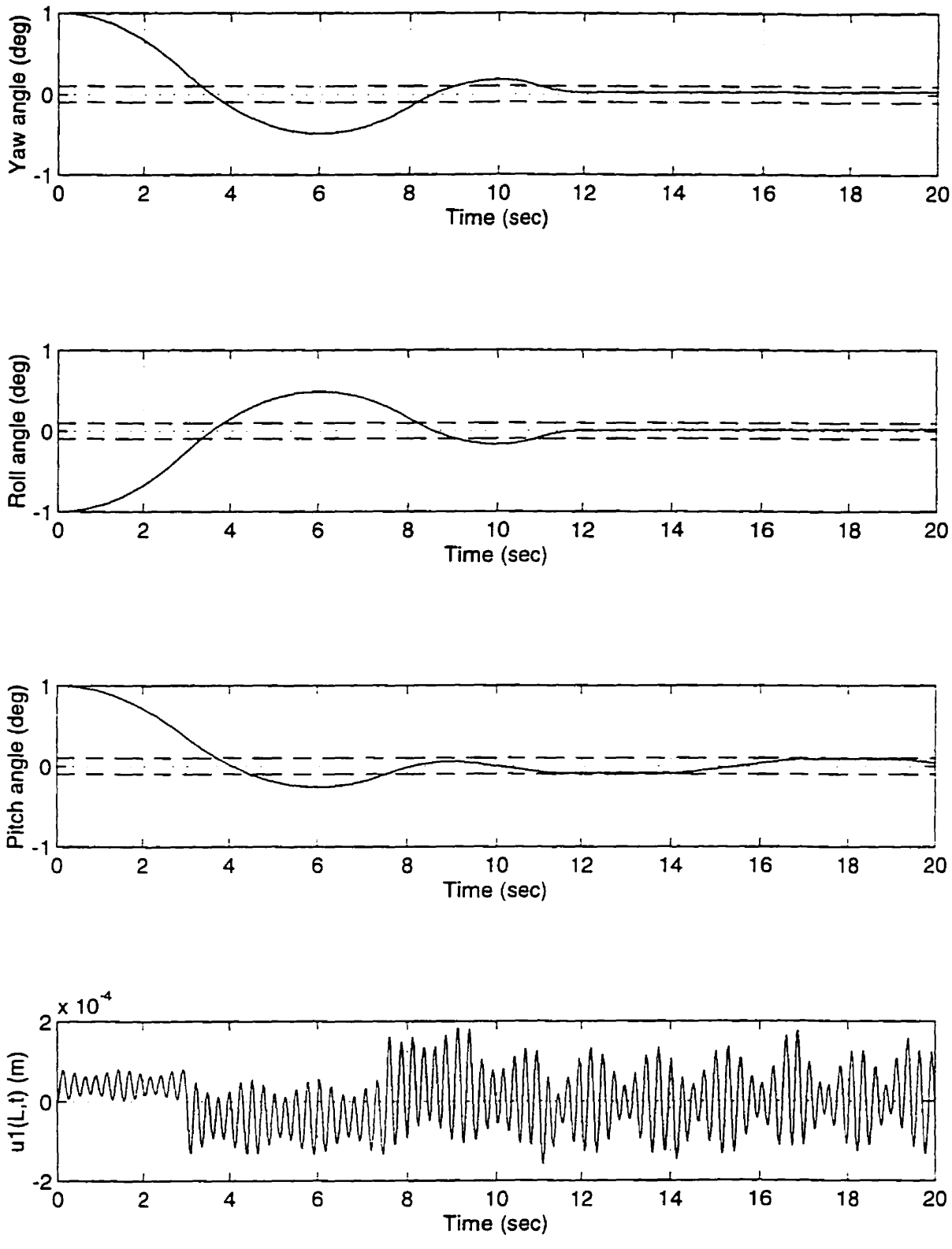

Figure 5.7a Three-Axis Stabilization: Attitude Angles, In-Plane Tip Vibration (Flexible Case, Circular cross-section, η=0.0, $EI_{in}=10^3$ Nm^2, $EI_{out}=10^3$ Nm^2)

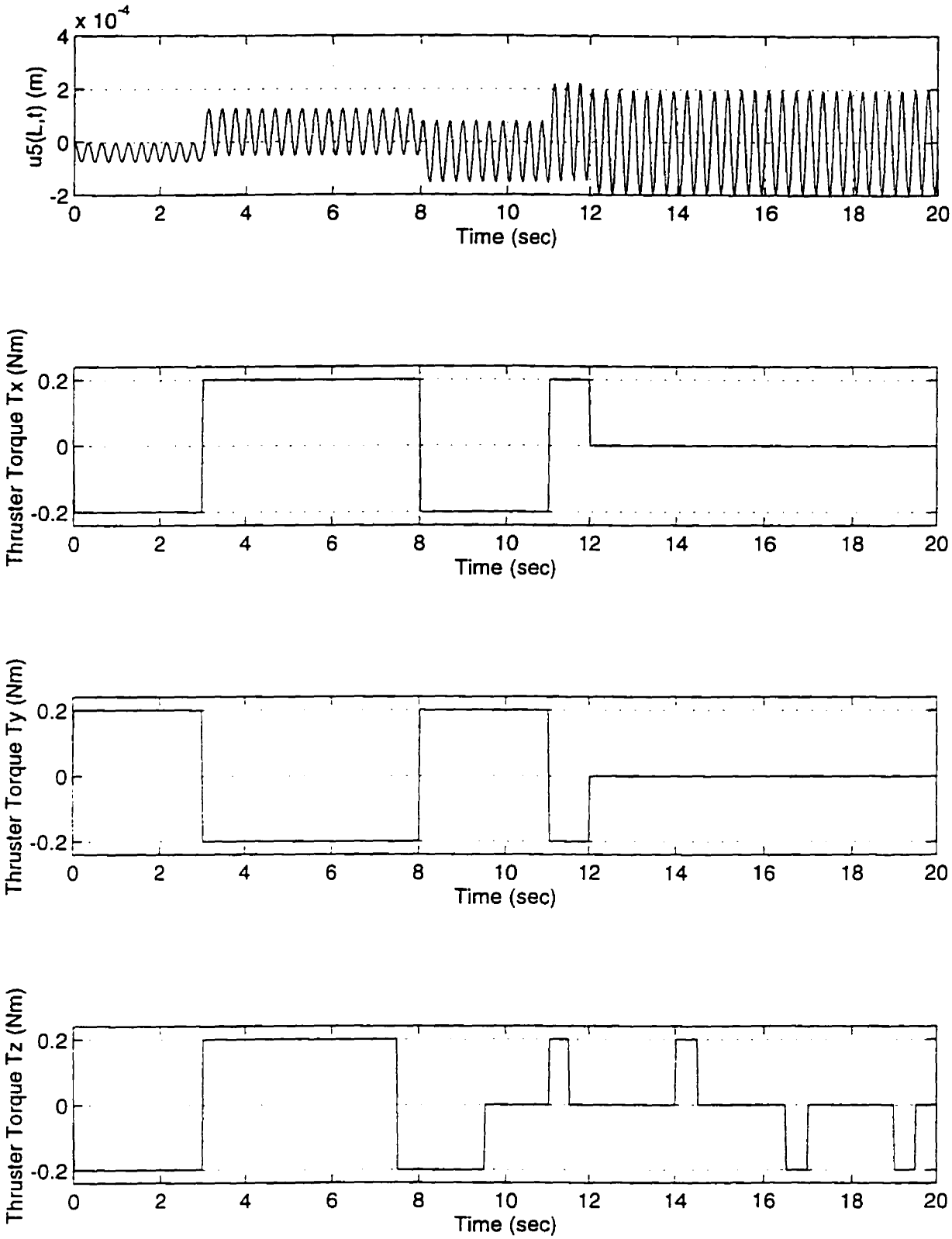

Figure 5.7b Three-Axis Stabilization: Out of plane Tip Vibration, Thruster Torques (Flexible Case, Circular cross-section, η=0.0, $EI_{in}=10^3$ Nm^2, $EI_{out}=10^3$ Nm^2)

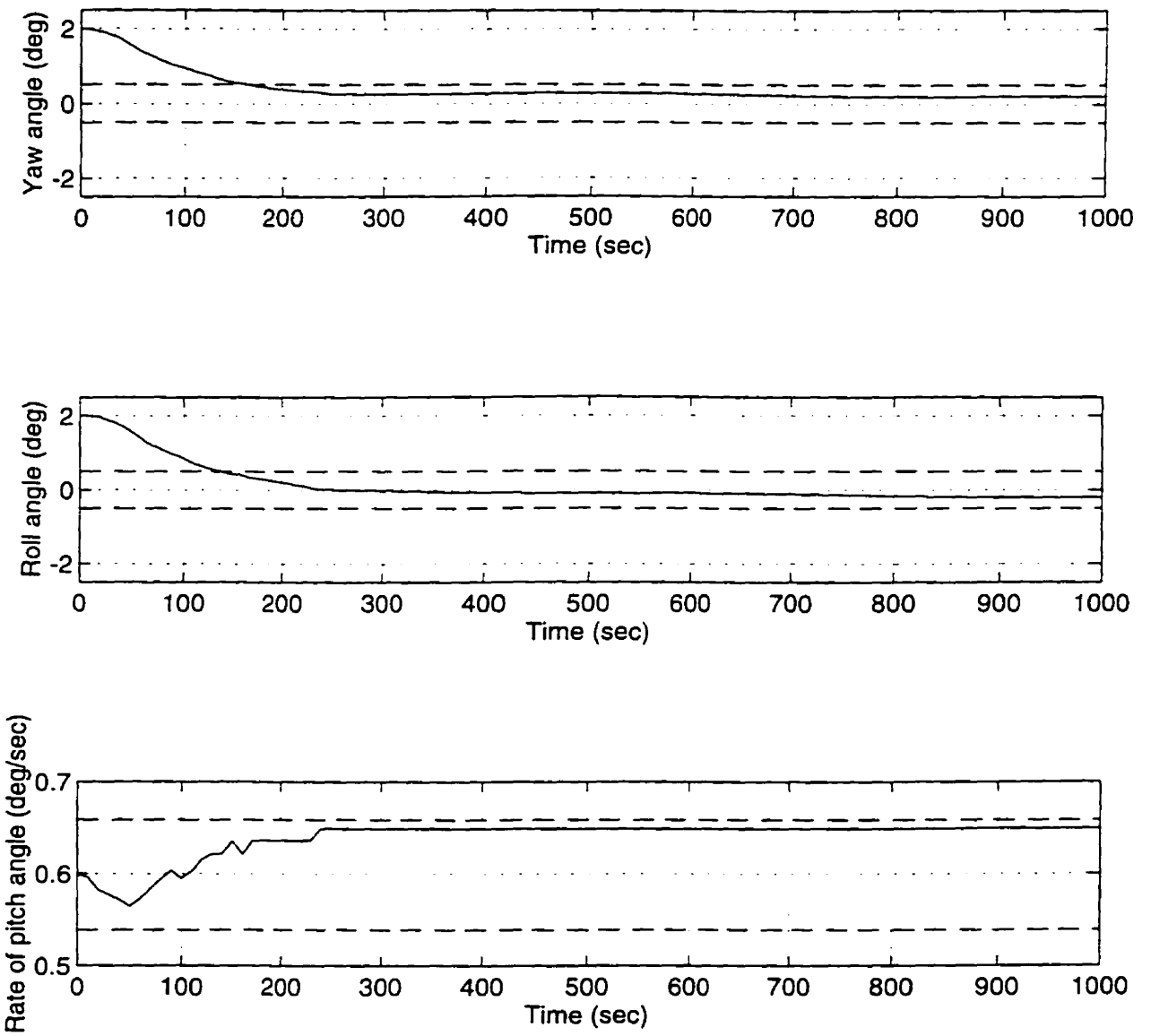

Figure 5.8a Spin Stabilization: Attitude Angles
(Rigid Case, No Disturbances, Start at Perigee)

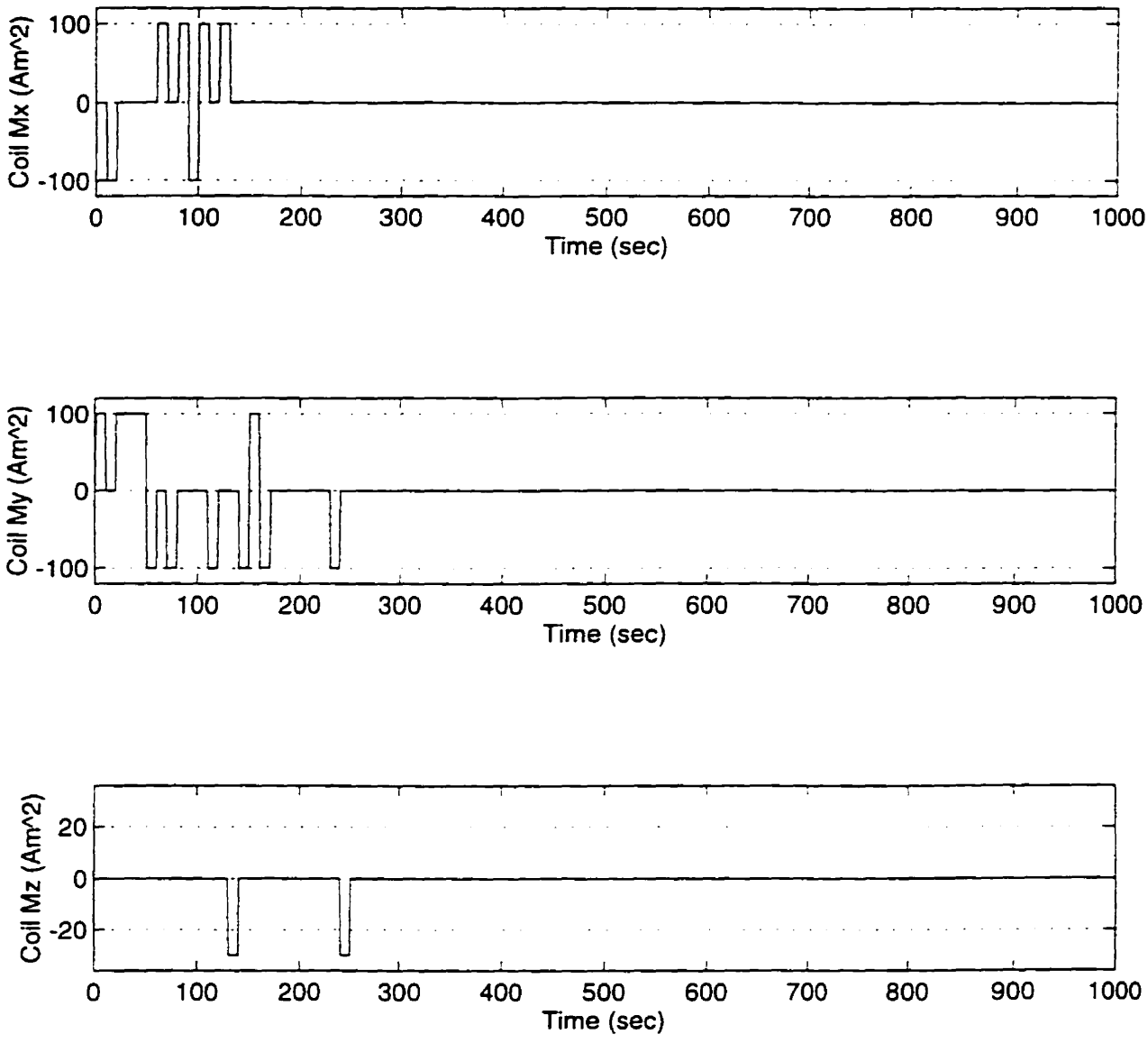

Figure 5.8b Spin Stabilization: Coil Switching
(Rigid Case, No Disturbances, Start at Perigee)

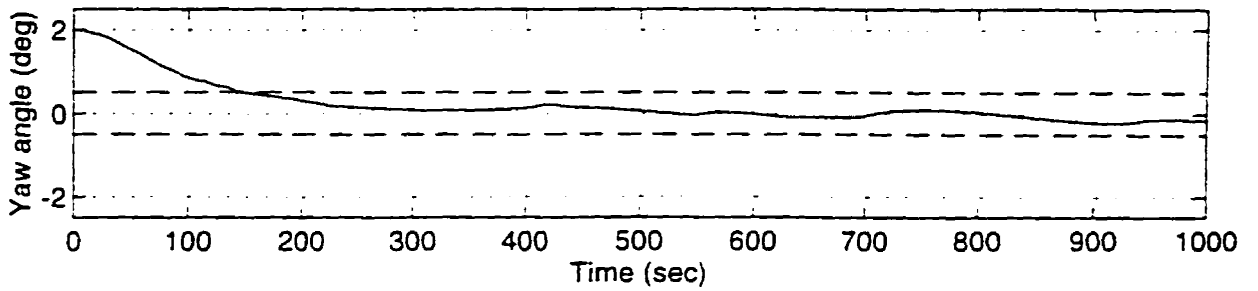

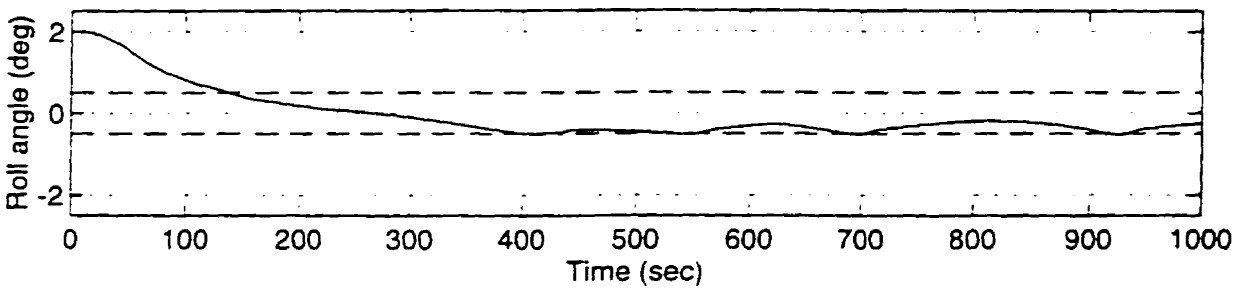

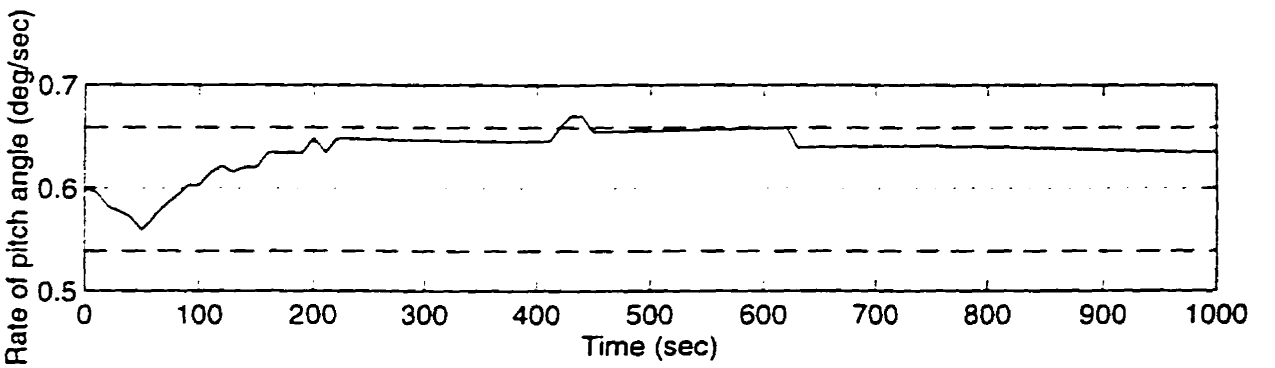

Figure 5.9a Spin Stabilization: Attitude Angles

(Rigid Case, With Disturbances, Start at Perigee)

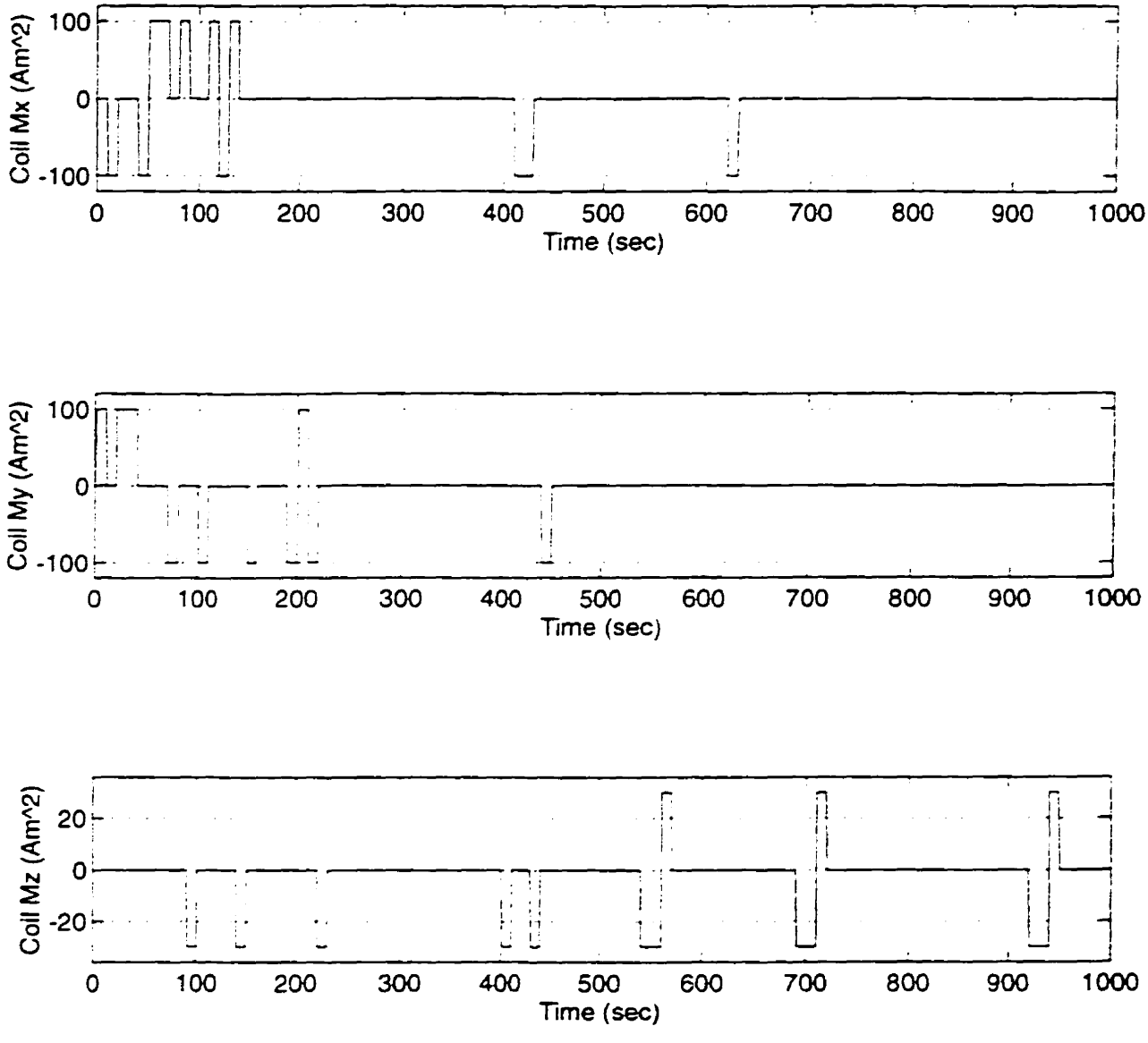

Figure 5.9b Spin Stabilization: Coil Switching

(Rigid Case, With Disturbances, Start at Perigee)

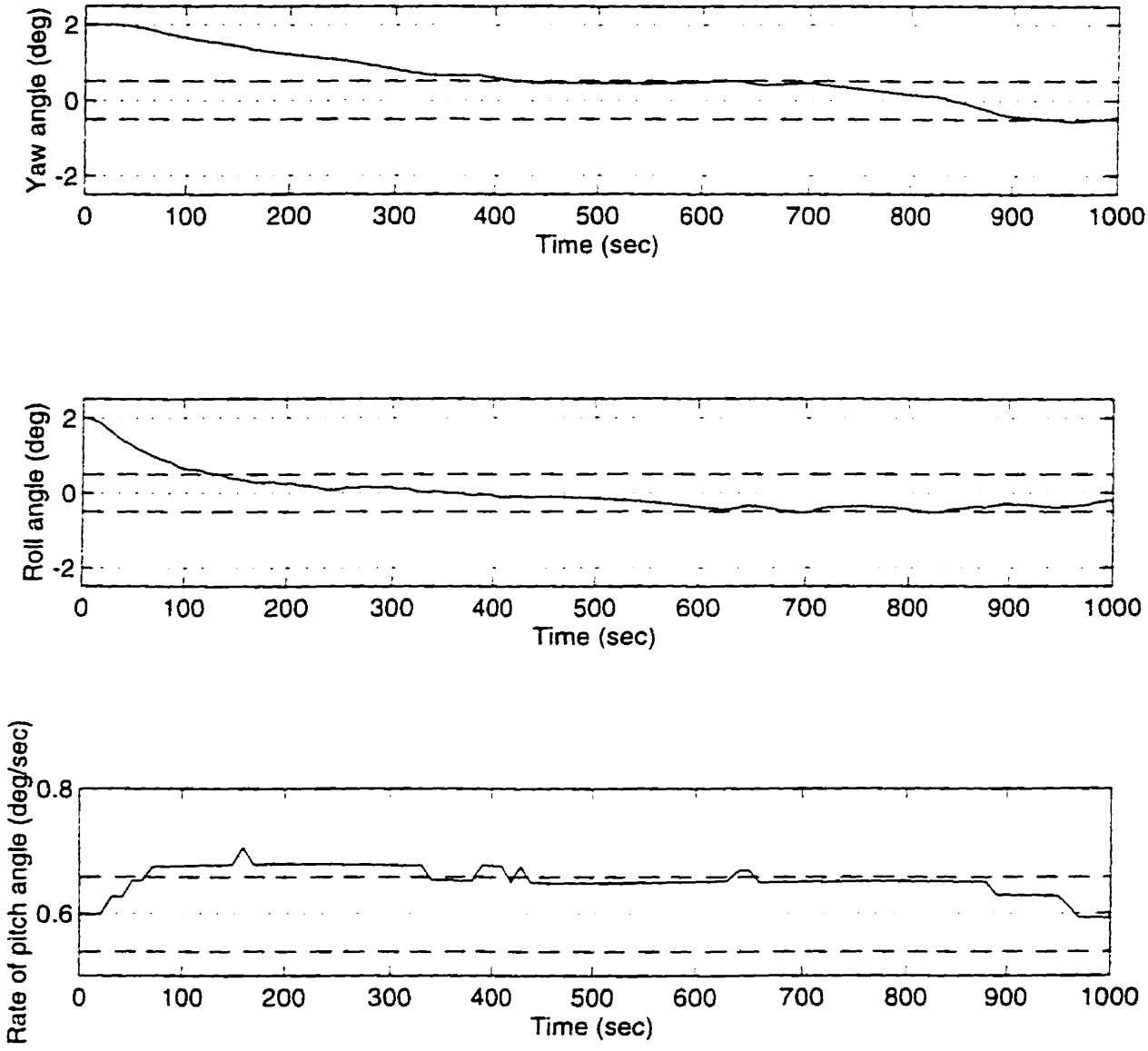

Figure 5.10a Spin Stabilization: Attitude Angles

(Rigid Case, Start at North Pole)

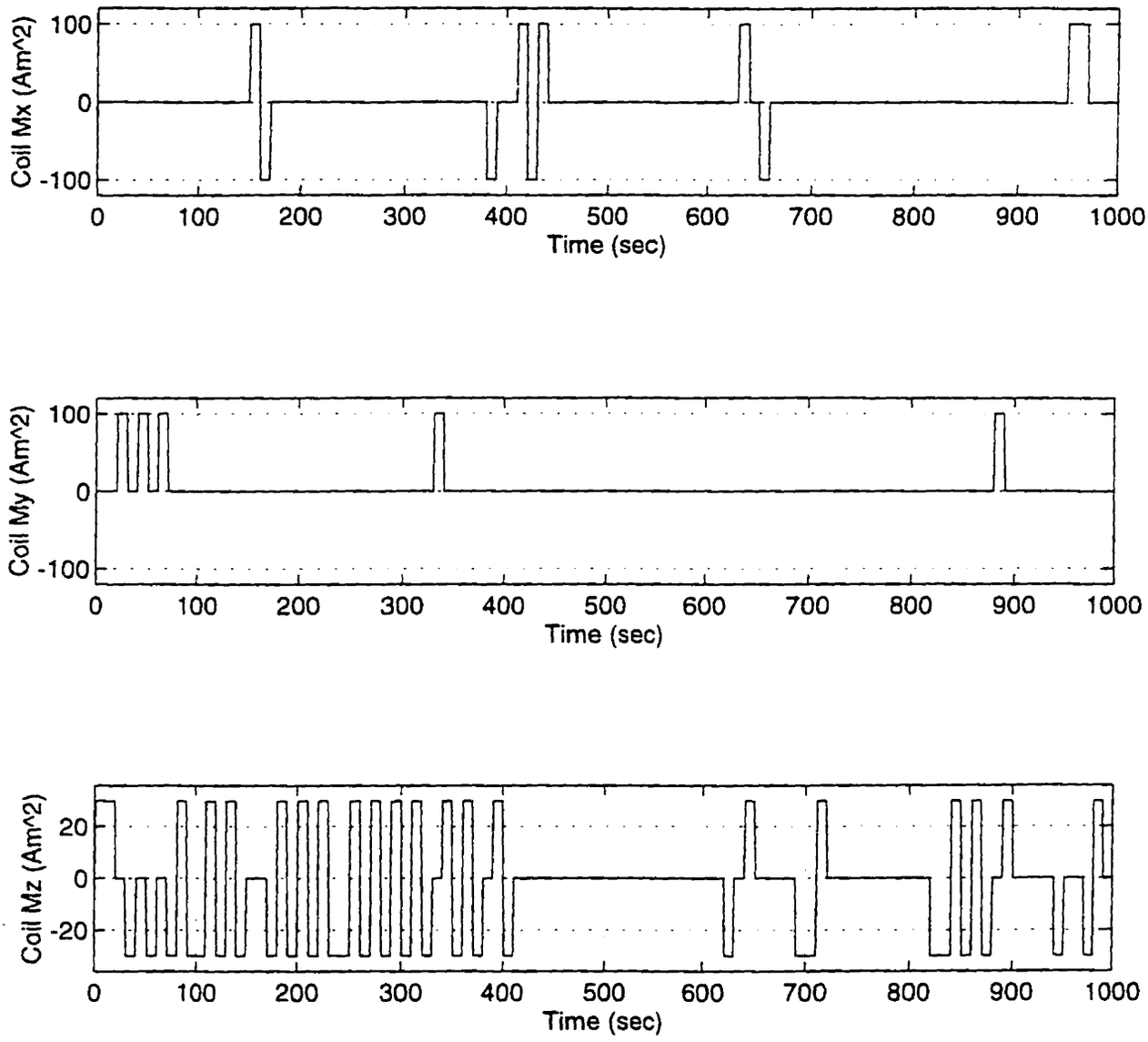

Figure 5.10b Spin Stabilization: Coil Switching

(Rigid Case, Start at North Pole)

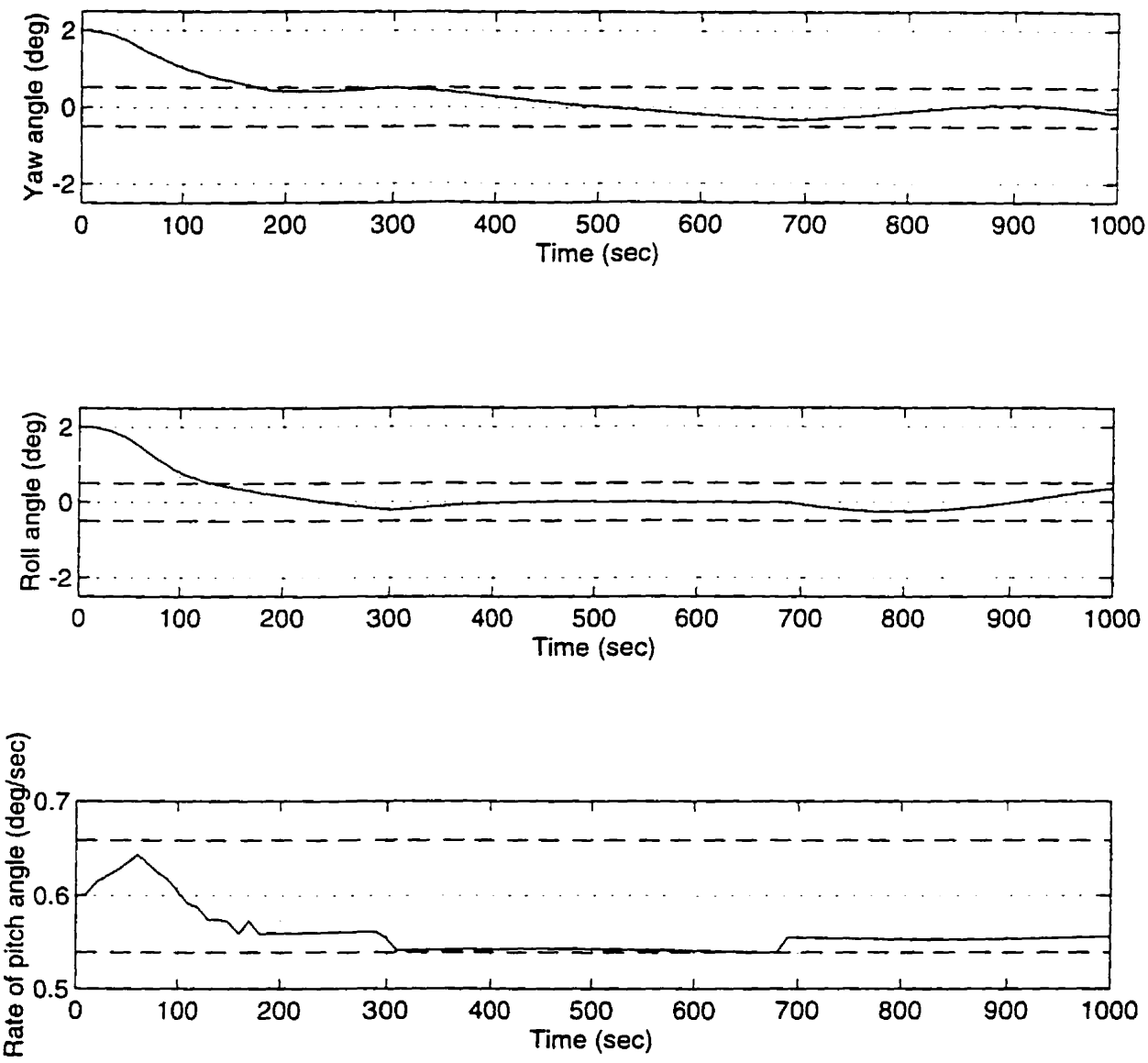

Figure 5.11a Spin Stabilization: Attitude Angles

(Rigid Case, Start at Apogee)

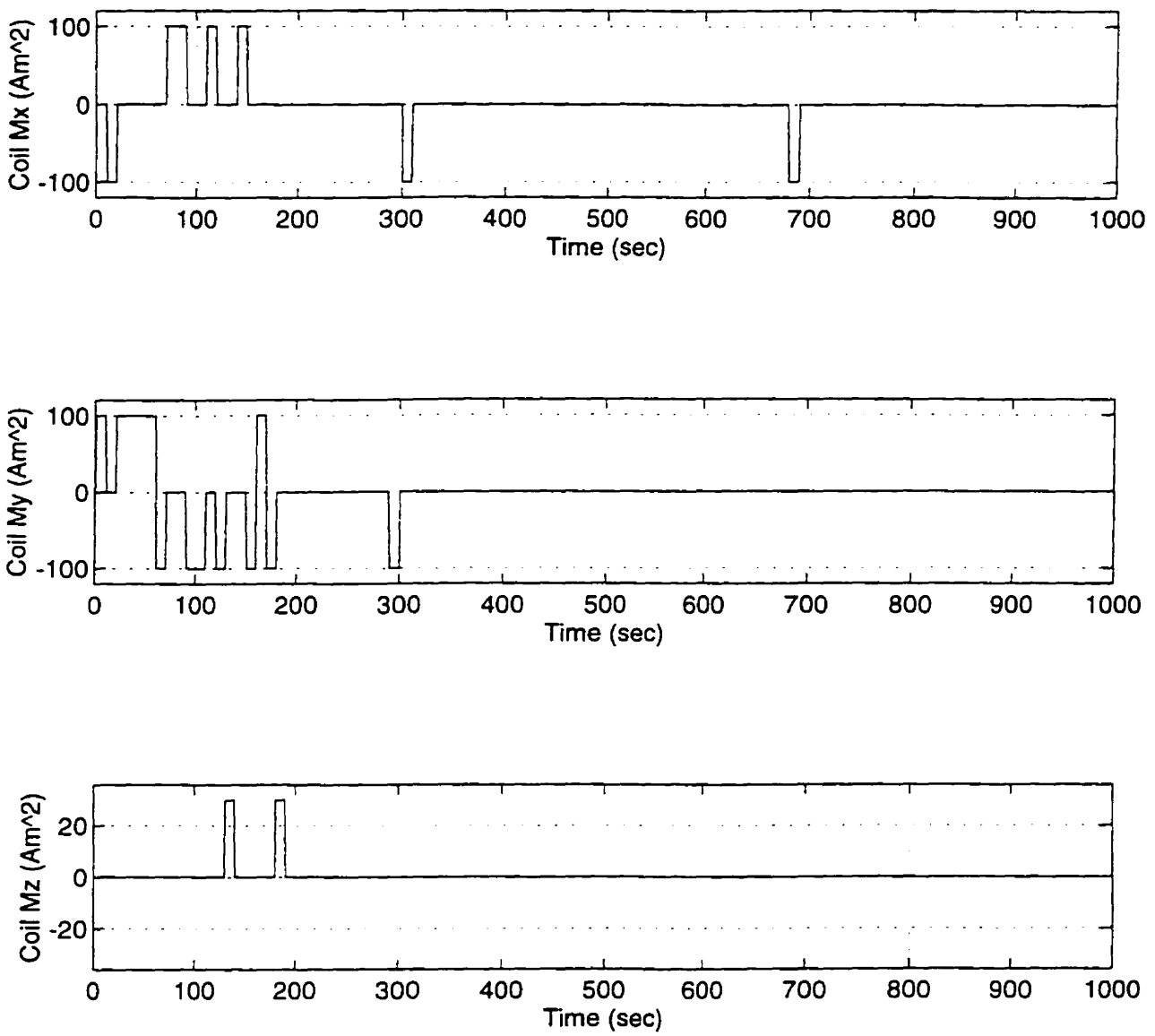

Figure 5.11b Spin Stabilization: Coil Switching

(Rigid Case, Start at Apogee)

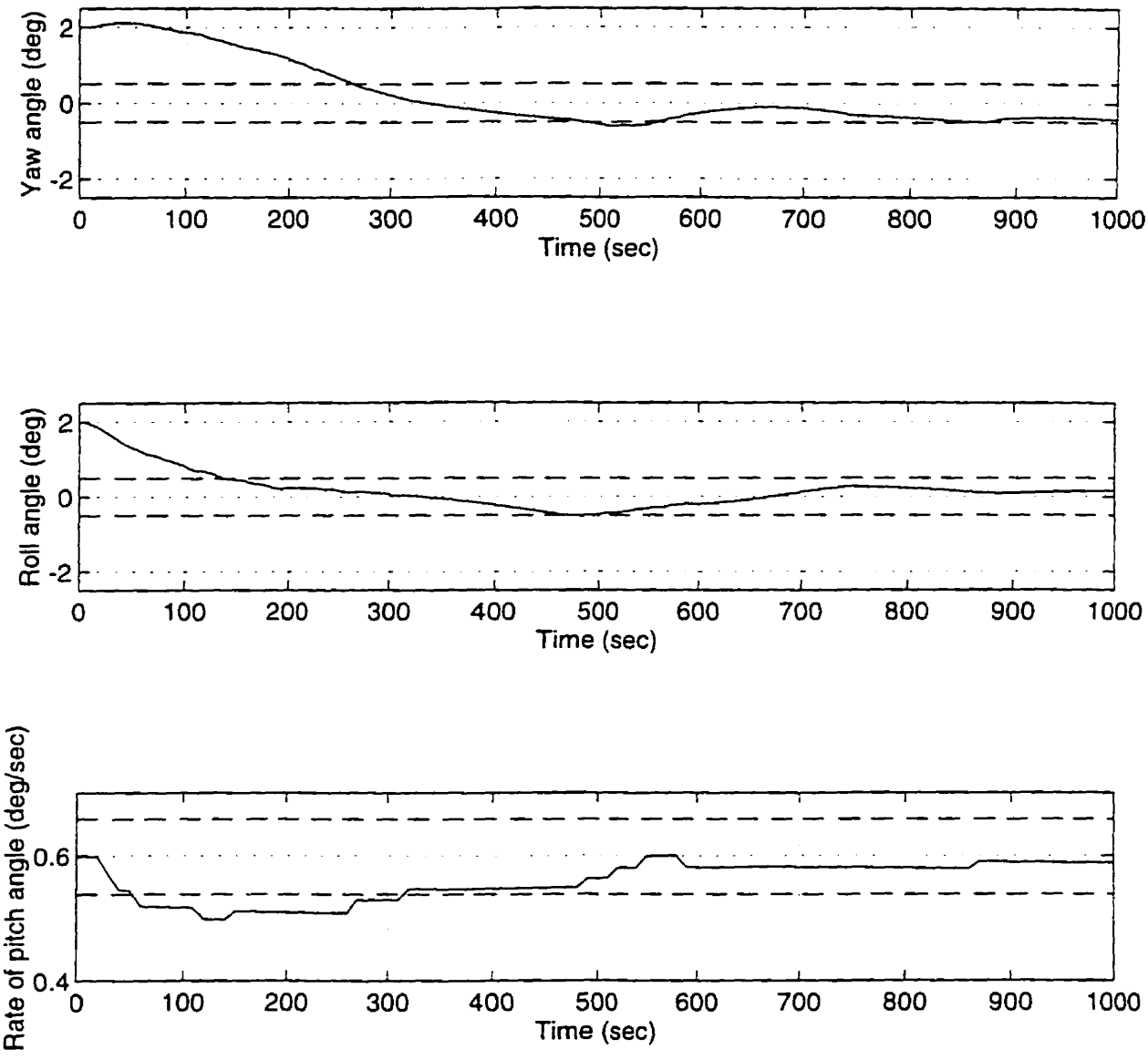

Figure 5.12a Spin Stabilization: Attitude Angles

(Rigid Case, Start at South Pole)

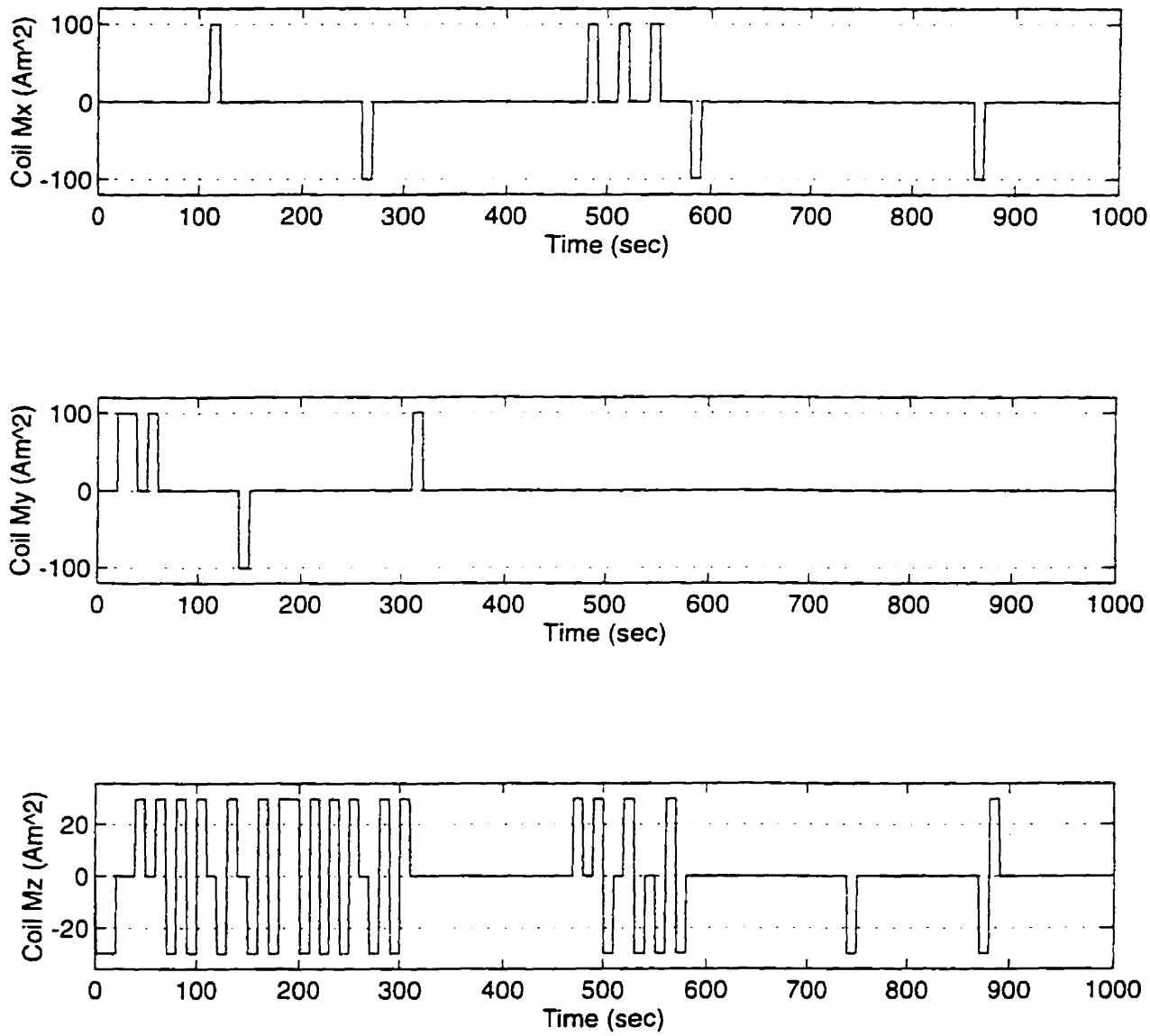

Figure 5.12b Spin Stabilization: Coil Switching

(Rigid Case, Start at South Pole)

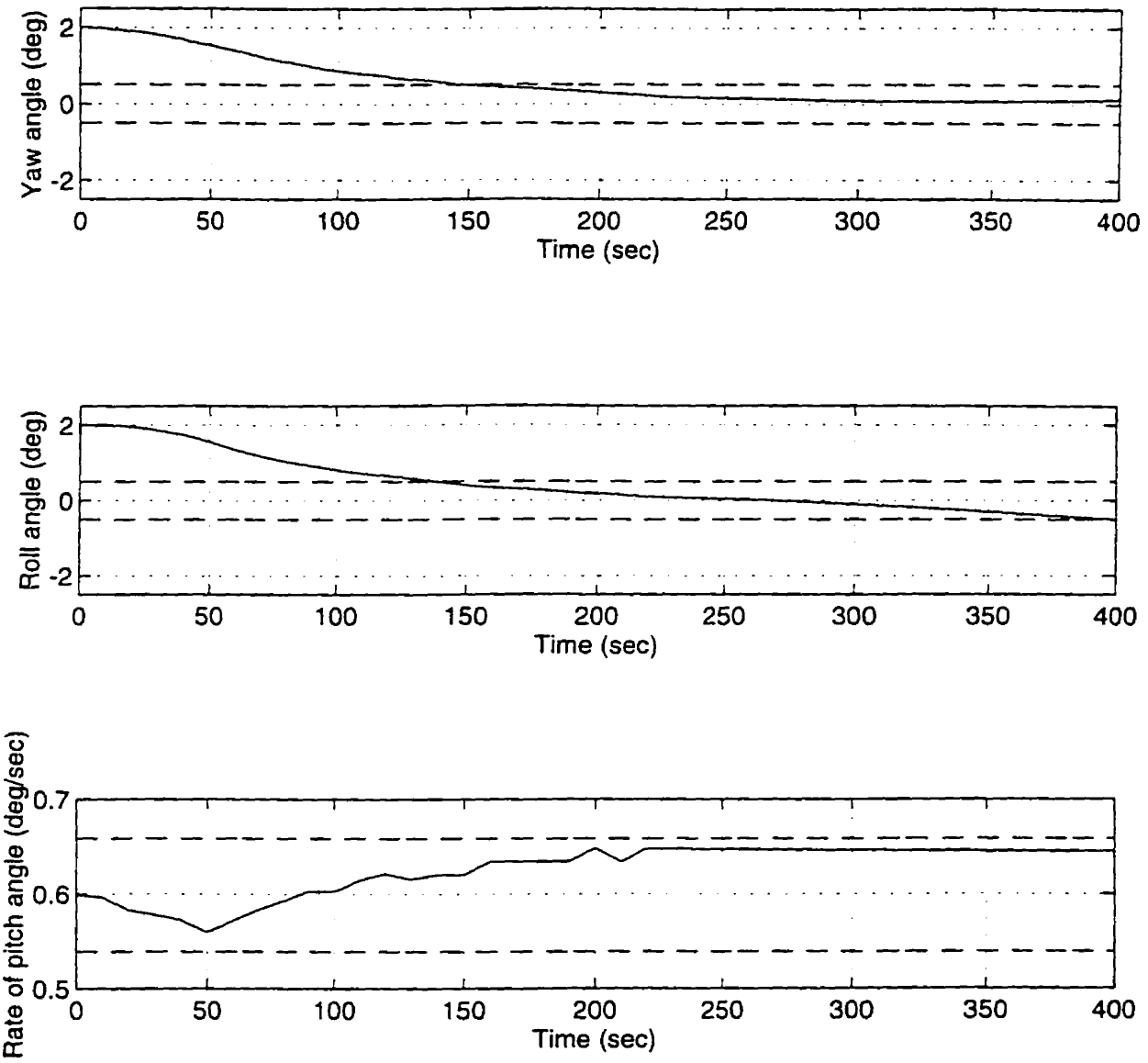

Figure 5.13a Spin Stabilization: Attitude Angles

(Expansion of Figure 5.9a)

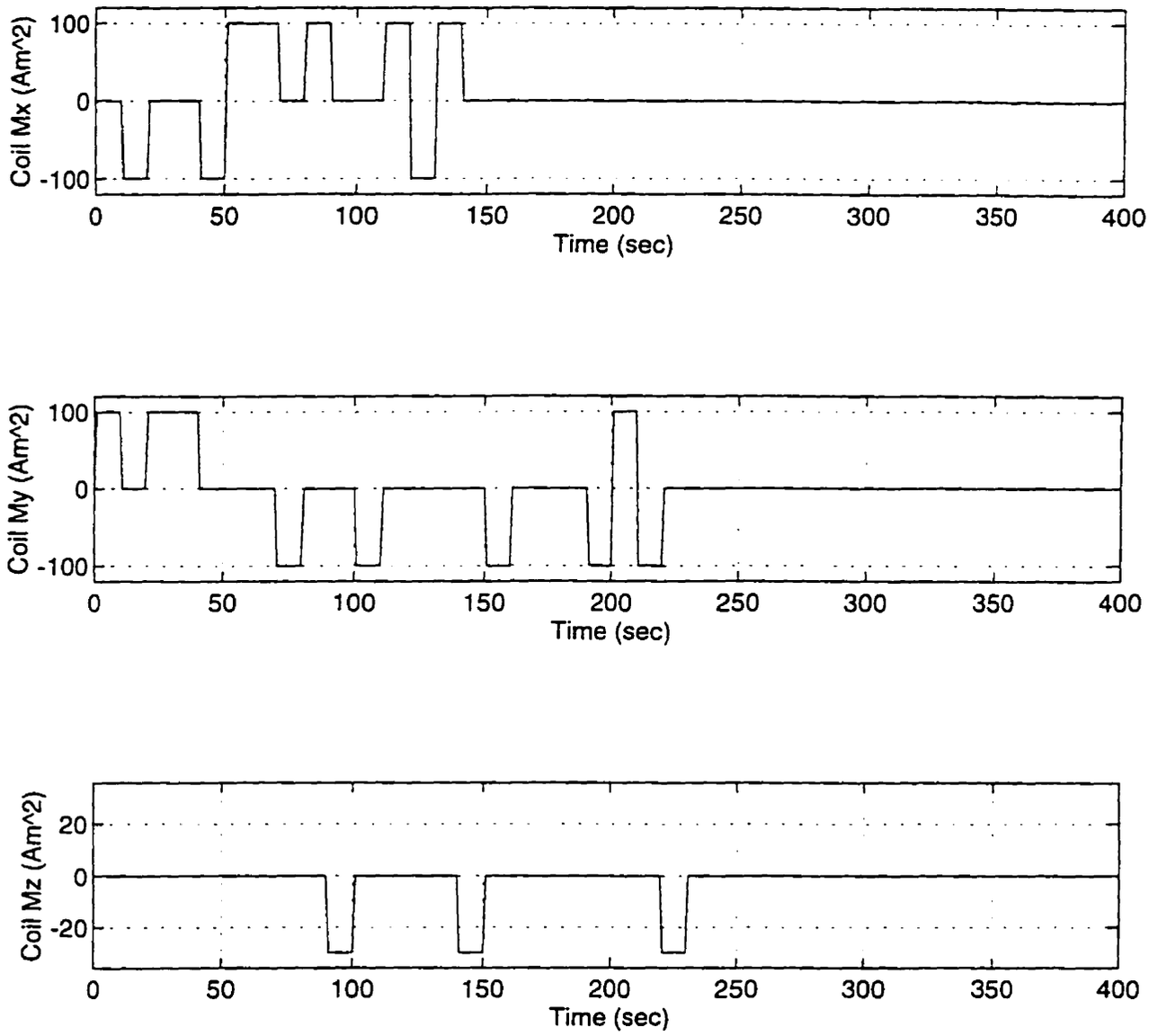

Figure 5.13b Spin Stabilization: Coil Switching

(Expansion of Figure 5.9b)

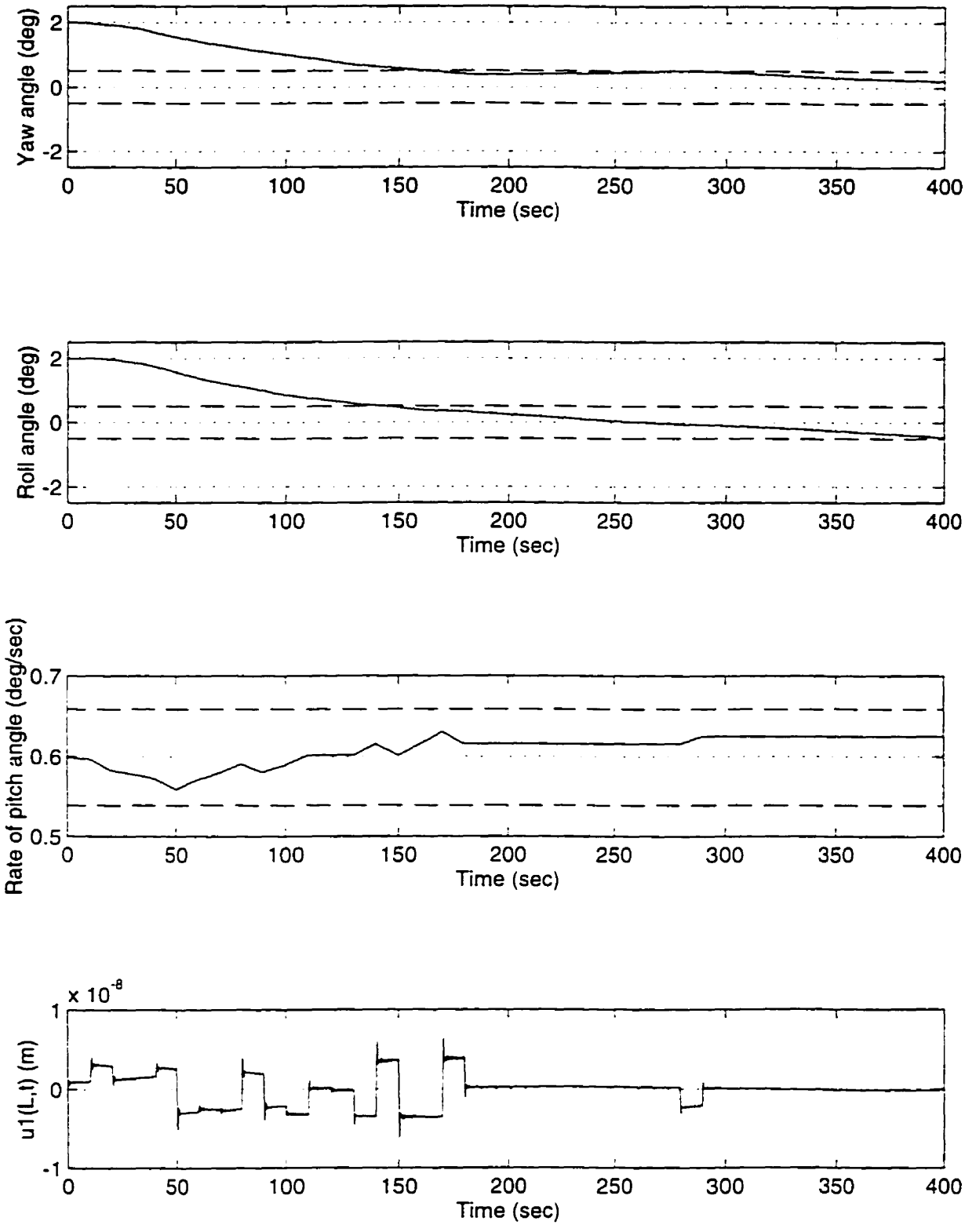

Figure 5.14a Spin Stabilization: Attitude Angles, In-Plane Tip Vibration
(Flexible Case, Rectangular cross-section, η=0.005, $EI_{in}=10^5$ Nm^2, $EI_{out}=10^3$ Nm^2)

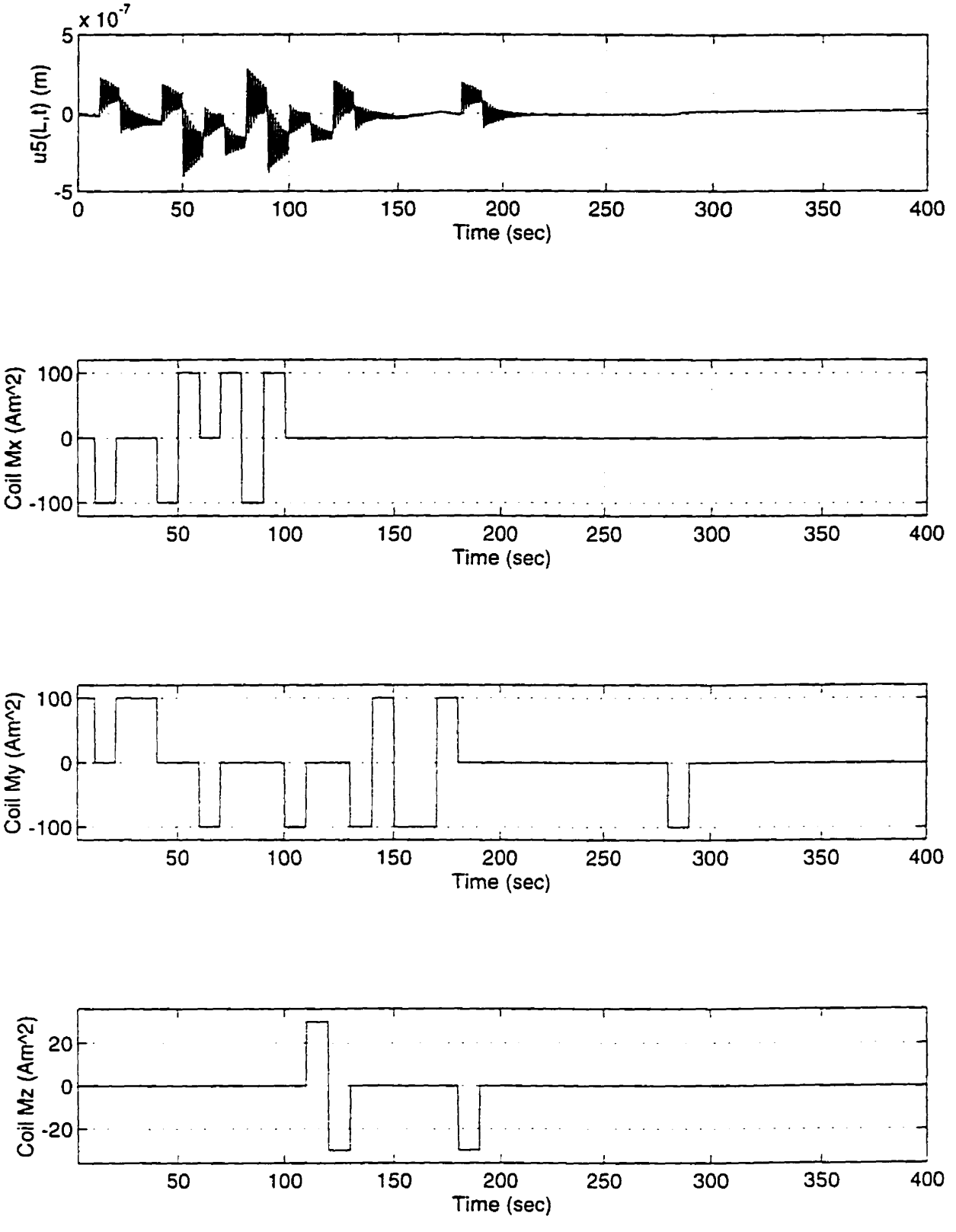

Figure 5.14b Spin Stabilization: Out of plane Tip Vibration, Coil Switching (Flexible Case, Rectangular cross-section, η=0.005, $EI_{in}=10^5$ Nm^2, $EI_{out}=10^3$ Nm^2)

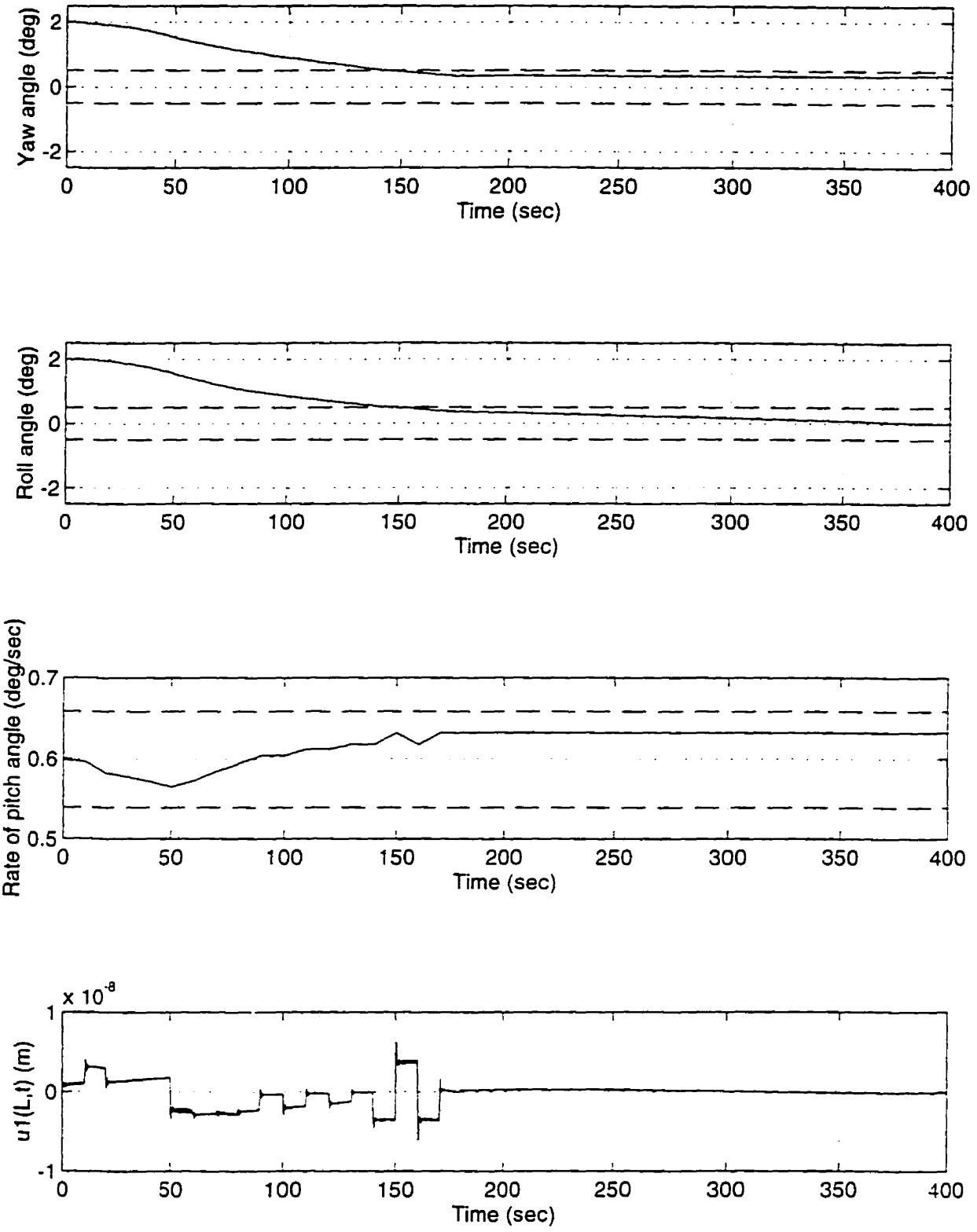

Figure 5.15a Spin Stabilization: Attitude Angles, In-Plane Tip Vibration

(Flexible Case, Rectangular cross-section, η=0.005, $EI_{in}=10^5$ Nm^2, $EI_{out}=10^2$ Nm^2)

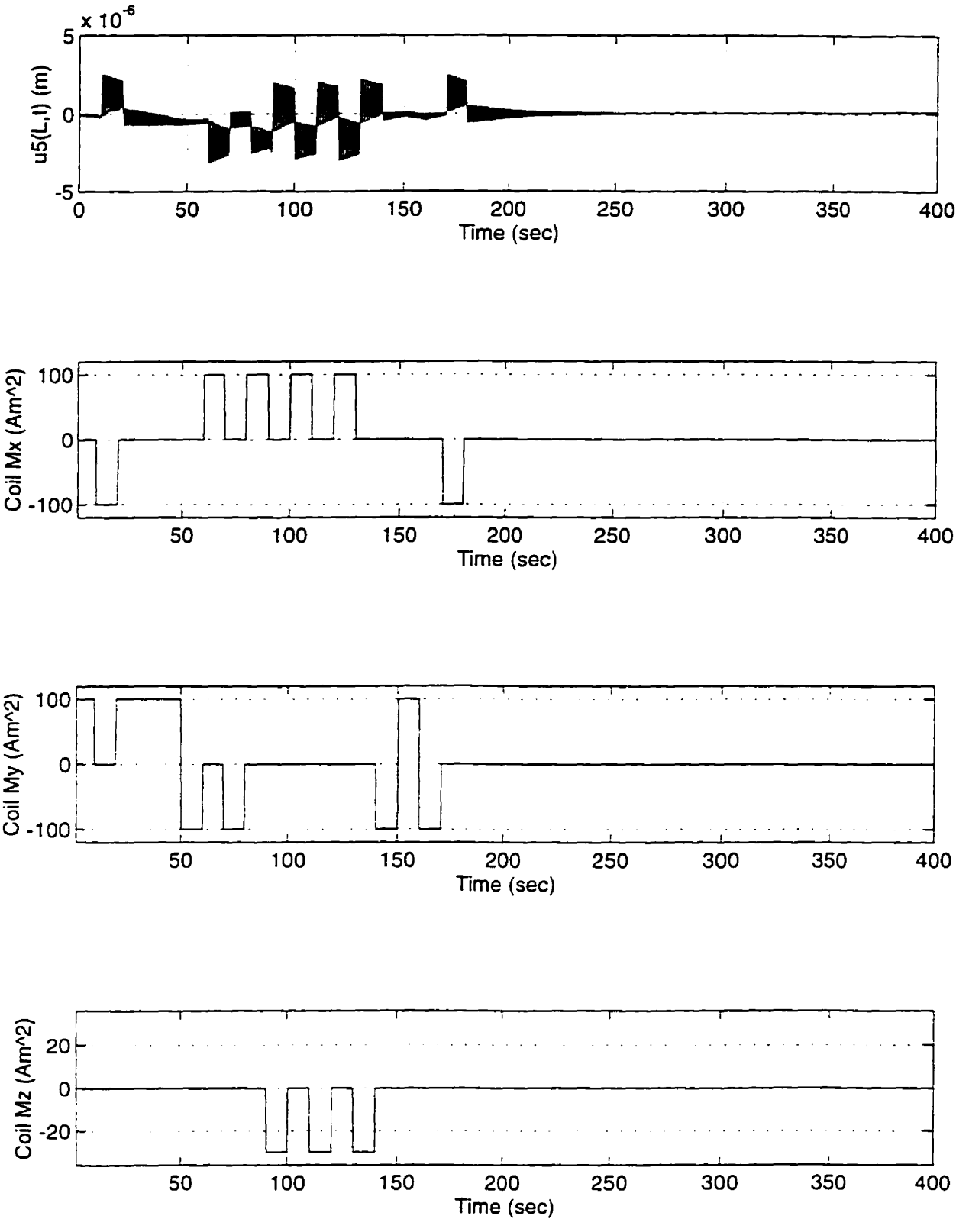

Figure 5.15b Spin Stabilization: Out of plane Tip Vibration, Coil Switching (Flexible Case, Rectangular cross-section, η=0.005, $EI_{in}=10^5$ Nm^2, $EI_{out}=10^2$ Nm^2)

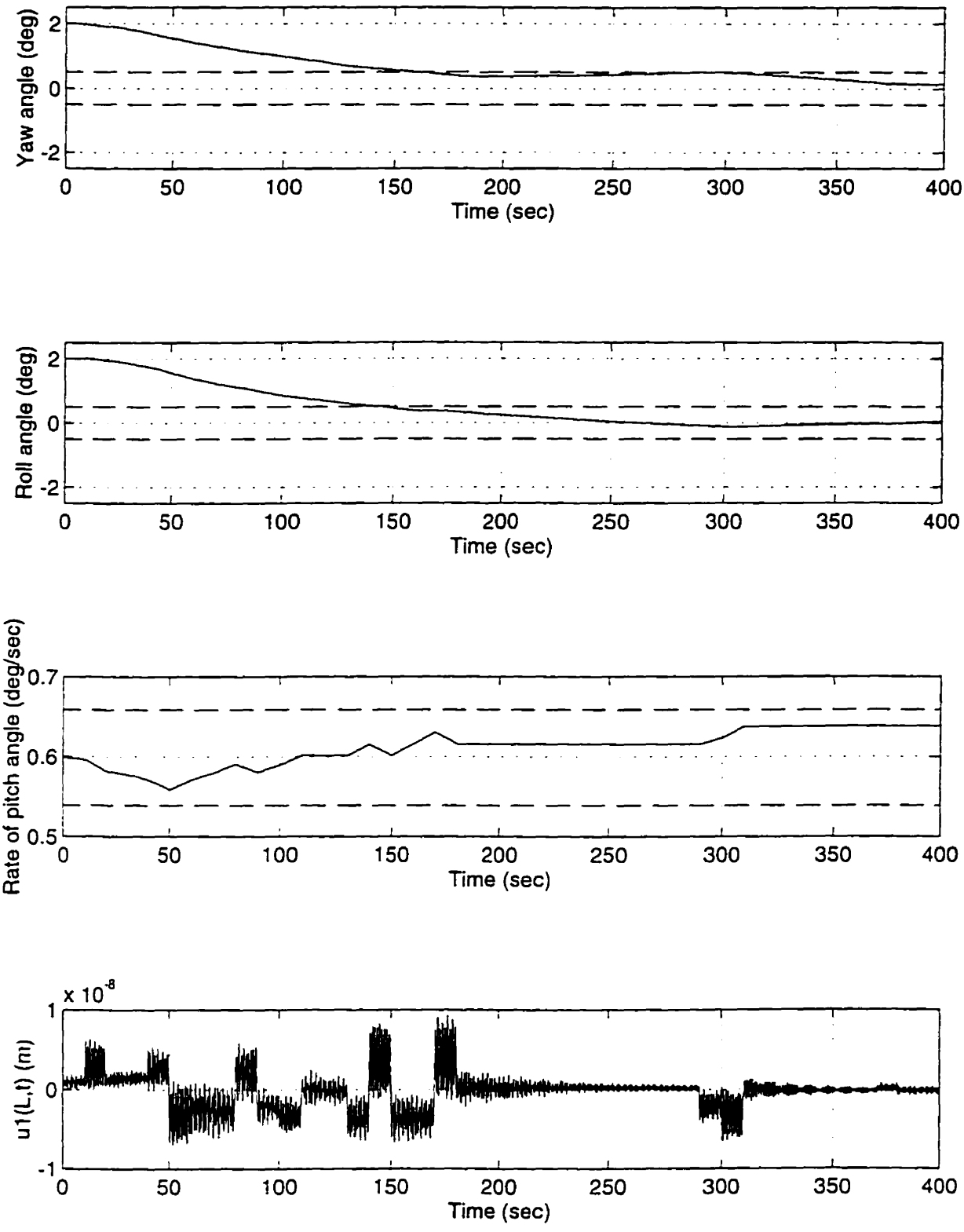

Figure 5.16a Spin Stabilization: Attitude Angles, In-Plane Tip Vibration
(Flexible Case, Rectangular cross-section, η=0.0, $EI_{in}=10^5$ Nm^2, $EI_{out}=10^2$ Nm^2)

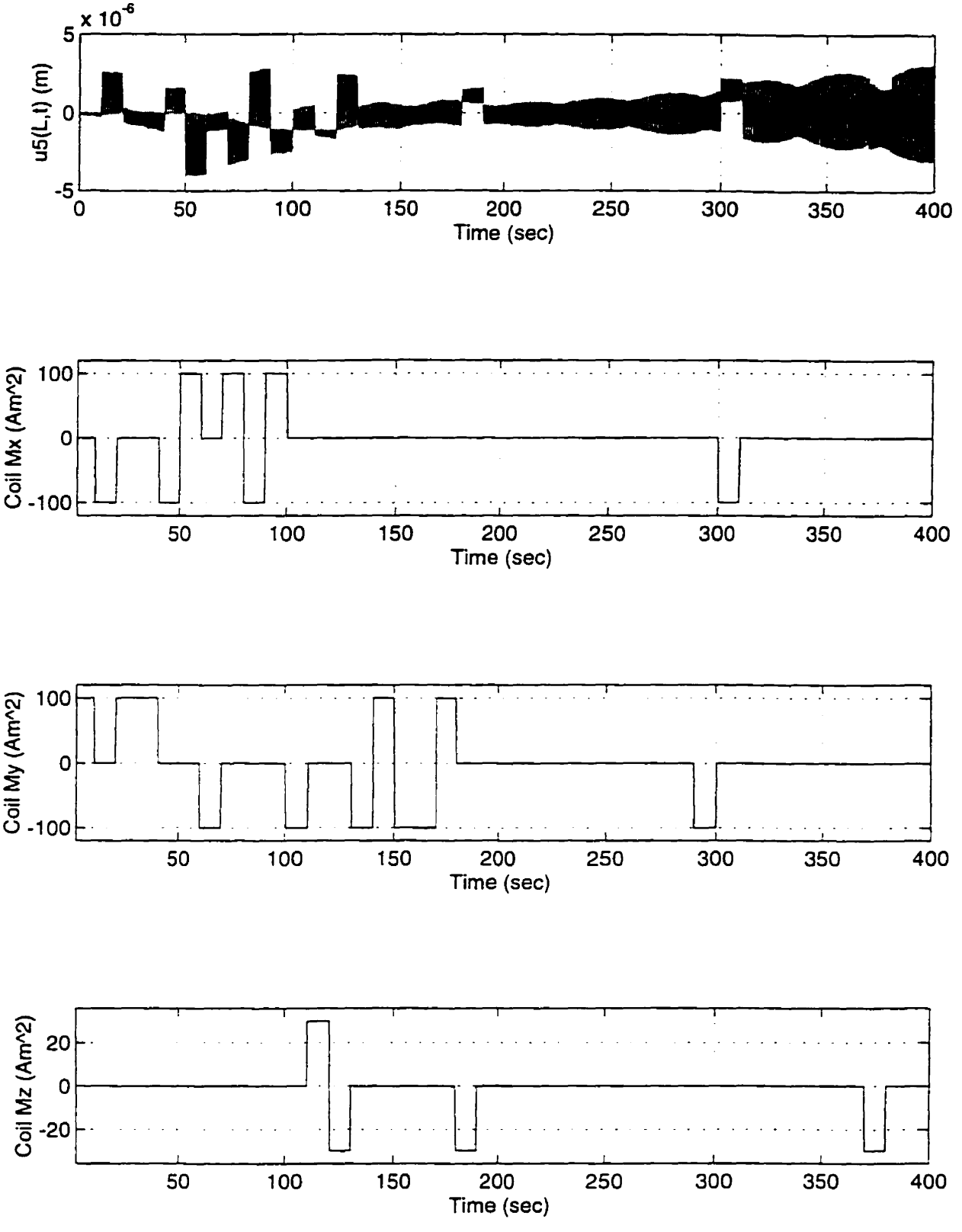

Figure 5.16b Spin Stabilization: Out of plane Tip Vibration, Coil Switching
(Flexible Case, Rectangular cross-section, η=0.0, $EI_{in}=10^5$ Nm^2, $EI_{out}=10^2$ Nm^2)

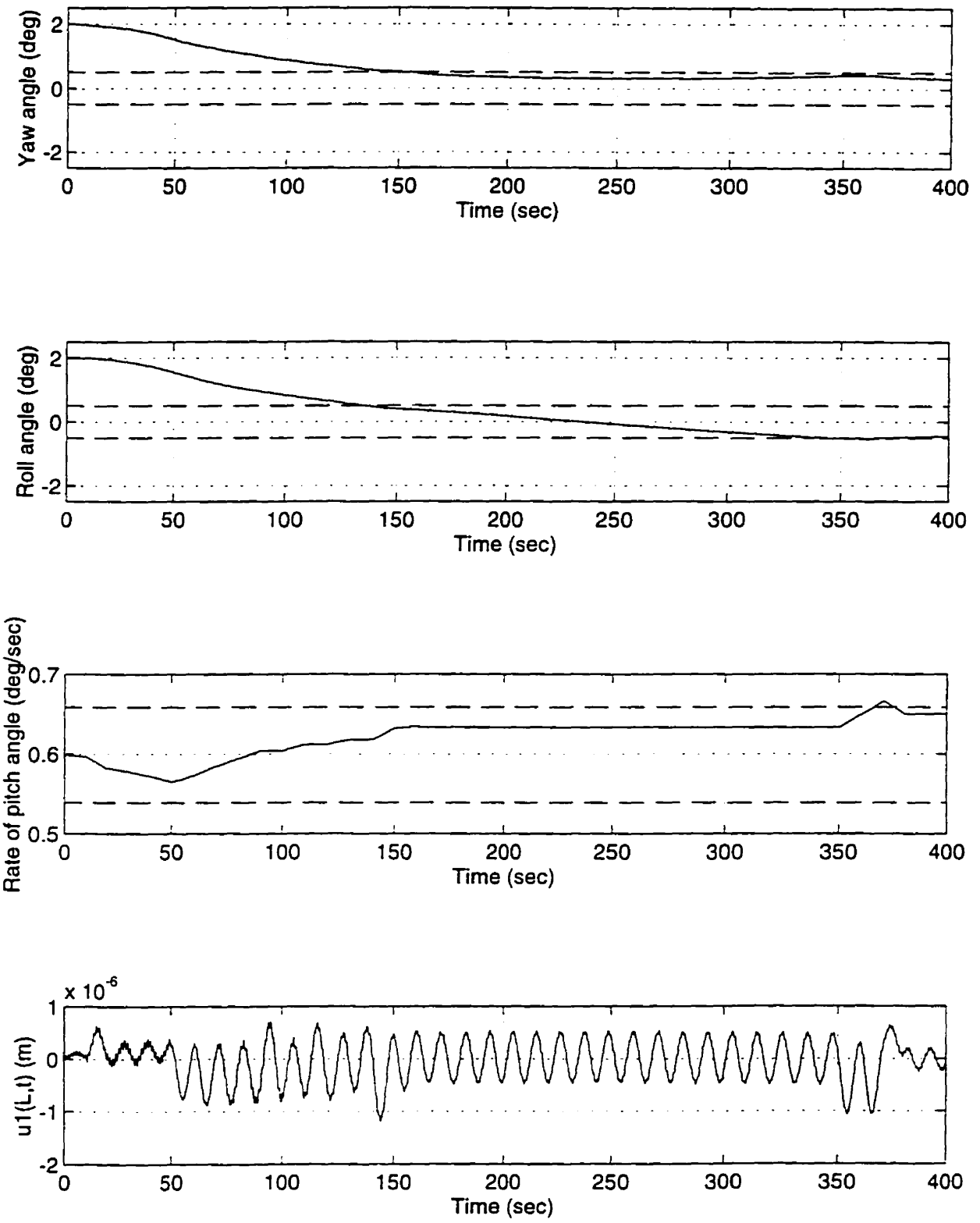

Figure 5.17a Spin Stabilization: Attitude Angles, In-Plane Tip Vibration (Flexible Case, Circular cross-section, η=0.0, $EI_{in}=10^3$ Nm^2, $EI_{out}=10^3$ Nm^2)

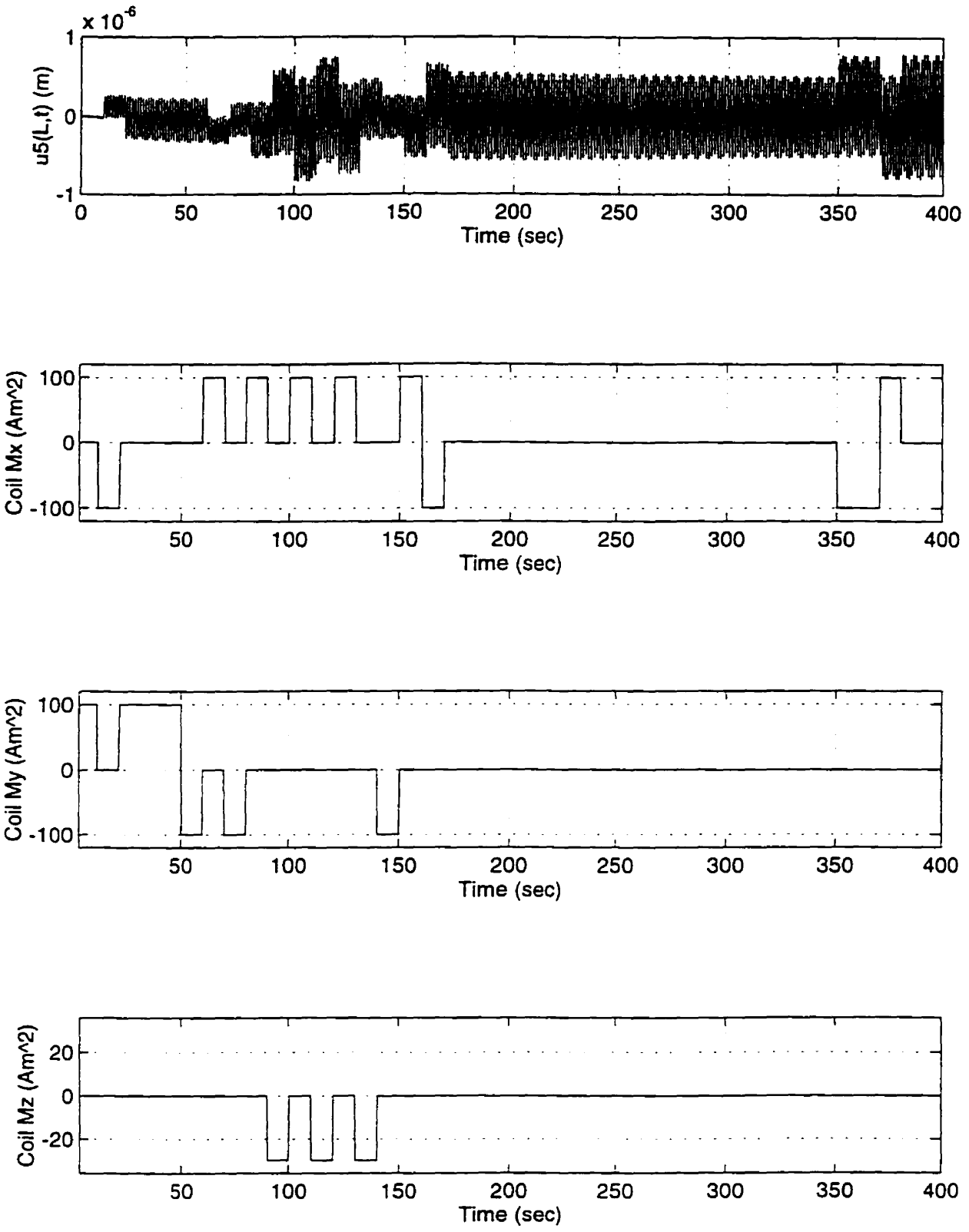

Figure 5.17b Spin Stabilization: Out of plane Tip Vibration, Coil Switching (Flexible Case, Circular cross-section, η=0.0, $EI_{in}=10^3$ Nm^2, $EI_{out}=10^3$ Nm^2)

Chapter 6

CLOSURE

6.1 Conclusion

This thesis studied the attitude control of a small satellite using fuzzy logic. A realistic satellite was modelled as a central rigid body with a set of flexible appendages. Equations of motion governing the bending vibrations of the appendages and the attitude motion of the satellite were derived using the Lagrangian method. The discretization of the flexible structures was carried out using the assumed mode method.

Two attitude controllers using fuzzy logic have been examined: one using small thrusters for a three-axis stabilization and a second one using magneto-torquers fed by a constant current for spin stabilization around the pitch axis. For each case, a set of control rules based on fuzzy logic was derived to control the polarity and switching time of the actuators.

In the case of three-axis stabilization, it was observed that the attitude motion can be controlled rapidly with thrusters of constant magnitude applied for a constant duration. Only four rules were needed to control each rotation. Even in the presence of environmental disturbances and uncontrolled vibrations of the appendages, the control could be achieved inside prescribed deadbands.

This successful approach was partly used in the design of the more complex controller for the spin stabilization about the orbit normal. When using magneto-torquers, severe constraints arise through the availability of the magnetic torque with the orbital position and due to the cross coupling between the axes. Also, additional constraints were imposed in order to deal with simplified actuators: coils have a constant magnitude and are

active for a constant duration. In spite of these control constraints and in the presence of environmental and flexible disturbances, the attitude motion could be controlled if small prescribed attitude errors are tolerated.

Through various simulations presented in this thesis, it has been shown that fuzzy logic control may be an alternative control scheme suitable for the attitude regulation of a spacecraft.

6.2 Recommendations

There are many possibilities for extension of the present work. Some of them are listed below.

(i) In the closed loop part of the control system, sensing of the attitude errors was considered as perfect. In general however, sensors include some noise and could be taken into account as an additional disturbance.

(ii) All state variables were assumed to be available. State observers could be considered in the control loops for the attitude regulation of the satellite.

(iii) In this thesis, controllers were designed to achieve some specific objectives without any optimization, which could be studied in future work.

(iv) Other simple flexible appendages could be introduced in the attitude dynamics model, such as paraboloid antennas.

(v) The reduction of the state vector of the flexible appendages can induce control spillover, which could be studied.

(vi) Stability of a fuzzy logic controller can rarely be proven analytically. New stability criteria should then be developed.

(vii) Difficulty in fuzzy logic control design lies in the definition of the membership functions and in the tuning of the control rules, which often requires a trial and error approach. However, this could be avoided by considering meta-rules tuning automatically the control rules and resulting in a self-adapting controller.

REFERENCES

[Balas'78] Balas M. J., "Active Control of Flexible Systems,"*Journal of Optimization Theory and Applications*, Vol. 25, No. 3, pp. 415-436.

[Banerjee et al.'90] Banerjee A. K., Dickens J. M., "Dynamics of an Arbitrary Flexible Body in Large Rotation and Translation," *Journal of Guidance, Control and Dynamics*, Vol. 13, No. 2, pp. 221-227.

[Berenji et al.'93] Berenji H. R., Lea R. N., Jani Y., Khedkar P., Malkani A., Hoblit J., "Space Shuttle Attitude Control by Reinforcement Learning and Fuzzy Logic," *1993 IEEE International Conference on Fuzzy Systems*, Vol. 2, pp. 1396-1401.

[Blakely'95] Blakely R. J., "Geomagnetic Field Potential Theory in Gravity and Magnetic Applications," *Cambridge University Press*, 1995, pp. 154-169.

[Bryson'94] Bryson A. E., *Control of Spacecraft and Aircraft*, Princeton University Press, 1994.

[Chiang et al.'94] Chiang R. Y., Jang J.-S. R., "Fuzzy Logic Attitude Control for Cassini Spacecraft," *1994 IEEE International Conference on Fuzzy Systems*, Vol. 3, pp. 1532-1537.

[Cvetkovic et al.'93] Cvetkovic S. R., Robertson G. J., "Spacecraft Design Considerations for Small Satellite Remote Sensing," *IEEE Transactions on Aerospace and Electronic*

Systems, Vol. 29, No. 2, pp. 391-403.

[Hanagud et al.'89] Hanagud S., Sarkar S., "Problem of the Dynamics of a Cantilever Beam Attached to a Moving Base," *Journal of Guidance, Control and Dynamics*, Vol. 12, No. 3, pp. 438-441.

[Hodgart et al.'87] Hodgart M. S., Wright P. S., "Attitude Determination, Control and Stabilization of UoSat-2," *Journal of the Institution of Electronic and Radio Engineers*, Vol. 57, No.5 (Supplement), pp. S151-S162.

[Horais'91] Horais B., "Small-Satellite Technology and Applications," *Proceedings of SPIE - The International Society for Optical Engineering*, International Society for Optical Engineering, Bellingham, WA, USA, Vol. 1495, 287 pages (28 papers), 1991.

[Hughes'73] Hughes P. C., "Recent Advances in the Attitude Dynamics of Spacecraft with Flexible Solar Arrays," *Canadian Aeronautics and Space Journal*, Vol. 19, No. 4, pp. 165-171.

[Hughes'86] Hughes P. C., *Spacecraft Attitude Dynamics*, J. Wiley, 1986.

[Huston'91] Huston R. L., "Multibody Dynamics - Modeling and Analysis Methods," *Applied Mechanics Reviews*, Vol. 44, No. 3, pp. 109-117.

[Huston et al.'95] Huston R. L., Zhang D., "Recent Advances in Modeling Flexible Multibody Systems," *Advances in the Astronautical Sciences*, Vol. 90, Part 2, pp. 1453-1472.

[Junkins'90] Junkins J. L., "Mechanics and Control of Large Flexible Structures," *Progress in Astronautics and Aeronautics*, Vol. 129.

[Kalaycioglu'87] Kalaycoglu S., "Effect of Offset of the Point of Attachment on the Dynamics and Stability of Spinning Flexible Appendages," *AAS/AIAA Astrodynamics Specialist Conference*, Kalispell, Montana, August 10-13, 1987.

[Kane et al.'87] Kane T. R., Ryan R. R., Banerjee A. K., "Dynamics of a Cantilever Beam Attached to a Moving Base," *Journal of Guidance, Control and Dynamics*, Vol. 10, No. 2, pp. 139-151.

[Kaplan'76] Kaplan M. H., *Modern Spacecraft Dynamics and Control*, John Wiley and Sons, 1976.

[Karray et al.'93] Karray F., Modi V. J., Mah H., "A Composite Control Scheme For Joint Tracking and Active Vibration Suppression of Mobile Flexible Manipulator Systems," *Advances in the Astronautical Sciences*, Vol. 85, Part 3, pp. 2283-2300.

[Lee'90] Lee C. C., "Fuzzy Logic in Control Systems: Fuzzy Logic Controller, Part I&II," *IEEE Transactions on Systems, Man, and Cybernetics*, Vol. 20, No. 2, pp. 404-435.

[Likins et al.'71] Likins P. W., Bouvier H. K., "Attitude Control of Nonrigid Spacecraft," *Astronautics and Aeronautics*, Vol. 9, No. 5, pp. 64-71.

[Matsuzaki et al.'94] Matsuzaki Y., Abe S., "Fuzzy Logic Control of Three-Dimensional Motion of a Tethered Satellite System," *Proceedings of the AIAA/ASME/AHS/ASC Structures, Structural Dynamics, and Material Conference*, Vol. 4, 1994, New York, NY, USA, AIAA-94-1617-CP, pp. 2378-2383.

[Meirovitch et al.'66] Meirovitch L., Nelson H. D., "High-Spin Motion of a Satellite Containing Elastic Parts," *Journal of Spacecraft and Rockets*, Vol. 3, No. 11, pp. 1597-1602.

[Meirovitch et al.'77] Meirovitch L., Van Landingham H. F. ,"Control of Spinning Flexible Spacecraft by Modal Synthesis," *Acta Astronautica*, Vol. 4, pp. 985-1010.

[Meirovitch et al.'83] Meirovitch L., Baruh H., Öz H., "A Comparison of Control Techniques for Large Flexible Systems," *Journal of Guidance, Control and Dynamics*, Vol. 6, No. 4, pp. 302-310.

[Meirovitch'91] Meirovitch L., "Hybrid State Equations of Motion for Flexible Bodies in Terms of Quasi-Coordinates," *Journal of Guidance, Control and Dynamics*, Vol. 14, No. 5, pp. 1008-1013.

[Modi'74] Modi V. J., "Attitude Dynamics of Satellites with Flexible Appendages - A Brief Review," *Journal of Spacecraft*, Vol. 11, No. 11, pp. 743-751.

[Öz et al.'80] Öz H., Meirovitch L., "Optimal Modal-Space Control of Flexible Gyroscopic Systems," *Journal of Guidance and Control*, Vol. 3, No. 1, pp. 218-226.

[Sadigh et al.'93] Sadigh M. J., Misra A. K., "More on the so-called Dynamic Stiffening Effect," *Advances in the Astronautical Sciences*, Vol. 85, Part 3, pp. 2301-2320.

[Satyadas et al.'95] Satyadas A., Krishnakumar K., "GA-optimized Fuzzy Controller for Spacecraft Attitude Control," *IEEE International Conference on Industrial Automation and Control, Proceedings 1995*, IEEE, Piscataway, NJ, USA, 95TH8005, pp. 121-126.

[Steyn'94] Steyn W. H., "Comparison of Low-Earth-Orbit Satellite Controllers Submitted to Controllability Constraints," *Journal of Guidance, Control and Dynamics*, Vol. 17, No. 4, pp. 795-804.

[Tribble'95] Tribble A. C., *The Space Environment: Implications for Spacecraft Design*, Princeton University Press, 1995.

[Vigneron'71] Vigneron F. R., "Stability of a Freely Spinning Satellite of Crossed-Dipole Configuration," *Transactions of the Canadian Aeronautics and Space Institute*,Vol. 3, No. 1, pp. 8-19.

[Ying et al.'90] Ying H., Siler W., Buckley J. J., "Fuzzy Control Theory: A Nonlinear Case," *Automatica*, Vol. 26, No. 3, pp. 513-520.

[Wang'94] Wang L.-X., *Adaptive Fuzzy Systems and Control: Design and Stability Analysis*, Englehoods Cliffs, Prentice Hall, 1994.

Appendix A

ADMISSIBLE FUNCTIONS AND ASSOCIATED INTEGRALS

The eigenfunctions of a cantilever beam undergoing bending are given by:

$$\Phi_n(\xi) = [\cosh(\lambda_n\xi) - \cos(\lambda_n\xi)] - \sigma_n[\sinh(\lambda_n\xi) - \sin(\lambda_n\xi)],\ 0 \le \xi \le 1 \qquad (A.1)$$

$$\text{where } \sigma_n = \frac{\cos(\lambda_n) + \cosh(\lambda_n)}{\sin(\lambda_n) + \sinh(\lambda_n)}, \qquad (A.2)$$

and λ_n are the roots of the characteristic equation:

$$\cos(\lambda)\cosh(\lambda) + 1 = 0 \qquad (A.3)$$

The vectors and matrices defined in Eqs.(2.8), (2.9), (2.14) and (2.21) can be obtained analytically and are presented in the following two tables.

Vector	Expression	Example
$\mathbf{c}_{1i}$	$\frac{2}{\lambda_i^2}$	$(\mathbf{c}_1)_1$=0.5688
$\mathbf{c}_{2i}$	$\frac{2\sigma_i}{\lambda_i}$	$(\mathbf{c}_2)_1$=0.7829

Table A.1 Expressions of Nondimensional Vectors

Matrix	Expression		Example
$\mathbf{M}_{ij}$	δ_{ij}		$\mathbf{M}_{11}=1$
$\mathbf{D}_{ij}$	$\delta_{ij}\lambda_i^2$		$\mathbf{D}_{11}=3.5160$
$\mathbf{K}_{ij}$	$\delta_{ij}\lambda_i^4$		$\mathbf{K}_{11}=12.3623$
$\mathbf{C}_{3ij}$	$i=j$	$\frac{5}{4}+\frac{\sigma_i^2\lambda_i^2}{3}-\frac{\sigma_i\lambda_i}{2}$	$(\mathbf{C}_3)_{11}=1.1933$
	$i\neq j$	$-\frac{16(-1)^{i+j}\lambda_i^4\lambda_j^4}{(\lambda_j^4-\lambda_i^4)^2}-\frac{2\lambda_i^2\lambda_j^2(\sigma_j\lambda_j-\sigma_i\lambda_i)}{\lambda_j^4-\lambda_i^4}$	$(\mathbf{C}_3)_{12}=-0.6858$
$\mathbf{C}_{4ij}$	$i=j$	$2+\frac{\sigma_i^2\lambda_i^2}{2}-\sigma_i\lambda_i$	$(\mathbf{C}_4)_{11}=1.5708$
	$i\neq j$	$\frac{8\lambda_i^2\lambda_j^2}{(\lambda_j^2+(-1)^{i+j}\lambda_i^2)^2}-\frac{4\lambda_i^2\lambda_j^2(\sigma_j\lambda_j-\sigma_i\lambda_i)}{\lambda_j^4-\lambda_i^4}$	$(\mathbf{C}_4)_{12}=-0.4223$

Table A.2 Expressions of Nondimensional Matrices

Appendix B

SPACECRAFT INERTIA AND APPENDAGE EQUATIONS

B.1 Spacecraft Inertia Matrix

The inertia matrix **I** of the spacecraft about its centre of mass and expressed in the body fixed frame can be written as:

$$\mathbf{I} = \begin{bmatrix} A & -F & -E \\ -F & B & -D \\ -E & -D & C \end{bmatrix} \tag{B.1}$$

where (A, B, C) and (D, E, F) are respectively the moments and the products of inertia of the spacecraft about its centre of mass.

The moments of inertia can be written in terms of the generalized coordinates:

$$\begin{aligned} A(\mathbf{q}) = {} & I_{Tcb} + 2\rho L(a^2 + 2h^2 + \frac{L^2}{3} + aL) + 2\rho L^2 h(\mathbf{q}_7 - \mathbf{q}_5 + \mathbf{q}_6 - \mathbf{q}_8)^T \mathbf{c}_2 \\ & - \rho L^3[\mathbf{q}_2^T(\frac{a}{L}\mathbf{C}_4 + \mathbf{C}_3)\mathbf{q}_2 + \mathbf{q}_4^T(\frac{a}{L}\mathbf{C}_4 + \mathbf{C}_3)\mathbf{q}_4 + \mathbf{q}_6^T(\frac{a}{L}\mathbf{C}_4 + \mathbf{C}_3)\mathbf{q}_6 + \mathbf{q}_8^T(\frac{a}{L}\mathbf{C}_4 + \mathbf{C}_3)\mathbf{q}_8] \\ & + \rho L^3(\mathbf{q}_1^T\mathbf{M}\mathbf{q}_1 + \mathbf{q}_3^T\mathbf{M}\mathbf{q}_3 + \mathbf{q}_5^T\mathbf{M}\mathbf{q}_5 + \mathbf{q}_6^T\mathbf{M}\mathbf{q}_6 + \mathbf{q}_7^T\mathbf{M}\mathbf{q}_7 + \mathbf{q}_8^T\mathbf{M}\mathbf{q}_8) \end{aligned} \tag{B.2}$$

$$\begin{aligned} B(\mathbf{q}) = {} & I_{Tcb} + 2\rho L(a^2 + 2h^2 + \frac{L^2}{3} + aL) + 2\rho L^2 h(\mathbf{q}_7 - \mathbf{q}_5 + \mathbf{q}_6 - \mathbf{q}_8)^T \mathbf{c}_2 \\ & - \rho L^3[\mathbf{q}_1^T(\frac{a}{L}\mathbf{C}_4 + \mathbf{C}_3)\mathbf{q}_1 + \mathbf{q}_3^T(\frac{a}{L}\mathbf{C}_4 + \mathbf{C}_3)\mathbf{q}_3 + \mathbf{q}_5^T(\frac{a}{L}\mathbf{C}_4 + \mathbf{C}_3)\mathbf{q}_5 + \mathbf{q}_7^T(\frac{a}{L}\mathbf{C}_4 + \mathbf{C}_3)\mathbf{q}_7] \\ & + \rho L^3(\mathbf{q}_2^T\mathbf{M}\mathbf{q}_2 + \mathbf{q}_4^T\mathbf{M}\mathbf{q}_4 + \mathbf{q}_5^T\mathbf{M}\mathbf{q}_5 + \mathbf{q}_6^T\mathbf{M}\mathbf{q}_6 + \mathbf{q}_7^T\mathbf{M}\mathbf{q}_7 + \mathbf{q}_8^T\mathbf{M}\mathbf{q}_8) \end{aligned} \tag{B.3}$$

$$C(\mathbf{q}) = I_{Zb} + 4\rho L(a^2 + \frac{L^2}{3} + aL) + \rho L^3(\mathbf{q}_1^T\mathbf{M}\mathbf{q}_1 + \mathbf{q}_2^T\mathbf{M}\mathbf{q}_2 + \mathbf{q}_3^T\mathbf{M}\mathbf{q}_3 + \mathbf{q}_4^T\mathbf{M}\mathbf{q}_4)$$
$$-\rho L^3[\mathbf{q}_1^T(\frac{a}{L}\mathbf{C}_4 + \mathbf{C}_3)\mathbf{q}_1 + \mathbf{q}_3^T(\frac{a}{L}\mathbf{C}_4 + \mathbf{C}_3)\mathbf{q}_3 + \mathbf{q}_5^T(\frac{a}{L}\mathbf{C}_4 + \mathbf{C}_3)\mathbf{q}_5 + \mathbf{q}_7^T(\frac{a}{L}\mathbf{C}_4 + \mathbf{C}_3)\mathbf{q}_7] \quad (B.4)$$
$$-\rho L^3[\mathbf{q}_2^T(\frac{a}{L}\mathbf{C}_4 + \mathbf{C}_3)\mathbf{q}_2 + \mathbf{q}_4^T(\frac{a}{L}\mathbf{C}_4 + \mathbf{C}_3)\mathbf{q}_4 + \mathbf{q}_6^T(\frac{a}{L}\mathbf{C}_4 + \mathbf{C}_3)\mathbf{q}_6 + \mathbf{q}_8^T(\frac{a}{L}\mathbf{C}_4 + \mathbf{C}_3)\mathbf{q}_8]$$

Similarly, the products of inertia are:

$$D(\mathbf{q}) = -\rho L^3(\mathbf{q}_1^T\mathbf{M}\mathbf{q}_5 + \mathbf{q}_3^T\mathbf{M}\mathbf{q}_7) + \frac{\rho L^2 h}{2}(-\mathbf{q}_2^T\mathbf{C}_4\mathbf{q}_2 + \mathbf{q}_4^T\mathbf{C}_4\mathbf{q}_4 - \mathbf{q}_6^T\mathbf{C}_4\mathbf{q}_6 + \mathbf{q}_8^T\mathbf{C}_4\mathbf{q}_8) \quad (B.5)$$
$$+\rho L^2 h(\mathbf{q}_1 - \mathbf{q}_3)^T\mathbf{c}_2 + \rho L^3(\mathbf{q}_6 + \mathbf{q}_8)^T(\mathbf{c}_1 + \frac{a}{L}\mathbf{c}_2)$$

$$E(\mathbf{q}) = -\rho L^3(\mathbf{q}_4^T\mathbf{M}\mathbf{q}_8 + \mathbf{q}_2^T\mathbf{M}\mathbf{q}_6) + \frac{\rho L^2 h}{2}(-\mathbf{q}_1^T\mathbf{C}_4\mathbf{q}_1 + \mathbf{q}_3^T\mathbf{C}_4\mathbf{q}_3 - \mathbf{q}_5^T\mathbf{C}_4\mathbf{q}_5 + \mathbf{q}_7^T\mathbf{C}_4\mathbf{q}_7) \quad (B.6)$$
$$+\rho L^2 h(\mathbf{q}_4 - \mathbf{q}_2)^T\mathbf{c}_2 - \rho L^3(\mathbf{q}_5 + \mathbf{q}_7)^T(\mathbf{c}_1 + \frac{a}{L}\mathbf{c}_2)$$

$$F(\mathbf{q}) = \rho L^3(\mathbf{q}_1 - \mathbf{q}_2 + \mathbf{q}_3 - \mathbf{q}_4)^T(\mathbf{c}_1 + \frac{a}{L}\mathbf{c}_2) \quad (B.7)$$

The components of the angular momentum vector $\Gamma(\mathbf{q}, \dot{\mathbf{q}})$ appearing in Eq.(2.5) are given as follows:

$$\Gamma_x(\mathbf{q}, \dot{\mathbf{q}}) = \rho L^3(\dot{\mathbf{q}}_1^T\mathbf{M}\mathbf{q}_5 - \dot{\mathbf{q}}_5^T\mathbf{M}\mathbf{q}_1 + \dot{\mathbf{q}}_3^T\mathbf{M}\mathbf{q}_7 - \dot{\mathbf{q}}_7^T\mathbf{M}\mathbf{q}_3) + \rho L^2 h(\dot{\mathbf{q}}_3 - \dot{\mathbf{q}}_1)^T\mathbf{c}_2$$
$$+\rho L^3(\dot{\mathbf{q}}_6 + \dot{\mathbf{q}}_8)^T(\frac{a}{L}\mathbf{c}_2 + \mathbf{c}_1) + \rho L^2 h(\dot{\mathbf{q}}_2^T\mathbf{C}_4\mathbf{q}_2 - \dot{\mathbf{q}}_4^T\mathbf{C}_4\mathbf{q}_4 + \dot{\mathbf{q}}_6^T\mathbf{C}_4\mathbf{q}_6 - \dot{\mathbf{q}}_8^T\mathbf{C}_4\mathbf{q}_8) \quad (B.8)$$

$$\Gamma_y(\mathbf{q}, \dot{\mathbf{q}}) = \rho L^3(\dot{\mathbf{q}}_6^T\mathbf{M}\mathbf{q}_2 - \dot{\mathbf{q}}_2^T\mathbf{M}\mathbf{q}_6 + \dot{\mathbf{q}}_8^T\mathbf{M}\mathbf{q}_4 - \dot{\mathbf{q}}_4^T\mathbf{M}\mathbf{q}_8) + \rho L^2 h(\dot{\mathbf{q}}_4 - \dot{\mathbf{q}}_2)^T\mathbf{c}_2$$
$$+\rho L^3(\dot{\mathbf{q}}_5 + \dot{\mathbf{q}}_7)^T(\frac{a}{L}\mathbf{c}_2 + \mathbf{c}_1) + \rho L^2 h(\dot{\mathbf{q}}_3^T\mathbf{C}_4\mathbf{q}_3 - \dot{\mathbf{q}}_1^T\mathbf{C}_4\mathbf{q}_1 + \dot{\mathbf{q}}_7^T\mathbf{C}_4\mathbf{q}_7 - \dot{\mathbf{q}}_5^T\mathbf{C}_4\mathbf{q}_5) \quad (B.9)$$

$$\Gamma_z(\mathbf{q}, \dot{\mathbf{q}}) = \rho L^3(\dot{\mathbf{q}}_1 + \dot{\mathbf{q}}_3 + \dot{\mathbf{q}}_2 + \dot{\mathbf{q}}_4)^T(\mathbf{c}_1 + \frac{a}{L}\mathbf{c}_2) \quad (B.10)$$

B.2 Appendage Equations

Following the method developed in section 2.6, the vibrational equations are given in terms of the generalized coordinates vectors $\mathbf{q}_i$, for i =2 to 8:

$$\mathbf{M}\ddot{\mathbf{q}}_2 + 2\eta_2\omega_{in}\mathbf{D}\dot{\mathbf{q}}_2 + [\omega_{in}^2\mathbf{K} - (\omega_y^2+\omega_z^2)\mathbf{M} + (\omega_x^2+\omega_z^2)(\frac{a}{L}\mathbf{C}_4 + \mathbf{C}_3) + \frac{h}{L}(\dot{\omega}_x - \omega_y\omega_z)\mathbf{C}_4]\mathbf{q}_2$$
$$-2\omega_y\mathbf{M}\dot{\mathbf{q}}_6 - (\dot{\omega}_y + \omega_x\omega_z)\mathbf{M}\mathbf{q}_6 = \frac{1}{\rho L^3}(\mathbf{f}_{e.2} - \frac{\partial V_g}{\partial \mathbf{q}_2}) + \frac{h}{L}(\dot{\omega}_y + \omega_x\omega_z)\mathbf{c}_2 - (\dot{\omega}_z - \omega_x\omega_y)(\frac{a}{L}\mathbf{c}_2 + \mathbf{c}_1) \quad \text{(B.11)}$$

$$\mathbf{M}\ddot{\mathbf{q}}_3 + 2\eta_3\omega_{in}\mathbf{D}\dot{\mathbf{q}}_3 + [\omega_{in}^2\mathbf{K} - (\omega_x^2+\omega_z^2)\mathbf{M} + (\omega_y^2+\omega_z^2)(\frac{a}{L}\mathbf{C}_4 + \mathbf{C}_3) + \frac{h}{L}(\dot{\omega}_y + \omega_x\omega_z)\mathbf{C}_4]\mathbf{q}_3$$
$$+2\omega_x\mathbf{M}\dot{\mathbf{q}}_7 + (\dot{\omega}_x - \omega_y\omega_z)\mathbf{M}\mathbf{q}_7 = \frac{1}{\rho L^3}(\mathbf{f}_{e.3} - \frac{\partial V_g}{\partial \mathbf{q}_3}) - \frac{h}{L}(\dot{\omega}_x - \omega_y\omega_z)\mathbf{c}_2 - (\dot{\omega}_z + \omega_x\omega_y)(\frac{a}{L}\mathbf{c}_2 + \mathbf{c}_1) \quad \text{(B.12)}$$

$$\mathbf{M}\ddot{\mathbf{q}}_4 + 2\eta_4\omega_{in}\mathbf{D}\dot{\mathbf{q}}_4 + [\omega_{in}^2\mathbf{K} - (\omega_y^2+\omega_z^2)\mathbf{M} + (\omega_x^2+\omega_z^2)(\frac{a}{L}\mathbf{C}_4 + \mathbf{C}_3) - \frac{h}{L}(\dot{\omega}_x - \omega_y\omega_z)\mathbf{C}_4]\mathbf{q}_4$$
$$-2\omega_y\mathbf{M}\dot{\mathbf{q}}_8 - (\dot{\omega}_y + \omega_x\omega_z)\mathbf{M}\mathbf{q}_8 = \frac{1}{\rho L^3}(\mathbf{f}_{e.4} - \frac{\partial V_g}{\partial \mathbf{q}_4}) - \frac{h}{L}(\dot{\omega}_y + \omega_x\omega_z)\mathbf{c}_2 - (\dot{\omega}_z - \omega_x\omega_y)(\frac{a}{L}\mathbf{c}_2 + \mathbf{c}_1) \quad \text{(B.13)}$$

$$\mathbf{M}\ddot{\mathbf{q}}_5 + 2\eta_5\omega_{out}\mathbf{D}\dot{\mathbf{q}}_5 + [\omega_{out}^2\mathbf{K} - (\omega_x^2+\omega_y^2)\mathbf{M} + (\omega_y^2+\omega_z^2)(\frac{a}{L}\mathbf{C}_4 + \mathbf{C}_3) - \frac{h}{L}(\dot{\omega}_y + \omega_x\omega_z)\mathbf{C}_4]\mathbf{q}_5$$
$$-2\omega_x\mathbf{M}\dot{\mathbf{q}}_1 - (\dot{\omega}_x + \omega_y\omega_z)\mathbf{M}\mathbf{q}_1 = \frac{1}{\rho L^3}(\mathbf{f}_{e.5} - \frac{\partial V_g}{\partial \mathbf{q}_5}) - \frac{h}{L}(\omega_x^2+\omega_y^2)\mathbf{c}_2 - (\dot{\omega}_y - \omega_x\omega_z)(\frac{a}{L}\mathbf{c}_2 + \mathbf{c}_1) \quad \text{(B.14)}$$

$$\mathbf{M}\ddot{\mathbf{q}}_6 + 2\eta_6\omega_{out}\mathbf{D}\dot{\mathbf{q}}_6 + [\omega_{out}^2\mathbf{K} - (\omega_x^2+\omega_y^2)\mathbf{M} + (\omega_x^2+\omega_z^2)(\frac{a}{L}\mathbf{C}_4 + \mathbf{C}_3) + \frac{h}{L}(\dot{\omega}_x - \omega_y\omega_z)\mathbf{C}_4]\mathbf{q}_6$$
$$+2\omega_y\mathbf{M}\dot{\mathbf{q}}_2 + (\dot{\omega}_y - \omega_x\omega_z)\mathbf{M}\mathbf{q}_2 = \frac{1}{\rho L^3}(\mathbf{f}_{e.6} - \frac{\partial V_g}{\partial \mathbf{q}_6}) + \frac{h}{L}(\omega_x^2+\omega_y^2)\mathbf{c}_2 - (\dot{\omega}_x + \omega_y\omega_z)(\frac{a}{L}\mathbf{c}_2 + \mathbf{c}_1) \quad \text{(B.15)}$$

$$\mathbf{M}\ddot{\mathbf{q}}_7 + 2\eta_7\omega_{out}\mathbf{D}\dot{\mathbf{q}}_7 + [\omega_{out}^2\mathbf{K} - (\omega_x^2+\omega_y^2)\mathbf{M} + (\omega_y^2+\omega_z^2)(\frac{a}{L}\mathbf{C}_4 + \mathbf{C}_3) + \frac{h}{L}(\dot{\omega}_y + \omega_x\omega_z)\mathbf{C}_4]\mathbf{q}_7$$
$$-2\omega_x\mathbf{M}\dot{\mathbf{q}}_3 - (\dot{\omega}_x + \omega_y\omega_z)\mathbf{M}\mathbf{q}_3 = \frac{1}{\rho L^3}(\mathbf{f}_{e.7} - \frac{\partial V_g}{\partial \mathbf{q}_7}) + \frac{h}{L}(\omega_x^2+\omega_y^2)\mathbf{c}_2 - (\dot{\omega}_y - \omega_x\omega_z)(\frac{a}{L}\mathbf{c}_2 + \mathbf{c}_1) \quad \text{(B.16)}$$

$$\mathbf{M}\ddot{\mathbf{q}}_8 + 2\eta_8\omega_{out}\mathbf{D}\dot{\mathbf{q}}_8 + [\omega_{out}^2\mathbf{K} - (\omega_x^2+\omega_y^2)\mathbf{M} + (\omega_x^2+\omega_z^2)(\frac{a}{L}\mathbf{C}_4 + \mathbf{C}_3) - \frac{h}{L}(\dot{\omega}_x - \omega_y\omega_z)\mathbf{C}_4]\mathbf{q}_8$$
$$+2\omega_y\mathbf{M}\dot{\mathbf{q}}_4 + (\dot{\omega}_y - \omega_x\omega_z)\mathbf{M}\mathbf{q}_4 = \frac{1}{\rho L^3}(\mathbf{f}_{e.8} - \frac{\partial V_g}{\partial \mathbf{q}_8}) - \frac{h}{L}(\omega_x^2+\omega_y^2)\mathbf{c}_2 - (\dot{\omega}_x + \omega_y\omega_z)(\frac{a}{L}\mathbf{c}_2 + \mathbf{c}_1) \quad \text{(B.17)}$$

Appendix C

PROOF OF EQUATION (2.18)

Let us take partial derivatives of the gravitational potential in Eq.(2.12) with respect to the vector of Euler angles:

$$\frac{\partial V_g}{\partial \alpha} = \frac{3\mu}{r_G^3}\left(\frac{\partial \mathbf{c}(\alpha)}{\partial \alpha}\right)^T \mathbf{I}(\mathbf{q})\mathbf{c}(\alpha) \tag{C.1}$$

The unit radial vector **c** is expressed in the body fixed frame in Eq.(C.1): this vector represents the first column of the rotation matrix **R** that describes the transformation from the orbital frame to the body-fixed frame:

$$\mathbf{c}(\alpha) = \mathbf{R}(\alpha)\mathbf{X}_o \tag{C.2}$$

The following algebra is used to obtain the partial derivative of the unit radial vector **c** with respect to the vector of Euler angles.

On the one hand, the time derivative of **R** can be obtained as follows:

$$\dot{\mathbf{R}} = \sum_{i=1}^{3} \frac{\partial \mathbf{R}}{\partial \alpha_i}\dot{\alpha}_i \tag{C.3}$$

On the other hand, the time derivative of **R** can be calculated from the angular velocity ω_R, associated with the rotation **R**:

$$\dot{\mathbf{R}} = -\omega_R^{\times}\mathbf{R} \tag{C.4}$$

where from Eq.(2.15):

$$\omega_R = \mathbf{P}(\alpha)\dot{\alpha} \tag{C.5}$$

The following equation is obtained by combining Eqs.(C.3) and (C.4):

$$\sum_{i=1}^{3} \frac{\partial \mathbf{R}}{\partial \alpha_i} \dot{\alpha}_i = -\omega_R^{\times} \mathbf{R} \tag{C.6}$$

Let us multiply both sides of Eq.(C.6) by the unit vector $\mathbf{X}_o$ and use Eq.(C.2):

$$\sum_{i=1}^{3} \frac{\partial \mathbf{c}}{\partial \alpha_i} \dot{\alpha}_i = \frac{\partial \mathbf{c}}{\partial \alpha} \dot{\alpha} = -\omega_R^{\times} \mathbf{c} = \mathbf{c}^{\times} \omega_R \tag{C.7}$$

Substituting Eq.(C.5) into Eq.(C.7), one obtains:

$$\frac{\partial \mathbf{c}}{\partial \alpha} \dot{\alpha} = \mathbf{c}^{\times} \mathbf{P} \dot{\alpha} \tag{C.8}$$

Since Eq.(C.8) holds for all $\dot{\alpha}$, the partial derivative of the radial vector $\mathbf{c}$ with respect to the vector of Euler angles can be obtained:

$$\frac{\partial \mathbf{c}}{\partial \alpha} = \mathbf{c}^{\times} \mathbf{P} \tag{C.9}$$

Taking the tranpose of Eq.(C.9) results in the following equation:

$$\left(\frac{\partial \mathbf{c}}{\partial \alpha} \right)^{T} = -\mathbf{P}^{T} \mathbf{c}^{\times} \tag{C.10}$$

Finally, the gravity gradient torque of the spacecraft can be obtained by substituting Eq.(C.10) in Eq.(C.1) and using Eq.(2.18):

$$\tau_g = -\left(\mathbf{P}^{-1}\right)^{T} \left(\frac{\partial V_g}{\partial \alpha} \right) = \frac{3\mu}{r_G^3} \mathbf{c}^{\times}(\alpha) \mathbf{I}(\mathbf{q}) \mathbf{c}(\alpha) \tag{C.11}$$

Appendix D

GEOMAGNETIC FIELD MODEL

According to the International Reference Field model, the predominant portion of the geomagnetic field vector can be obtained as the gradient of the magnetic potential function V_m:

$$\mathbf{b} = -\nabla V_m \tag{D.1}$$

where V_m can be conveniently represented by a series of spherical harmonics:

$$V_m(r,\phi,\theta) = R_e \sum_{n=1}^{k} \left(\frac{R_e}{r}\right)^{n+1} \sum_{m=0}^{n} \left(g_n^m \cos m\phi + h_n^m \sin m\phi\right) P_n^m(\theta) \tag{D.2}$$

where R_e is the Earth radius; g_n^m and h_n^m are the Gaussian coefficients; r, θ, ϕ are respectively the geocentric distance, the coelevation, and the East longitude from Greenwich meridian, and P_n^m are the Legendre functions.

As shown in [Blakely'95], the dipole model represents a reasonably good approximation of the magnetic field and is the model chosen in this thesis. By expanding the field potential to the first degree, Eq.(D.2) becomes:

$$V_m(r,\phi,\theta) = \frac{R_e^3}{r^2}\left(g_1^0 \cos\theta + g_1^1 \cos\phi \sin\theta + h_1^1 \sin\phi \sin\theta\right) \tag{D.3}$$

From the 1990 IGRF data in [Blakely'95], the Gaussian coefficients used in the dipole model are:

$$\begin{aligned} g_1^0 &= -29775 \text{ nT} \\ g_1^1 &= -1851 \text{ nT} \\ h_1^1 &= 5411 \text{ nT} \end{aligned} \tag{D.4}$$

As a result, the dipole strength of the Earth can be defined as:

$$M_e = R_e^3 \sqrt{g_1^{0^2} + g_1^{1^2} + h_1^{1^2}} = 7.84\ 10^6 \text{T km}^3 \tag{D.5}$$

The coelevation angle of the dipole is:

$$\theta_m = \arccos\left(\frac{g_1^0 R_e^3}{M_e}\right) = 169.12° \tag{D.6}$$

The East longitude of the dipole is:

$$\phi_m = \arctan\left(\frac{h_1^1}{g_1^1}\right) = 108.88° \tag{D.7}$$

Thus, the first-order geomagnetic field model is due to a dipole with northern magnetization pointed toward the southern hemisphere. From Eqs.(D.6) and (D.7), the extension of the magnetic dipole in the northern hemisphere intersects the Earth's surface at 79.12°N and 288.88°E.

IMAGE EVALUATION
TEST TARGET (QA-3)

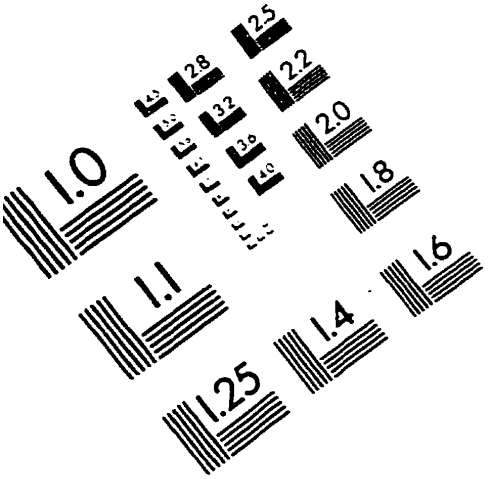

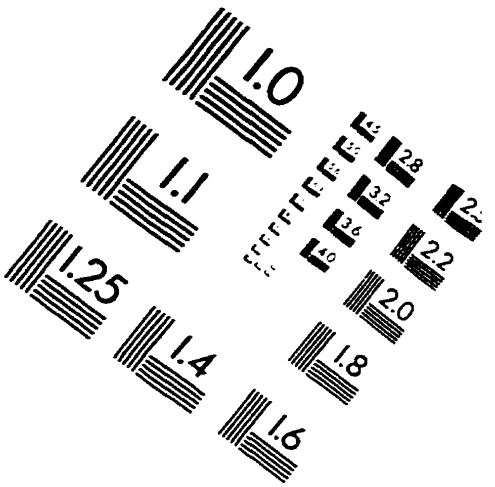

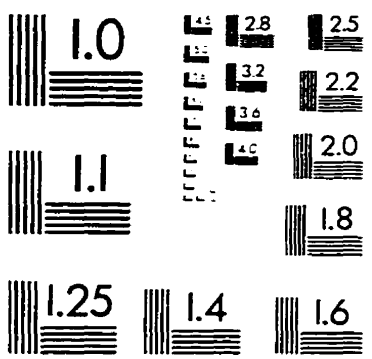

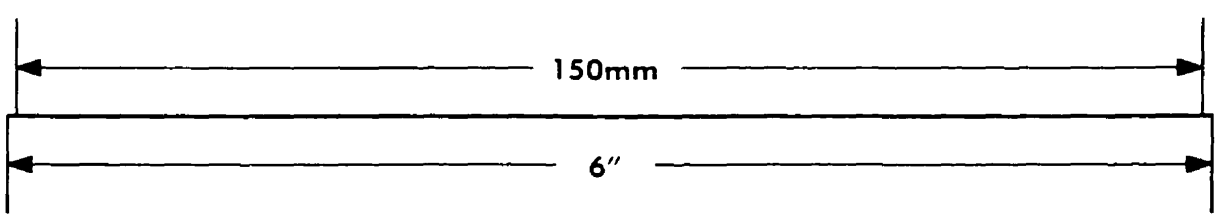

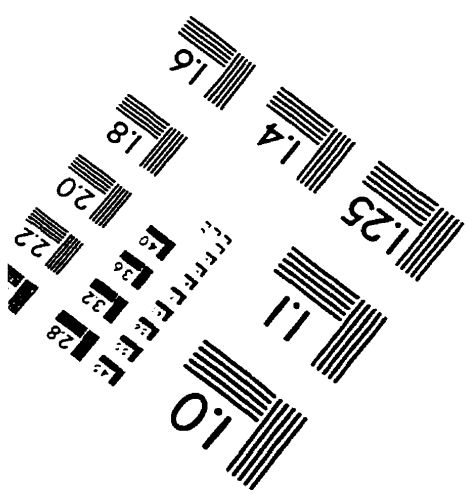

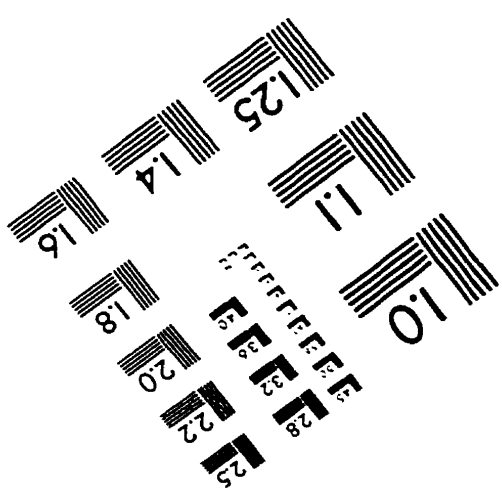

APPLIED IMAGE, Inc
1653 East Main Street
Rochester, NY 14609 USA
Phone: 716/482-0300
Fax: 716/288-5989